# FINAL REPORT

## Practical Assessment and Optimization of Redox-Based Groundwater Remediation Technologies

## SERDP Project ER-2308

MARCH 2017

Paul G. Tratnyek
Richard L. Johnson
**Oregon Health & Science University**

*Distribution Statement A*
*This document has been cleared for public release*

SERDP
DOD ▪ EPA ▪ DOE

*Page Intentionally Left Blank*

This report was prepared under contract to the Department of Defense Strategic Environmental Research and Development Program (SERDP). The publication of this report does not indicate endorsement by the Department of Defense, nor should the contents be construed as reflecting the official policy or position of the Department of Defense. Reference herein to any specific commercial product, process, or service by trade name, trademark, manufacturer, or otherwise, does not necessarily constitute or imply its endorsement, recommendation, or favoring by the Department of Defense.

*Page Intentionally Left Blank*

# REPORT DOCUMENTATION PAGE

*Form Approved*
*OMB No. 0704-0188*

Public reporting burden for this collection of information is estimated to average 1 hour per response, including the time for reviewing instructions, searching existing data sources, gathering and maintaining the data needed, and completing and reviewing this collection of information. Send comments regarding this burden estimate or any other aspect of this collection of information, including suggestions for reducing this burden to Department of Defense, Washington Headquarters Services, Directorate for Information Operations and Reports (0704-0188), 1215 Jefferson Davis Highway, Suite 1204, Arlington, VA 22202-4302. Respondents should be aware that notwithstanding any other provision of law, no person shall be subject to any penalty for failing to comply with a collection of information if it does not display a currently valid OMB control number. **PLEASE DO NOT RETURN YOUR FORM TO THE ABOVE ADDRESS.**

**1. REPORT DATE** *(DD-MM-YYYY)*
03-10-2017

**2. REPORT TYPE**
Final Report

**3. DATES COVERED** *(From - To)*

**4. TITLE AND SUBTITLE**

Practical Assessment and Optimization of Redox-Based Groundwater Remediation Technologies

**5a. CONTRACT NUMBER**

**5b. GRANT NUMBER**

**5c. PROGRAM ELEMENT NUMBER**

**6. AUTHOR(S)**

Tratnyek, Paul G.
Johnson, Richard L.

**5d. PROJECT NUMBER**

**5e. TASK NUMBER**

**5f. WORK UNIT NUMBER**

**7. PERFORMING ORGANIZATION NAME(S) AND ADDRESS(ES)**

Oregon Health & Science University
20000 NW Walker Road
Beaverton, OR 97006

**8. PERFORMING ORGANIZATION REPORT NUMBER**

**9. SPONSORING / MONITORING AGENCY NAME(S) AND ADDRESS(ES)**
Strategic Environmental Research and Development Program
4800 Mark Center Drive, Suite 17D03

**10. SPONSOR/MONITOR'S ACRONYM(S)**
SERDP

**11. SPONSOR/MONITOR'S REPORT NUMBER(S)**
ER-2308

**12. DISTRIBUTION / AVAILABILITY STATEMENT**

U

**13. SUPPLEMENTARY NOTES**

**14. ABSTRACT**

This project took a "chemical probe reaction" approach, which involves adding chemical reactivity or redox probes (CRPs) that react with the medium, and the resulting change in speciation of the CRP is monitored either spectrophotometrically (i.e., by measuring the color change) or potentiometrically (i.e., with a Pt electrode). Variations on this method can be used to characterize thermodynamic, kinetics, and capacity aspects of the redox conditions in a sample. CRPs could be used at field sites in push-pull tests, or for ex situ characterization of preserved samples. Ultimately, the project aimed to relate CRP results to contaminant degradation under in situ conditions.

**15. SUBJECT TERMS**

| **16. SECURITY CLASSIFICATION OF:** | | | **17. LIMITATION OF ABSTRACT** | **18. NUMBER OF PAGES** | **19a. NAME OF RESPONSIBLE PERSON** |
|---|---|---|---|---|---|
| **a. REPORT** | **b. ABSTRACT** | **c. THIS PAGE** | | | Paul Tratnyek |
| U | U | U | U | 43 | **19b. TELEPHONE NUMBER** *(include area code)* 503-346-2431 |

**Standard Form 298 (Rev. 8-98)**
**Prescribed by ANSI Std. Z39.18**

*Page Intentionally Left Blank*

# 1. TABLE OF CONTENTS


**1. Table of Contents** ..... **ii**
**2. List of Tables** ..... **iv**
**3. List of Figures** ..... **v**
**4. List of Acronyms** ..... **xi**
**5. Keywords** ..... **xii**
**6. Acknowledgements** ..... **xii**
**7. Abstract** ..... **1**
**8. Objectives** ..... **3**
**9. Background** ..... **4**
*9.1. Limitations of Conventional Tools for Redox Assessment* ..... *4*
*9.2. Alternative Approaches to Redox Assessment* ..... *5*
*9.3. Field Deployment of Chemical Probes with Push-Pull Tests* ..... *8*
**10. Results and Discussion** ..... **9**
*10.1. Objective 1—Conceptual Development of Probes* ..... *9*
10.1.1. Model System Selection ..... 10
10.1.2. Conceptual Development of Thermodynamic Probes ..... 11
10.1.3. Conceptual development of Kinetic Probes ..... 14
10.1.4. Conceptual development of Capacity Probes ..... 15
*10.2. Objective 2(A)—Bench Scale Testing of Probes* ..... *16*
10.2.1. Introduction ..... 17
10.2.2. Experimental ..... 18
10.2.3. Results and Discussion ..... 20
10.2.4. Supporting Information for Fan et al. 2016 [*108*] ..... 28
10.2.4.1. Experimental Details ..... 28
10.2.4.2. Characterization of Iron Oxides ..... 29
*10.3. Objective 2(B)—Bench Scale Applications to nZVI* ..... *40*
10.3.1. Introduction ..... 40
10.3.2. Experimental ..... 42
10.3.3. Results and Discussion ..... 43
10.3.4. Supporting Information for Fan et al. 2015 [*184*] ..... 52
10.3.4.1. Method Details ..... 52
*10.4. Objective 3—Column-Pilot Scale Demonstration* ..... *61*
10.4.1. Introduction ..... 61
10.4.2. Methods ..... 62
10.4.2.1. Column setup ..... 62
10.4.2.2. Thermodynamic measurements ..... 63
10.4.2.3. Selection of appropriate redox dye ..... 63
10.4.2.4. Design of the pull-push-pull tests ..... 63
10.4.2.5. Calculation of ECRP ..... 64
10.4.2.6. Kinetic measurements ..... 64
10.4.2.7. Determination of rate constants ..... 65
10.4.3. Results ..... 66
10.4.3.1. Thermodynamic measurements ..... 66
10.4.3.2. Kinetic measurements ..... 67

10.4.3.3. Comparison of thermodynamic and kinetic data for the columns.....69
10.4.3.4. Strengths and weaknesses of CRP pull-push-pull tests.....70
10.4.4. Supporting Information for Johnson et al. 2017 [*189*] ..... 71
10.4.4.1. Flow system for the columns .....71
10.4.4.2. Chemical reactivity probes.....72
10.4.4.3. Experimental setup for the flow-through columns.....73
10.4.4.4. Flow Modeling .....74
10.4.4.5. Ancillary Column Data .....75
10.4.4.6. UV-vis and modeling data for all columns and ports.....76
*10.5. Objective 4—Outreach and Technology Transfer..... 78*
10.5.1. Collaborations to deploy CRPs for Field Site Characterization ..... 78
10.5.2. Other Collaborations on Field Sites..... 80
10.5.3. Training via Short Courses and Webinars ..... 80
10.5.3.1. Short Courses and Webinars .....80
10.5.3.2. SERDP ESTCP Webinar.....80
**11. Overall Conclusions and Implications .....81**
**12. References.....82**
**13. Appendices.....97**
*13.1. Supporting Data..... 97*
*13.2. List of Scientific/Technical Publications ..... 97*
*13.3. Other Supporting Materials..... 97*

# 2. LIST OF TABLES

Table 1. Examples of chemical probes for in situ redox processes. .....9

Table 2. Selected thermodynamic probes .....12

Table 3. Results of fitting SSA data in Figure S1 for Bayferrox iron oxides .....29

Table 4. Nomenclature and Properties of Thermodynamic Chemical Reactivity Probes (CRPs). .....31

Table 5. Summary of the experimental conditions, the CRPs selected for calculating the $E_{CRP}$ of each iron minerals, the calculated $E_{CRP}$, and measured $E_{Pt}$ under each condition .....33

Table 6. Observed reduction rate constants ($k_{obs}$) for three contaminants .....35

Table 7. Published reduction rate constants of nitrobenzene (including 4Cl-nitrobenzene), carbon tetrachloride, and trichloroethene (and tetrachloroethene) by magnetite. .....36

Table 8. Published reduction rate constants of nitrobenzene (including 4Cl-nitrobenzene), carbon tetrachloride, and trichloroethene (and tetrachloroethene) by Fe(II) sorbed onto Fe(III) oxide. .....37

Table 9. Published reduction rate constants of nitrobenzene (including 4Cl-nitrobenzene), carbon tetrachloride, and trichloroethene (and tetrachloroethene) by green rust .....38

Table 10. Published reduction rate constants of nitrobenzene (including 4Cl-nitrobenzene), carbon tetrachloride, and trichloroethene (and tetrachloroethene) by mackinawite .....39

# 3. LIST OF FIGURES

Figure 1. Conceptual representation of the relationship between measures of contaminant degradation. ....6

Figure 2. Eh-pH diagram from (31), illustrating equilibrium speciation of a labile chemical probe (Q for quinone) vs. the (less labile) iron system. Iron associated with minerals and quinones—which are associated with natural organic matter (NOM)—can contribution to the abiotic natural attention of groundwater contaminants like TCE. ....6

Figure 3. Redox buffering capacity diagram for iron from (35), showing maximum buffering capacity (β) at the stability field boundaries. ....7

Figure 4. Schematic representation of a sequence of three push-pull tests consisting of single injections followed by multiple extractions. A cocktail of chemicals (thermodynamic, kinetic, and capacity probes plus a conservative tracer) could allow the effects of redox manipulation to be quantitatively assessed. ....8

Figure 5. Conceptual representation of the relationship between measures of contaminant degradation (in this case rate) and measures of the conditions of reducing materials (shown also as a rate). RAZ, RSF, I2S, and MV are all possible probes. The question marks are to reinforce that the pairings of contaminant and probe shown were hypothetical when this plot was developed. ....10

Figure 6. Surface normalized reaction rate constants ($k_{sa}$) vs. mass normalized reaction rate constants ($k_m$) for abiotic reduction of CT and TCE/PCE by a variety of reduced iron and sulfur minerals, measured in laboratory batch experiments. (Based on a compilation of data from previously published work summarized in [*55*]). ....11

Figure 7. Redox couples for the two probes we are currently focusing on. Colors represent approximate color of the species. Properties are summarized in Table 2. ....12

Figure 8. (A) Resorufin (left axis) and I2S (right axis) reduction in homogeneous Fe(II) solution and heterogeneous Fe(II)-mineral heterogeneous suspension; (B) Eh in Fe(II)-mineral suspensions vs. the ratio between oxidized and reduced I2S. Eh value was based on ORP measurement (vs. Ag/AgCl) performed after 20-h Fe(II) adsorption period. The absorbance was measured 1-hr after probe addition to Fe(II)-mineral suspensions. ....13

Figure 9. Reduction of Resofurin (left) and I2S (right) in the presence of aquifer materials and various reductants. Note that the time scale needed for these data with natural materials is significantly longer than for the model system results

(Figure 8), presumably due to greater quantity of available oxide surface area in the latter. .....14

Figure 10. Pseudo-first order reduction kinetics of carbon tetrachloride by goethite + various amount of Fe(II). .....15

Figure 11. Preliminary data illustrating results obtained by titrating model aquifer sediment with two types of chemical oxidants. The experimental protocol for this is straight-forward, but the conceptual basis of generalizing the results (i.e., format of the figure) was an area of study. .....16

Figure 12. The effects of (A) oxide type, (B) goethite loading, (C) Fe(II) loading with magnetite, and (D) Fe(II) loading with goethite on reduction of CRPs by Fe(II) + iron oxide suspensions. The CRP was AQDS for (A) and (B) and AQS for (C) and (D). All spectra were taken after 20 hr of exposure to the mineral suspensions. .....21

Figure 13. Summary of the $E_{CRP}$ values determined for different reducing iron minerals under various conditions. Each marker is labeled with the specific value of the varied parameter (bold labels). The plain text annotation above each subcolumn indicates the experimental parameter that was constant in that series of experiments. For reference, reduction potentials of the four CRPs at pH = 7 ($E_H'$) are plotted in the far left column for reference. For comparison, formal reduction potentials reported in prior studies are plotted in the far right column. Tabulated values are from Stumm [*102*] and measured values are based on Orsetti et al. [*86*] and Gorski et al. [*72*]. .....23

Figure 14. (A) The $E_{Pt}$ of mineral suspension as a function of time measured by a 3 mm Pt electrode (rotated at 2000 rpm) and a Ag/AgCl reference electrode under Ar headspace (arrows indicate the time aliquots of thermodynamic CRPs were added); (B) Potentiometrically measured $E_{Pt}$ vs. $E_{CRP}$ shown in Figure 13.....25

Figure 15. Pseudo-first order rate constants (log $k_{SA}$) for reduction of 4Cl-NB, 2-CAP, and CT by iron minerals versus mineral reduction potentials determined by chemical reactivity probes ($E_{CRP}$) Fitting results (slope, intercept, $r^2$) are −0.029±0.005, −6±1, 0.839; −0.008±0.001, −5.8±0.3, 0.885; and −0.011±0.003, −6.1±0.6, 0.738 for 4-Cl-NB, 2-CAP, and CT, respectively. (Oxide loading (g/L), type, and Fe(II) concentration (mM) for each data point are annotated next to the marker). .....26

Figure 16. Mass-normalized reduction rate constants ($k_M$) of kinetic CRPs (including nitroaromatics and chlorinated alkanes) and chlorinated ethenes with various reducing iron minerals (open symbols: values reported in literature; solid

symbols: value determined in this study). Literature data used in this plot are summarized in Table 7 to Table 10.....27

Figure 17. Specific surface areas of Bayferrox iron oxides determined by $N_2$ gas adsorption by the BET method. Open symbols represent independent replicate measurements, starting with 0.7 to 1.0 g of fresh sample each time. The instrument (Micromeritics Gemini V Surface Area & Pore size Analyzer) had recently received manufacturer maintenance and verification. The absolute accuracy of the instrument was determined to be within 3.5% using a carbon black standard. .....30

Figure 18. Absorbance spectra of (A) RSF, (B) I2S, (C) AQDS, and (D) AQS after reduction by lepidocrocite + 0.5 mM Fe(II) (solid line) and after exposing to ambient air (dash line) .....32

Figure 19. Mineral reduction potential ($E_{CRP}$) and aqueous Fe(II) concentration measured before probe addition for goethite and lepidocrocite at different mineral loadings with 1 mM initial Fe(II) concentration.....34

Figure 20. Determination of the apparent stoichiometry of I2S reaction with nZVI: (A) decrease in aqueous absorbance at 610 nm due to reduction of $I2S_{ox}$ by freshly-prepared CMC-nZVI diluted to the specified initial concentrations. The asterisk represents $Abs_{610}$ measured after sample reoxidation. (Data was recorded continuously, but markers are only shown every 1000 data points.) (B) Correlation between the amount of I2S reduction and nZVI oxidation for fresh and aged CMC-nZVI (each data point is derived from an individual I2S reduction curve, including the examples in A, shown by solid diamonds. The solid line corresponds to the linear regression coefficients given in the graph).....44

Figure 21. Second-order kinetic modeling: (A) Fitting of representative data for I2S reduction by freshly-prepared CMC-nZVI diluted to 2 and 4 mg/L in pH 7.2 HEPES buffer (the concentration was calculated based on the absorbance data shown in Figure 1A), (B) Correlation between oxidized nZVI determined by fitting and oxidized nZVI determined by absorbance.....47

Figure 22. Effect of Fe(II) on I2S reduction by Fe(0): (**A**) I2S reduction by mixtures of Fe(II) and nZVI with the total iron concentration of 10 mg/L and equal concentrations of nZVI without Fe(II). (**B**) I2S reduction by 4 mg/L nZVI with aqueous Fe(II) concentrations from 0 to 15 mg/L (open symbols are experimental data, and solid lines are second-order kinetic fits). (C) Second-order rate constant (left axis) and amount of I2S reduction (right axis) extracted from fitting the data in Figure 21B. .....48

Figure 23. Quantifying the lifetime of nZVI in DO/DI water: Kinetics of Fe(0) oxidation by water with 50, 100, and 200 mg/L initial nZVI concentrations (in 10 mM HEPES buffer at pH 7.2) and 200 mg/L initial nZVI concentration (in 10 mM HEPES buffer of pH 8.5). Each data point was determined by I2S reduction in subsamples of the nZVI suspension). Labels are ORP measured with a Pt electrode and reported vs. SHE. .....49

Figure 24. Eh-pH diagram for species of I2S and iron (Fe(II) = 4 mg/L; Temperature = 298 K; Suppressed iron phases: hematite). Speciation modeling for iron performed using the Geochemist's Workbench modeling package (RockWare Inc., Golden, CO). Thermodynamic data for I2S from references [*99, 171*]. The vertical lines in blue separate the fully protonated, monoanionic, and dianionic species of $I2S_{RED}$ (respectively from left to right). .....53

Figure 25. Absorbance spectra of ~140 µM $I2S_{ox}$ and $I2S_{red}$ and 4 mg/L $nZVI_{ox}$ and $nZVI_{red}$ in deoxygenated 10 mM HEPES buffer at pH 7.2. ($I2S_{red}$ was prepared by adding 1 drop of freshly-prepared 1 M sodium dithionite into the $I2S_{ox}$ solution; $nZVI_{ox}$ was prepared by exposing the $nZVI_{red}$ suspension to ambient air). .....54

Figure 26. Calibration curves ($y = ax + b$) for absorbance at 610 nm for $I2S_{ox}$ and freshly-prepared CMC-nZVI ($nZVI_{red}$), both in 10 mM HEPES buffer at pH 7.2. Spectrophoto-metry performed in a screw-cap sealed optical glass cuvette with 1-cm path length. .....55

Figure 27. Change in $Abs_{610}$ due to reduction of I2S by 10 mg/L aqueous Fe(II) (without nZVI) at pH 7.2 and 8.5 with 10 mM HEPES buffer. The initial concentration of I2S was ~140 µM. .....56

Figure 28. Change in Fe(0) concentration due to reaction with water only (without I2S) in 10 mM HEPES buffer at pH 7.2 and 8.5. Initial concentrations of CMC-nZVI were 2, 4, and 6 mg/L. Fe(0) concentrations are calculated by the $Abs_{610}$ using the calibration curve of $nZVI_{red}$ shown in Figure 26. .....57

Figure 29. Decrease in Fe(0) content over time (due to oxidation in water, etc.) for the freshly-synthesized CMC-nZVI stock solutions and solutions of nZVI diluted to 200 mg/L nZVI in DI/DO and in pH 7.2 10 mM HEPES buffer. The latter data (gray symbols) are also shown in Figure 4 of the main text. .....58

Figure 30. Effects of anions on the reduction capacity of Fe(0), represented by the amount of I2S reduction by nZVI suspension after 24 h exposure ([anion] = 0.5 mM, [nZVI] = 200 mg/L, pH = 7.2. For I2S reduction, 200 mg/L nZVI was further diluted to 4 mg/L in 10 mM HEPES buffer at pH 7.2). .....59

Figure 31. Transmission electron micrographs of (**A**) original CMC-nZVI aged for 24 h, (**B**) 200 mg/L CMC-nZVI aged for 24 h in DO/DI water, (**C**) 200 mg/L CMC-nZVI aged for 24 h in pH 7.2 HEPES buffer, and (**D**) 100 mg/L CMC-nZVI after complete oxidation by I2S. .....60

Figure 32. Schematic drawing of the experimental setup for the abiotic kinetic experiments. .....65

Figure 33. $E_{CRP}$ values for sub-samples taken from all sample ports on the control and sulfate columns. .....66

Figure 34. Average reduction potential values for all ports on both columns. Values were determined by chemical reactivity probe and by platinum electrode corrected to the standard hydrogen electrode. .....67

Figure 35. (A) example of absorbance data from the continuous-flow tests. This example is for Port 1 of the sulfate column. Other data are shown as supporting information, below, in Section 1.7.4.6. (B) mass balance (represented as the sum of the absorbances) for Port 1 on the sulfate column .....68

Figure 36. First order reduction rate constants for the control and sulfate columns measured at the four ports on the columns. .....70

Figure 37. Flow system for the columns .....71

Figure 38. Summary of nomenclature and properties of thermodynamic chemical reactivity probes (CRPs). (Same as Table 4) .....72

Figure 39. Experimental setup for the flow-through columns. Ceramic piston pumps for the eluent in the back, syringe pumps for CRPs in the foreground. The oxygen-free chamber containing the flow cell is shown above the red arrow. .....73

Figure 40. Black curve is the from the concentration model as well and squares are the experimental data. The red line represents the influent concentration at what would have been the column-end of the sample tube. (1/16th inch tube in Figure 33 in the main text). Both the lag time and the mixing observed in the experimental data were incorporated into the model .....74

Figure 41. Dissolved iron at sample ports along the control column. .....75

Figure 42. Dissolved iron and sulfate at sample ports along the sulfate column. .....75

Figure 43. Control column, Ports 1-4. The upper portion of each column (Port 4) was difficult to test because of gas accumulation at the top of the column. For the control column, the quality of the 350 nm data for Port 4 was compromised by dramatically changing baseline, so it was not included in this analysis. .....76

Figure 44. Sulfate column, Ports 1-4. .....77

Figure 45. Sample the CMC-nZVI injection test site in Ontario. .....78

Figure 46. Example data using CRPs to characterization the reduction potential and capacity of CMC-nZVI impacted waters sampled from the Ontario field site. .....79

Figure 47. Demonstration of CRP reduction upon contact with aquifer material in a column. Images represent pull, push, and pull, using resazurin at the CRP. Blue to pink indicates reduction. .....81

# 4. LIST OF ACRONYMS

| Acronym | Definition |
|---|---|
| β | Redox buffer capacity |
| 2-CAP | 2-Chloroacetophenone |
| 2-CPE | 2-Chlorophenylethanol |
| 4-Cl-NB | 4-Chloronitrobenzene |
| AQDS | Anthraquinone disulfonate |
| AQS | Anthraquinone sulfonate |
| BET | Surface Area Measurement Method |
| CMC | Carboxymethylcellulose |
| CRP | Chemical reactivity (or redox) probe |
| CT | Carbon tetrachloride |
| DCIP | Dichloroindophenol |
| DO/DIW | Deoxygenated/Deionized water |
| DOI | Digital object identifier |
| GR | Green rust |
| GT | Goethite |
| HCA | Hexachloroethane |
| HEPES | Biological buffer |
| HPLC | High-performance liquid chromatography |
| HT | Hematite |
| I2S | Indigo disulfate |
| INT, XTT, MTS | Biochemical molecular probe compounds |
| ISCO | In situ chemical oxidation |
| ISCR | In situ chemical reduction |
| ISTR | In situ thermal remediation |
| $k_M$ | Mass normalized rate constant |
| $k_{SA}$ | Surface area normalized rate constant |
| LEAP | Large experimental aquifer program |
| LFER | Linear free energy relationship |
| LP | Lepidocrocite |
| MNA | Monitored natural attenuation |
| MT | Magnetite |
| MV | Methyl viologen |
| NAC | Nitro aromatic compound |
| NOD | Natural oxidant demand |
| NOM | Natural organic matter |
| NRD | Natural reductant demand |
| nZVI | Nano zerovalent iron |
| ORP | Oxidation-reduction potential |
| PCE | Perchloroethene |
| RAZ | Reszurin |
| RDE | Rotating disk electrode |
| RNIP | Commercial nZVI |
| RSF | Resorufin |
| SHE | Standard hydrogen electrode |
| SSA | Specific surface area |
| TCE | Trichlorothene |
| TCFE | Trichloroflouroethene |

| | |
|---|---|
| TEAP | Terminal electron accepting process |
| TNT | Trinitrotoluene |
| UHP | Ultra high purity |
| XRD | X-ray diffraction |

# 5. KEYWORDS

Remediation, Groundwater, In Situ Chemical Reduction (ISCR), Oxidation-Reduction (Redox), ORP, Natural Reductant Demand (NRD), Dechlorination, Trichloroethylene (TCE), Push-Pull Test, Treatability Assessment.

# 6. ACKNOWLEDGEMENTS

We thank J.Z. Bandstra for his input on formulation of the kinetic model for aging. The surface areas of oxides were measured by Maria Fuentes-Deonate, while on an internship funded by the NSF Center for Coastal Margin Observation and Research. Andrew Barnum at Portland State University for collecting the transmission electron micrographs.

# 7. ABSTRACT

***Objectives***: Many approaches to remediation of contaminated groundwater rely on contaminant degradation processes that are, directly or indirectly, based on redox reactions. Predicting and optimizing such processes requires reliable methods for characterizing in situ redox conditions, but the existing methods (usually direct ORP measurement with a Pt electrode) have repeatedly been shown to be inadequate.

***Technical Approach***: This project took a "chemical probe reaction" approach, which involves adding chemical reactivity or redox probes (CRPs) that react with the medium, and the resulting change in speciation of the CRP is monitored either spectrophotometrically (i.e., by measuring the color change) or potentiometrically (i.e., with a Pt electrode). Variations on this method can be used to characterize thermodynamic, kinetics, and capacity aspects of the redox conditions in a sample. CRPs could be used at field sites in push-pull tests, or for ex situ characterization of preserved samples. Ultimately, the project aimed to relate CRP results to contaminant degradation under in situ conditions.

***Results***: A variety of CRPs were identified that have potential application for characterizing redox conditions in environmental materials, with several offering the most promise: resazurin, indigo disulfonate, and anthraquinone sulfonate. These CRPs are non-toxic, readily available, and undergo rapid redox reactions with minimal sorption. Using these CRPs, with spectrophotometric or potentiometric detection, the reducing properties of minerals such as magnetite, with and without added Fe(II), were characterized. This information is not available using traditional direct ORP measurements done without CRPs to mediate electron transfer between the mineral surface and the electrode.

Using other CRPs, the kinetics of reduction by minerals such as magnetite were measured reliably in relatively rapid tests (less than one week), whereas the kinetics of reduction of chlorinated solvents by mineral is much slower, and therefore, much harder to measure. Serial application of CRPs could also be done to provide a kind of redox titration, thereby characterizing the reducing capacity of aquifer materials.

Using a combination of thermodynamic and kinetic CRPs measurements, and data from prior work on abiotic reduction of contaminants, a correlation was obtained that predicts the kinetics of contaminant reduction from the reducing potentials of iron oxide minerals. This correlation includes the effect of Fe(II) sorbed to Fe(III) oxide minerals through the reduction potential of the resulting phase.

***Benefits***. The use of CRPs to characterize the redox properties of environmental materials—including aquifer solids, but also sediments, soils, and sludges—can overcome many of the fundamental and practical limitations to traditional Pt electrode (only) measurements. Probably, the most significant advantage is the ability of CRPs to detect redox conditions on mineral surfaces, which can be much more strongly reducing than the associated pore water, and are primarily responsible for abiotic natural attenuation.

The CRP-based methods that we developed here are also flexible so that they can be adapted to characterize not only redox potential, but also kinetic and capacity characteristics of environmental media. Therefore, only CRP-based methods are likely to be able to fully characterize all of the aspects of in situ redox conditions necessary to determine if abiotic natural attenuation (or other redox-based remediation strategies, both chemical and microbiological) is

likely to be successful as a remedy at particular sites. However, the methods were validated and optimized mainly with laboratory-based measurements, so some aspects of their implementation under field conditions remain to be explored. Some of this technology transfer is continuing through other SERDP projects (especially ER-2621), and other efforts are under development through collaborations with a variety of practitioners.

# 8. OBJECTIVES

Characterization of in situ redox conditions is an essential component in designing, optimizing, implementing, and monitoring redox-based remediation of contaminated subsurface. Redox assessment in current remedial practices heavily rely on measurement of oxidation-reduction potential (ORP) or $E_h$ and solution phase analysis of redox active species, such as dissolved oxygen, nitrate, Fe(II), or sulfide etc. However, the outcomes of these approaches often lack specificity for redox transformation pathways of contaminants and fail to predict the potential for contaminant degradation by redox processes due to redox disequilibrium.

This project aimed to overcome these insufficiencies by (*i*) re-evaluating traditional redox-based characterization methods in light of our current, improved understanding of subsurface redox processes; (*ii*) developing in situ chemical probe based redox characterization methods that are more precise and robust, and (*iii*) rigorously defining the relationship between results from these new characterization methods and the performance of redox-based remedies applied to particular sites.

The project addressed the three types of factors that determine the performance of redox technologies (thermodynamic, kinetic, and capacity) by focusing on chemical-probe based assays that represent dynamic, rather than static, characteristics of the system. For example, although they are widely used, platinum electrode measurements are of limited value in designing remediation systems because they respond to a wide range of redox-active species with variable and unknown sensitivities. In contrast, the chemical probes we are investigating can target the species that are of primary interest in the design of a particular remediation system. Furthermore, utilizing these probes as in situ “push-pull” tests for measurement of aquifer properties should yield more accurate results than laboratory measurements based on collected core samples.

The overall objective of this project was to develop a suite of diagnostic tools for assessment and optimization of redox-based remediation technologies for aquifers contaminated with chlorinated hydrocarbons. The chemical probes are of three general types: (*i*) “thermodynamic” probes that capture the redox potential of the medium for reaction with contaminants, (*ii*) “kinetic” probes that characterize the rate of contaminant degradation by redox processes, and (*iii*) “capacity” probes that characterize the “buffer capacity” of the system with respect to changes in redox conditions. We adopted existing probes, where they proved suitable, and sought to identify and demonstrate new probes, as necessary. Protocols were developed for in situ application of these tools to characterization of groundwater redox conditions, based mainly on push-pull type in situ methods.

The project was structured around four major objectives. Objective 1 was conceptual development of chemical reactivity or redox probes (CRPs), including compilation and analysis of data and preliminary testing and calculations. Objective 2 involved bench-scale testing of CRPs on model environmental materials. Objective 3 involved column scale testing using aquifer materials with and without added iron minerals. Objective 4 was to begin transfer of CRP redox assay technologies to practitioners through field-scale demonstrations and training.

# 9. BACKGROUND

## 9.1. Limitations of Conventional Tools for Redox Assessment

Characterization of in situ redox conditions that is both rigorous with respect to chemical fundamentals and practical with respect to application in the field continues to be a challenge due to confusion over appropriate use of pε to describe redox conditions in natural waters [*1-3*]. The parameter is defined in terms of the activity of solvated electrons in solution (i.e., $p\varepsilon = -\log [e^-_{aq}]$), but the species $e^-_{aq}$ does not exist under environmental conditions to any significant degree. The related concept of p*e* [*4*], referring to the activity of electrons in the electrode material, may have a more realistic physical basis with respect to measurable quantities, but it does not provide an improved basis for describing redox transformations in solution. The fundamental problem is that the mechanisms of oxidation and reduction under environmental conditions do not involve electron transfer from solution (or from electrode materials, except in the rare case of direct application of electrolysis to remediation). Instead, the mechanisms of contaminant degradation by redox reactions involve reactions with specific oxidant or reductant molecules, and it is these species that define the half-reactions on which estimates of environmental redox reactions should be based.

Electrode potentials measured with an inert electrode like platinum (i.e., *ORP* or $E_h$) are of little help because they are not a simple function of the concentrations of specific oxidants and reductants in the solution. Instead, the electrode gives a mixed potential in response to all the redox active species in a given solution, weighted by the sensitivity of the electrode to each species (i.e., the exchange current density) [*5*]. Resolving mixed potentials into concentrations of all the contributing species is not a practical way to characterize the availability of oxidants or reductants to react with a particular contaminant. In fact, the only environmental condition where measured electrode potentials have been related quantitatively to concentrations of redox-active species is in relatively simple systems dominated by relatively high concentrations of dissolved iron [*6-9*]. Inorganic oxidants, such as $O_2$ and $H_2O_2$, tend to have small exchange current densities, so their presence is not reliably indicated by electrode potential determinations [*10*].

A related problem with characterization of redox conditions of environmental materials is the lack of equilibrium among the chemical constituents of an environmental system [*11-14*] or between the environmental constituents and a sensor material [*15*]. This is especially true for the use of $H_2$ as an indicator of redox conditions [*16-18*] because redox reactions involving $H_2$ are highly dependent on catalysis to overcome kinetic limitations. Thus, while groundwater concentrations of $H_2$ may correlate with the dominant terminal electron-accepting process (TEAP) under some conditions [*19-21*], they are not expected to be in equilibrium with in situ redox active species generally. The same limitations apply to the use of other TEAP indicators (changes in concentrations of nitrate, ammonia, sulfate, sulfide, etc.) to characterize the potential for contaminant degradation by redox processes.

Natural oxidant demand (NOD) and natural reductant demand (NRD)[1] can have significant impacts on the efficacy of remediation system. They can significantly impact the delivery of oxidants and reductants, as well as the lifetime of those chemicals within the

[1] The concept of natural reductant demand (NRD) is new and not yet familiar to most practitioners. However, we expect that NRD will soon acquire a similar significant to practitioners of ISCR that NOD play in ISCO.

treatment zone. The implication of this is that both kinetic and capacity aspects of NOD and NRD are important. Conventional measurements typically involve laboratory measurements where the NOD/NRD is completely satisfied using an excess of oxidant or reductant and the demand is back-calculated based on the mass of unused chemical. An additional complication regarding current NOD/NRD assessment methods is that they utilize core samples that can be significantly altered as the result of handling (especially if they come from highly reduced aquifers). In situ testing of aquifer NOD has been reported [*22*], however the design of their test provided only total NOD information but no kinetics data. To our knowledge, there were no analogous measurements of in situ NRD. As a result, developing improved tools in this area was a goal of this project.

## 9.2. Alternative Approaches to Redox Assessment

To overcome the limitations of conventional redox assessment methods, chemical probe reactions offer the widest range of options. This approach is not entirely new, and a few prior studies have explicitly articulated the approach and its potential benefits to characterization of redox conditions in environmental media [*23, 24*]. A few other studies have employed chemical probes at the field scale as "reactive tracers" [*25, 26*], but the variety of redox processes targeted in these studies is narrow. Most evidence that chemical probes can be useful for characterization of redox conditions is from studies that are batch-scale only and make no effort to test field-scale conditions. The relative lack of development of this area means that there are not yet standard, or even widely adopted, chemical probes for characterizing in situ redox processes. Therefore, Task 1 of this project was to (re)assess prospective chemical probes and select those that have the greatest potential.

In order to assess the whole range of issues that contribute to the assessment/optimization of in situ remediation by redox processes, three general types of chemical probes need to be considered [*27*]: (*i*) "thermodynamic" probes that capture the redox potential of the medium for reaction with contaminants, (*ii*) "kinetic" probes that characterize the rate of contaminant degradation by redox processes, and (*iii*) "capacity" probes that represent the buffer capacity of the system with respect to changes in redox conditions. These three probe types correspond to the three fundamental, chemical criteria that need to be met for a successful remediation technology. That is, the remedy needs to provide a degradation process that is thermodynamically favorable, kinetically fast, and with sufficient capacity to sufficiently decrease the mass of contaminant. There is some overlap—both conceptually and operationally—between these three probe/criteria, as illustrated by the Venn diagram in Figure 1.

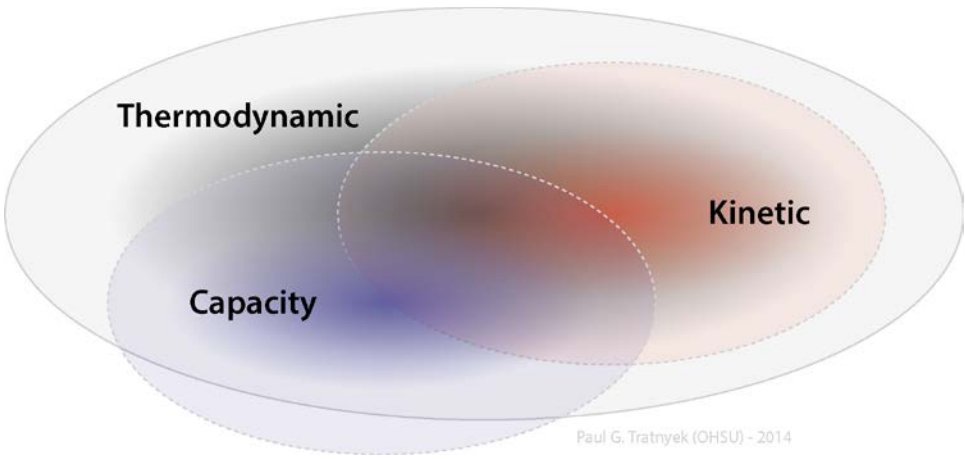


Figure 1. Conceptual representation of the relationship between measures of contaminant degradation.

*Thermodynamic* probes will determine which contaminants can be degraded by redox processes under the conditions of any particular site and treatment scenario. We proposed to overcome the main problems with traditional electrode measurements (i.e., ORP) by using chemical probes that rapidly and reversibly react with the species involved in redox-based contaminant degradation reactions. For example, while an ORP electrode does not give uniform response to all the relevant species involving iron [*5*, *7*], these species equilibrate rapidly with quinones [*28*], and speciation of these compounds is easy to determine colorimetrically [*29*, *30*]. By judicious selection of the chemical probe to match the target redox process (Figure 2), more or less selectivity for specific redox treatment agents can be designed into the assessment protocol.

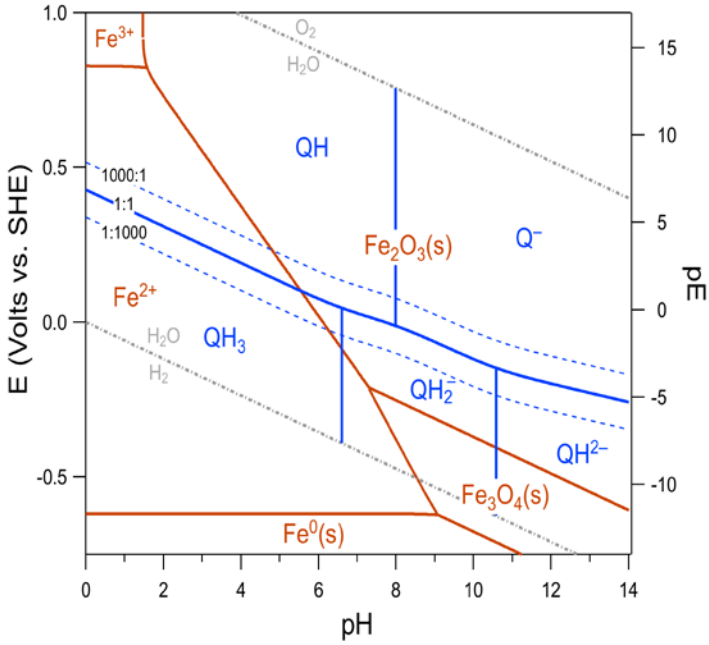


Figure 2. Eh-pH diagram from (31), illustrating equilibrium speciation of a labile chemical probe (Q for quinone) vs. the (less labile) iron system. Iron associated with minerals and quinones—which are associated with natural organic matter (NOM)—can contribution to the abiotic natural attention of groundwater contaminants like TCE.

*Kinetic probes* were selected to characterize rate-limited contaminant remediation processes, including both the degradation of the contaminant and the distribution among possible products. Using the contaminant, itself, for this purpose is obvious, yet but often not promising for several reasons: (*i*) any in situ test would be confounded by uncertainties in the distribution of preexisting contaminant by the concentration of the contaminant and its degradation products, (*ii*) the rate of many contaminant

degradation reactions is typically too slow to be observed in short-term tests, and (*iii*) any injection of the hazardous substance is likely to be restricted.

To overcome these obstacles, a variety of contaminant analogues have been used as kinetic probes for in situ applications. The two most relevant examples are trichlorofluoroethene (TCFE), which was used as a surrogate for TCE [*25*] and a suite of substituted nitro aromatic compounds (NACs), which can be considered as either analogs for explosive compounds like trinitrotoluene (TNT) or as a relatively non-specific and labile probes for reducing conditions generally [*32*]. The former was deployed using a push-pull test and the latter using in situ microcosm. However, there are limitations to the applicability of the probes to meeting the goals of this project. For example, the kinetics of TCFE reduction may be too slow, and the reduction of NACs may be too non-specific.

There are a variety of approaches that should provide kinetic probes that are better suited to application with in situ diagnostic tests (e.g., push-pull tests). One prospect would be to use brominated analogs to the chlorinated solvents. These dehalogenate more rapidly, but still show the branching between hydrogenolysis and reductive elimination pathways that is a key concern for chlorinated solvents. Some of the background necessary for this has already been reported [*33*], but such probes have not been applied under field conditions. An even more innovative prospect might employ brominated analogs to the chloroacetophenone-type probes introduced below. A limited amount of preliminary data is available on these as chemical probes in reducing sediments [*34*], but they have not been applied to groundwater systems.

*Capacity probes* are the third type of probe we proposed to develop, mainly for the purpose of characterizing NOD/NRD. In most cases, these probes will be the oxidant or reductant that is experiencing the NOD/NRD, however it could also be the products of those reactions (e.g., sulfate from persulfate). In current practice, NOD is almost always measured ex situ—using samples from site removed to the laboratory—even though in situ measurement would have at least two important advantages: (*i*) minimizing changes resulting from sample collection, handling, and preparation; and (*ii*) providing the opportunity to repeat measurements at the same location at multiple stages of the remediation process. Thus, the ability to measure NOD/NRD in situ using a *capacity* probe has several potential benefits. (Figure 3)

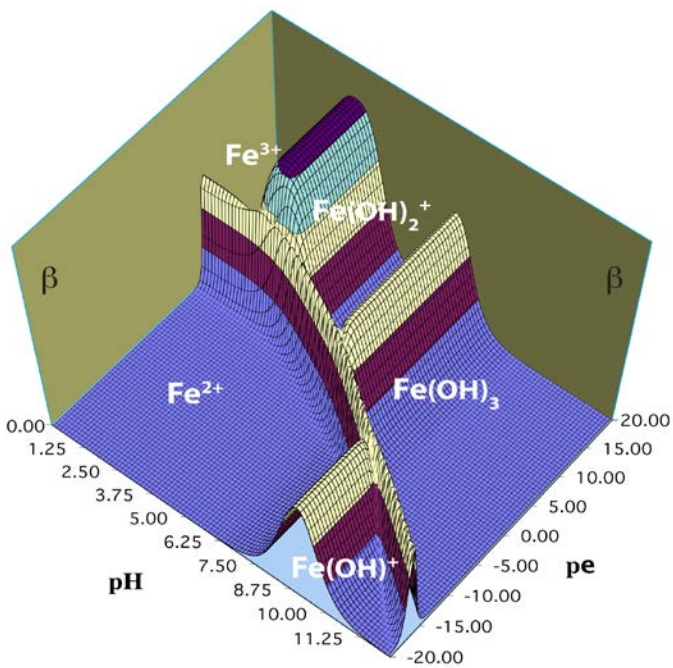


Figure 3. Redox buffering capacity diagram for iron from (35), showing maximum buffering capacity (β) at the stability field boundaries.

## 9.3. Field Deployment of Chemical Probes with Push-Pull Tests

To allow easy and rapid utilization of these chemical probes, they might be combined in protocols based on conventional "push-pull" tests. Because they are rapidly deployable and flexible, push-pull tests can range from simple single-injection/single-extraction tests to more complex tests involving a series of injections, each followed by multiple extractions. As a result, one of the beauties of this general approach is that the details of each test can be easily adjusted to meet specific needs. For example, a simple single injection/single-extraction test can be used to assess chemical state of a system using a thermodynamic probe.

Alternately, full assessment of the impact of oxidant/reductant injection can be accomplished using a sequence of injection/multiple extraction tests and a "cocktail" of probes. A conceptual representation of the latter is seen in Figure 4. The lower panel represents the repeat injection/multiple-extraction process while the data derived from such a test is shown conceptually in the upper panel. Briefly, following injection of a suite of chemicals (including chemical probes and conservative tracers), multiple small extractions can be used to observe changes in chemical state of the system as well as consumption of the capacity probe. As is observed in traditional laboratory redox titrations, repeated addition of titrant (in the current context, the capacity probe) will cause the consumption rate to slow or stop altogether, and allows the capacity (e.g., NOD, NRD) to be measured. In addition, if properly designed, these tests could provide contaminant degradation rate information over the range of conditions created during the redox manipulation process.

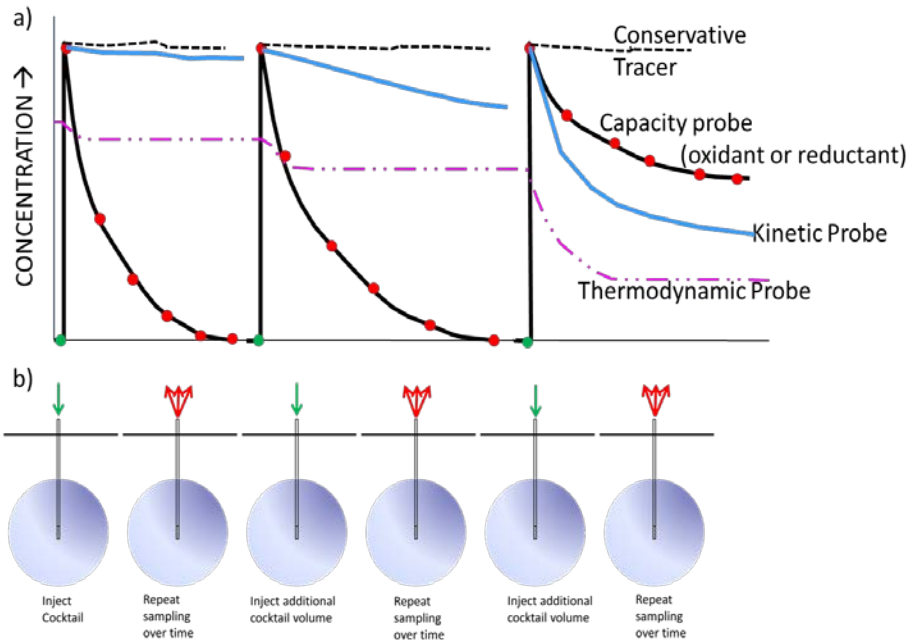


Figure 4. Schematic representation of a sequence of three push-pull tests consisting of single injections followed by multiple extractions. A cocktail of chemicals (thermodynamic, kinetic, and capacity probes plus a conservative tracer) could allow the effects of redox manipulation to be quantitatively assessed.

# 10. RESULTS AND DISCUSSION

The main results of this project are presented in three sections that correspond to the four major objectives of the proposal. Some of the sections is derived from one or more peer-reviewed publications, which are specified at the beginning of each section.

## 10.1. Objective 1—Conceptual Development of Probes

The main objective of this task was to systematically evaluate prospective chemical probes for flexible and reliable characterization of environmental redox processes.

A range of examples of candidates for which there is enough prior work to make a preliminary evaluation of their prospects are summarized in Table 1. In some cases, the assignment of probes between thermodynamic vs. kinetic categories depends on operational circumstances, and we are working on taking advantage of this flexibility as we refine our probe-based protocols.

**Table 1. Examples of chemical probes for in situ redox processes.**

| Probe Class, Family, Examples | Selection Criteria | References |
|---|---|---|
| **Thermodynamic Probes** | | |
| $Fe^{II}/Fe^{III}$ complexes with organic ligands: e.g., iron-tiron | Functional selectivity is potentially broad, and technical feasibility is potentially very good, but practicality is untested. | [*36, 37*] |
| Tetrazoliums<br>e.g., INT, XTT, MTS | Functional selectivity is potentially broad, and technical feasibility is promising. Practicality is likely limited. | [*38-40*] |
| Oxazines<br>e.g., Resazurin/Resorufin | Functional selectivity is mixed. Technical feasibility is promising. Practicality is promising. | [*29, 30, 41*] |
| **Kinetic Probes** | | |
| Labeled chlorinated solvents<br>e.g. TCFE | Functional selectivity is well-defined. Technical feasibility is proven. Practicality is promising. | [*25, 42-44*] |
| Substituted Nitro Aromatic Compounds (NACs)<br>e.g., 4-Nitrobenzene | Functional selectivity is broad. Technical feasibility is promising. Practicality uncertain. | [*32, 45*] |
| (Chlorinated) Acetophenones<br>e.g., 2-CAP | Functional selectivity is well-defined. Technical feasibility is proven. Practicality is uncertain. | [*23, 34, 46*] |
| **Capacity Probes** | | |
| Selective ISCO Oxidants<br>e.g., Permanganate | Functional selectivity is well-defined. Technical feasibility is proven. Practicality is promising. | [*22, 47-49*] |
| Non-selective ISCO Oxidants<br>e.g., Persulfate, Peroxide | Functional selectivity is very broad. Technical feasibility is promising, and practicality is proven. | [*50-52*] |
| ISCR Reductants<br>e.g., Dithionite | Functional selectivity is very broad. Technical feasibility is promising, and practicality is proven. | [*53, 54*] |

The selection criteria used include: (i) functional selectivity, (ii) technical feasibility, and (iii) practicality. The first of these criteria is the most fundamental. Basically, an indicator will have appropriate "functional selectivity" if it can be used to measure properties of aquifer media that correlate with contaminant degradation rates in a manner such as illustrated in Figure 5 below. This figure is hypothetical, but represents a conceptual model for the probe-based assays might be used.

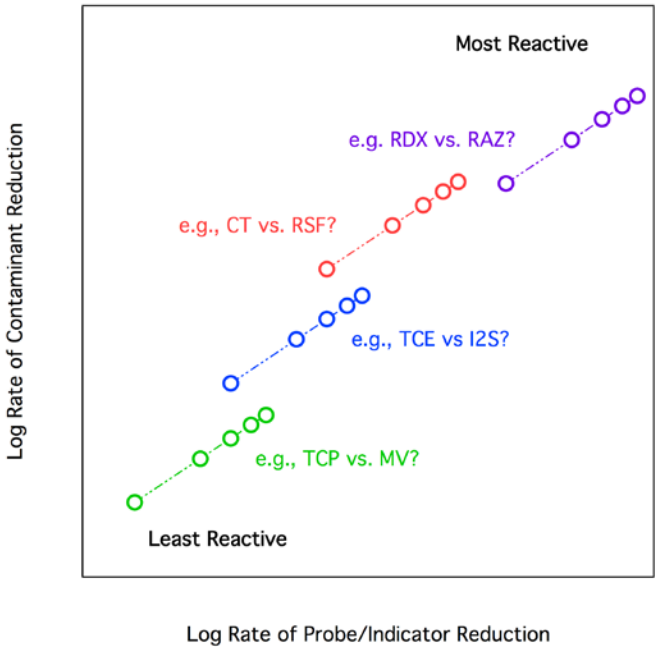


Figure 5. Conceptual representation of the relationship between measures of contaminant degradation (in this case rate) and measures of the conditions of reducing materials (shown also as a rate). RAZ, RSF, I2S, and MV are all possible probes. The question marks are to reinforce that the pairings of contaminant and probe shown were hypothetical when this plot was developed.

### 10.1.1. Model System Selection

In order to begin testing our probe selections, we needed a simple and well-characterized model system for reducing/aquifer materials. Iron and sulfur bearing mineral phases are the leading candidates because (*i*) they are extensively studied and characterized, and (*ii*) their roles in mediating and sustaining abiotic reductive dechlorination during in-situ bioremediation or long-term MNA attract increasing interests in remediation field. A large body of research has demonstrated a wide range of reactivity for most of the Fe(II)- or sulfide- containing mineral phases with chlorinated compounds at laboratory scale. Much of this data was compiled by He et al. [*55*].

We have extended He et al.'s analysis to by plotting the data for $k_{SA}$ vs. $k_M$ in Figure 6. The figure includes only tetra- and tri-chloroethene and carbon tetrachloride (CT), because these are the only three contaminants of strong relevance to the project and for which sufficient data are also available. The compiled batch kinetic data suggests that CT is generally reduced at much faster rates than chloroethenes in Fe(II)-Fe(III) oxide systems. The relatively slow reduction of TCE in these systems makes it difficult to do laboratory studies to evaluate the roles of these mineral phases in long-term abiotic natural attenuation process of TCE.

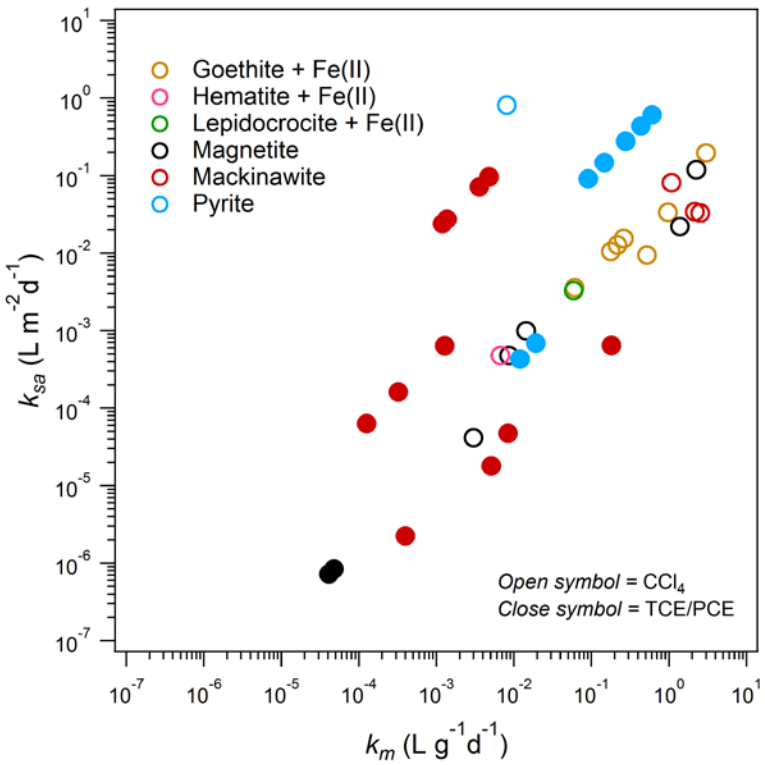


Figure 6. Surface normalized reaction rate constants ($k_{sa}$) vs. mass normalized reaction rate constants ($k_m$) for abiotic reduction of CT and TCE/PCE by a variety of reduced iron and sulfur minerals, measured in laboratory batch experiments. (Based on a compilation of data from previously published work summarized in [*55*]).

Besides providing insight into the relative reactivity of TCE/PCE vs. CT, the main purpose of **Figure 2** is to expose variations in reduction rates of these contaminants by different reducing mineral phases. Our goal is to be able to explain this variability by correlating with probe reaction response (e.g., as illustrated in **Figure 1**).

### 10.1.2. Conceptual Development of Thermodynamic Probes

While we have, and continue to, survey the full range of candidate redox probe compounds, currently we are focusing on two putative thermodynamic probes. One involves Resorufin (Rsf), which forms the redox couple shown in Figure 7A: i.e., reversible transformation to dihydroresorufin (in the absence of $O_2$). The process can be easily monitored by absorbance spectroscopy because resorufin has strong UV-vis absorbance (and fluorescence). Resorufin is safe and available, mobile, and very labile to redox reactions. We believe that it is reduced mainly by electron transfer mechanisms.

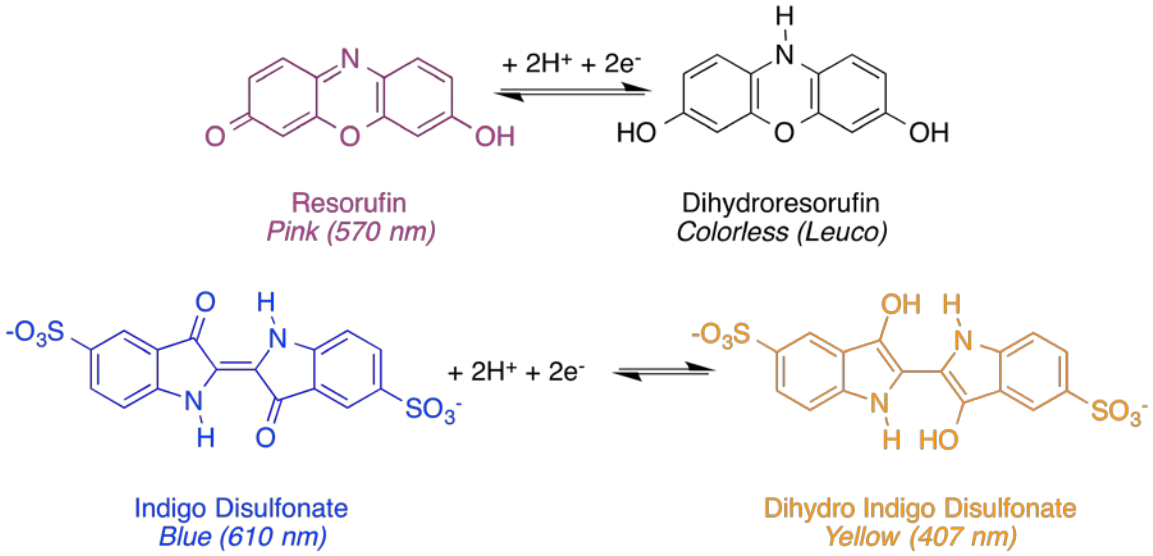


Figure 7. Redox couples for the two probes we are currently focusing on. Colors represent approximate color of the species. Properties are summarized in Table 2.

The other thermodynamic indicator we are pursuing currently is based on indigo disulfate (I2S). The oxidized form of this compound is blue, which turns yellow upon reduction. Intermediate mixtures of oxidized and reduced forms are conspicuously green. The redox couple for this indicator is shown above in Figure 7B. Very recently, we have also started testing the other two probes listed in Table 2: AQDS and AQS, which belong to anthraquinone group and have been extensively studied as electron shuttles. The more negative redox potentials of the latter two probes should make them useful as probes of strongly reducing conditions (such as are required for abiotic reduction of TCE).

Table 2. Selected thermodynamic probes

| Probe | Abbrev | $E_m^7$ (V) | $\lambda_{max}$ Ox (nm) | $\lambda_{max}$ Red (nm) |
|---|---|---|---|---|
| Resorufin | Rsf | -0.051 | 571 | Leuco |
| 5,5'-indigodisulfonate | I2S | -0.125 | 610 | 407 |
| 9,10-anthraquinone-2,6-disulfonate | AQDS | -0.184 | 326 | 386 |
| 9,10-anthraquinone-2-sulfonate | AQS | -0.225 | 326 | 403 |

Preliminary results obtained with batch tests using the Rsf and I2S probe in model systems composed of the various iron oxides with Fe(II)/oxide are shown in Figure 8 and Figure 9. The data show that while homogeneous 1.5 mM aqueous solutions of Fe(II) reduced Rsf completely to its colorless form, there was little reduction of I2S (Figure 8A). This is consistent with the reduction potentials of the probes relative to the $Fe^{3+}/Fe^{2+}$ couple. In heterogeneous Fe(II)-oxide systems, 0.5 mM Fe(II)-Goethite suspension reduced I2S rapidly, which indicates that a much stronger effective reductant is created by adsorbed Fe(II).

In contrast, ORP measured with a conventional Pt electrode gave a more negative value for homogeneous, 1.5 mM aqueous Fe(II) than heterogeneous 0.5 mM Fe(II) in a goethite suspension. The inconsistency between the ORP measurement and the probes assay results is most likely due to inaccuracy in the former, whereas the soluble redox indicator is able to interact with the reducing sites in the heterogeneous system (surface bound Fe(II)). Together with the insensitivity of I2S to aqueous Fe(II) suggests that it may be selective for heterogeneous Fe(II). Meanwhile, Rsf may serve as a more general redox probe to indicate mildly reducing conditions.

To verify the utility of the response of these probes, we have plotted the oxidation-reduction potential measured with a conventional Pt electrode versus the ratio of oxidized and reduced forms of the probe speciation (determined spectrophotometerically) in Figure 8B. This figure shows that Eh based on ORP measurement (symbols) generally were more positive than the calculated values based on I2S speciation (represented by the dashed line). In addition, Eh values obtained from the Pt electrode were not very reproducible. The deviation from the theoretical values and irreproducibility of ORP measurement might be due to the insensitivity of ORP electrode to the Fe(II) associated with the iron oxides, which should dominate this system.

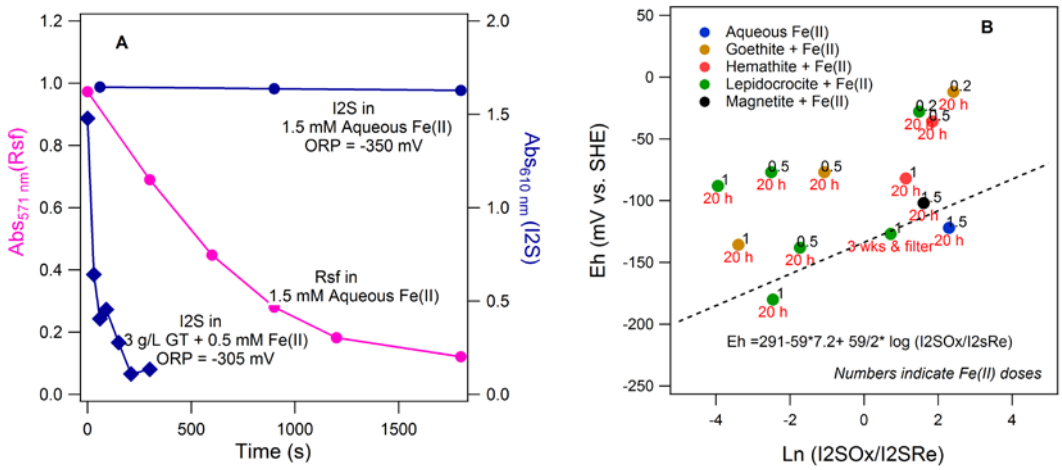


Figure 8. (A) Resorufin (left axis) and I2S (right axis) reduction in homogeneous Fe(II) solution and heterogeneous Fe(II)-mineral heterogeneous suspension; (B) Eh in Fe(II)-mineral suspensions vs. the ratio between oxidized and reduced I2S. Eh value was based on ORP measurement (vs. Ag/AgCl) performed after 20-h Fe(II) adsorption period. The absorbance was measured 1-hr after probe addition to Fe(II)-mineral suspensions.

Rsf and I2S were further tested in batches with aquifer materials for their potential applicability in field. Aquifer materials were extracted from a pilot-scale artificial porous media that has been previously used for studying bioremediation of toluene (in the “LEAP Tank” facility). The probes also showed good responses to different reductant amendments (Figure 9). For the I2S case, as reductant strength increased from Fe(II) to ZVI, the degree or probe reduction also increased.

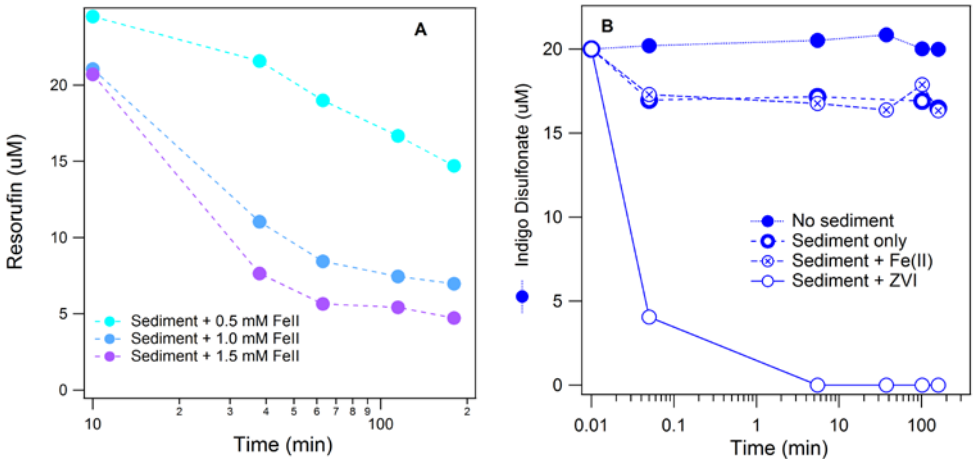


Figure 9. Reduction of Resofurin (left) and I2S (right) in the presence of aquifer materials and various reductants. Note that the time scale needed for these data with natural materials is significantly longer than for the model system results (Figure 8), presumably due to greater quantity of available oxide surface area in the latter.

Interpretation of the dyes as thermodynamic probes assumes the reversible reactions shown in Figure 7. In this context, interpretation of the probe requires that the reactions be at equilibrium. The data in Figure 9 suggest that equilibrium is achieved in a few minutes for I2S and a few hours for Rsf. Both of these time frames are well within the design parameters for field deployment in push pull tests. Furthermore, since the Eh intervals for the two dyes are different from one another (e.g., Rsf is largely reduced by Fe(II) while I2S is only partially reduced), they are complimentary to one another and together should provide a broader useful redox range for characterization of subsurface environments.

The data obtained to date on thermodynamic probes suggests that deployment of these probes in push-pull modes in field will be particularly advantageous when reactive solid phases are the primary reductants of interests. These scenarios include time periods following in situ redox manipulation and bioremediation, where formation of secondary reactive minerals is expected to sustain contaminant removal, and long-term natural attenuation, where indigenous reactive mineral phases play significant roles in dechlorination. In such cases, characterization of solid phase reactivity based on conventional (solution phase) ORP measurement performed in extracted groundwater samples is unlikely to be useful.

### 10.1.3. Conceptual development of Kinetic Probes

For kinetic probes, so far we have been using surrogate contaminants or model contaminants. One example of this is 2-chhloroacetophenone (2-CAP), which can be reduced by direct electron transfer to acetophenone or hydride transfer to 2-chlorophenylethanol (2-CPE) [*23*]. The latter pathway is mediated by hydride, which is specific to microbial processes [*56*]. We have tested this probe in batch experiments with materials extracted from different redox zones of an artificial porous media and are currently undergoing investigation in a series of incubations amended with different reducing agents. We are currently refining these batch experiments to determine the kinetics and pathways of reaction of this family of compounds in reducing media. (Data not shown).

Besides 2-CAP, the model contaminant we have been emphasizing so far in the kinetic probe studies is carbon tetrachloride (CT). Representative data in Figure 10.

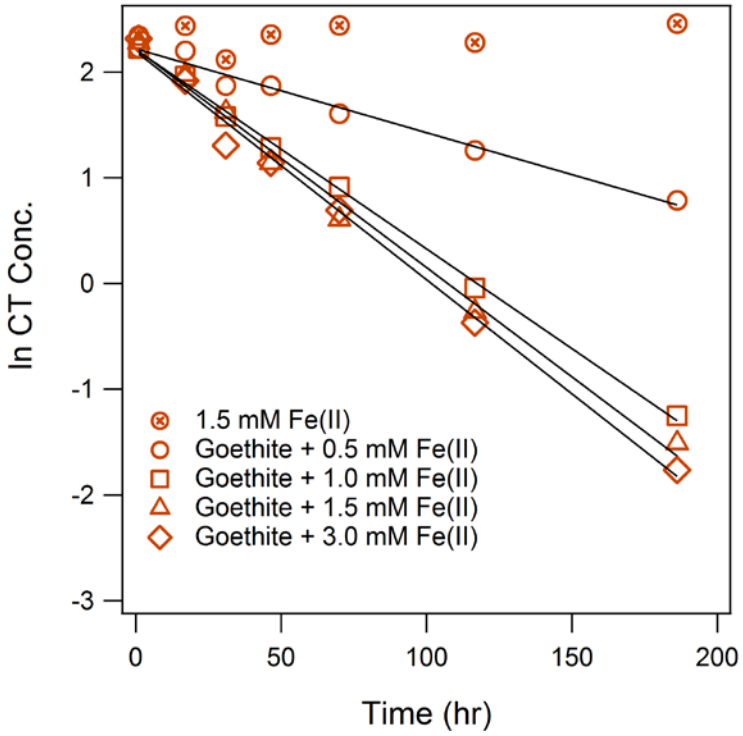


Figure 10. Pseudo-first order reduction kinetics of carbon tetrachloride by goethite + various amount of Fe(II).

The data in Figure 10 show that the reduction of carbon tetrachloride ($CCl_4$) by Fe(II)-Goethite suspensions follows pseudo-first order kinetics. In the aqueous Fe(II) only control, no appreciable $CCl_4$ reduction was observed. The pattern is consistent with the observation that aqueous Fe(II) alone did not reduce I2S. The higher Fe(II) dose (1 mM) was notably more yellow than the low Fe(II) dose (0.5 mM), which is consistent with higher $CCl_4$ reduction rate constant with 1 mM Fe(II) than 0.5 mM Fe (II).

The utility of using a model contaminant such as CT is that they can be chosen to have reaction rates may be fast enough to observe in field-scale push-pull tests, whereas contaminants like TCE react too slowly to be measured within the time frame of any sort of controlled experiment. The data in Figure 10 suggest that $CCl_4$ may react quickly enough to be useful in this context. Alternatively, or in addition, a probe like 2-CAP may be useful because it is reduced at rates comparable to CT, but mainly by different reductants. It may also be possible to use both together in a manner that broadens the reaction rate range for which the kinetic probes are applicable.

### 10.1.4. Conceptual development of Capacity Probes

We have only done preliminary testing of the capacity probe protocol that we anticipate using in later tasks. This is because the capacity probe protocol will be based on relatively conventional procedures used to characterize chemical reductant or oxidant demand (NRD and

NOD). An example of this type of data obtained from batch tests is given in Figure 11. One aspect of Objective 3 of this project was to explore the use of CRPs in push-pull tests.

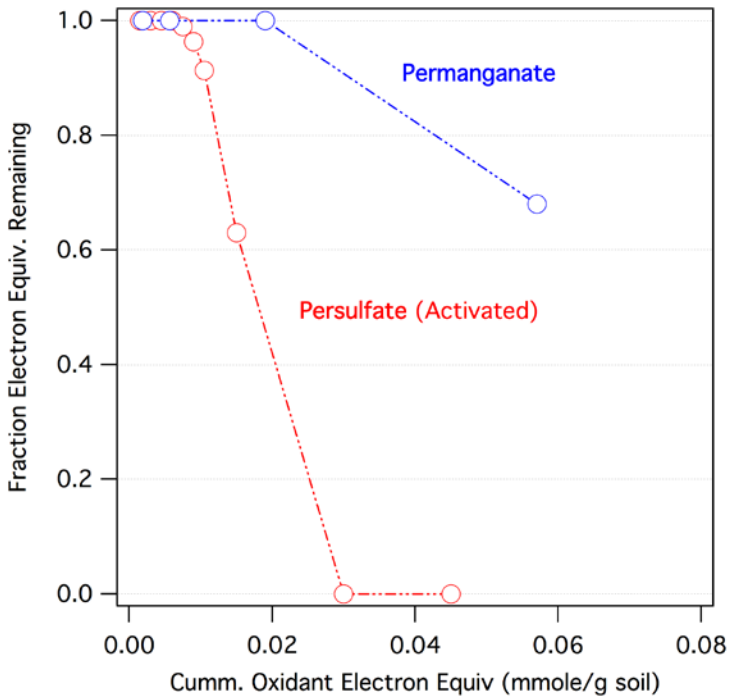


Figure 11. Preliminary data illustrating results obtained by titrating model aquifer sediment with two types of chemical oxidants. The experimental protocol for this is straight-forward, but the conceptual basis of generalizing the results (i.e., format of the figure) was an area of study.

## 10.2. Objective 2(A)—Bench Scale Testing of Probes

The major results of Objective 2 were published as Fan et al. 2016, the content of which is summarized in this section of the report.

Fan, D., M. Bradley, A. W. Hinkle, R. L. Johnson, and P. G. Tratnyek. 2016. **Chemical reactivity probes for assessing abiotic natural attenuation by reducing iron minerals**. *Environ. Sci. Technol.* 50(4): 1868-1876. [DOI: 10.1021/acs.est.5b05800].

**Abstract**: Increasing recognition that abiotic natural attenuation (NA) of chlorinated solvents can be important has created demand for improved methods to characterize the redox properties of the aquifer materials that are responsible for abiotic NA. This study explores one promising approach: using chemical reactivity probes (CRPs) to characterize the thermodynamic and kinetic aspects of contaminant reduction by reducing iron minerals. Assays of thermodynamic CRPs were developed to determine the reduction potentials ($E_{CRP}$) of suspended minerals by spectrophotometric determination of equilibrium CRP speciation and calculations using the Nernst equation. $E_{CRP}$ varied as expected with mineral type, mineral loading, and Fe(II) concentration. Comparison of $E_{CRP}$ with reduction potentials measured potentiometrically using a Pt electrode ($E_{Pt}$) showed that $E_{Pt}$ was 100–150 mV more negative than $E_{Pt}$. When $E_{Pt}$ was measured with small additions of CRPs, the systematic difference between $E_{Pt}$ and $E_{CRP}$ was eliminated, suggesting that these CRPs are effective mediators of electron transfer between

mineral and electrode surfaces. Model contaminants (4-chloronitrobenzene, 2-chloroacetophenone, and carbon tetrachloride) were used as kinetic CRPs. The reduction rate constants of kinetic CRPs correlated well with the $E_{CRP}$ for mineral suspensions. Using the rate constants compiled from literature for contaminants and relative mineral reduction potentials based on $E_{CRP}$ measurements, qualitatively consistent trends were obtained, suggesting that CRP-based assays may be useful for estimating abiotic NA rates of contaminants in groundwater.

## 10.2.1. Introduction

Abiotic reduction of contaminants by naturally-occurring reducing iron minerals (including iron oxides and sulfides) is an important component of natural attenuation (NA) [*55, 57-59*]. The abiotic reduction of chlorinated ethenes (e.g., trichloroethene, TCE) is of particular interest, and has been described in many laboratory studies using reducing iron minerals prepared by chemical synthesis [*60-63*], or in-situ precipitation [*64-66*], and aquifer materials obtained from contaminated field sites [*67-69*] However, the rates of these reactions are usually slow, making it impractical to assess in-situ rates of abiotic NA.

In contrast, much faster reaction rates with reducing minerals can be obtained with (model) contaminants, such as nitroaromatic compounds (NACs) or polyhalogenated alkanes (PHAs) [*32, 70-73*]. In principle, easily reducible model contaminants could serve as chemical probes to characterize the reactivity of reducing aquifer materials with more recalcitrant contaminants if the two groups of compounds share similar reactivity patterns [*74, 75*]. Using hexachloroethane (HCA) and 4-chloronitrobenzene (4Cl-NB) as probe compounds, Elsner et al. [*74*] showed qualitatively similar trends in the reduction rates of these two compounds by a range of ferrous-iron containing minerals, even though the two probe compounds are reduced by different mechanisms and the absolute rates differ by almost 3 to 4 orders of magnitude. Rates of HCA reduction have further been shown (qualitatively) to parallel literature data for TCE reduction by magnetite [*60*], green rust [*61*], and iron sulfides [*60*], suggesting that HCA and other surrogate chemical probes might help to predict relative rates of chloroethene reduction in abiotic NA.

The fundamental validity and practical reliability of using model contaminants as probes to predict rates of abiotic NA requires identifying mineral properties that determine the rates of probe/contaminant reduction. This is, however, challenging because of the profound and complex effects on mineral redox chemistry that arise from the diversity of reducing iron minerals, including surface Fe(II), structural Fe(II), and FeS. For Fe(II) sorbed onto iron oxides, a number of studies have suggested that the mineral reactivity correlates with the density of the sorbed Fe(II) [*70, 74*]. However, the interpretation of $Fe(II)_{ads}$ data estimated with traditional extraction methods is complicated by the finding of electron transfer from adsorbed Fe(II) into the bulk materials and that aqueous Fe(II) appears to be necessary for maintaining mineral reactivity [*76, 77*]. For mixed valent iron oxides, such as magnetite or green rust, the ratio of Fe(II) to Fe(III) has also been shown to affect the reduction kinetics of contaminants [*64, 78*].

In homogeneous systems with aqueous Fe(II)-ligand complexes as the reductants, the one electron reduction potential of the reducing species has been shown to give a linear free energy relationship (LFER) with the reduction rate constants for oxyamyl, a carbamate pesticide [*79*]. LFERs structured in this way—one contaminant vs. many environmental reactants—are

uncommon, compared with LFERs for many contaminants vs. one environmental reactant (e.g., NACs vs. Fe(II)porpyrin [*80*]), but the two approaches are complementary and combining them has potential value for diagnostic and predictive purposes. Although it is more difficult to obtain the analogous LFERs for heterogeneous reductants, such as Fe(II) minerals, the mineral redox potential is still the most likely descriptor variable in such relationships because it dictates the thermodynamic driving force of these reactions with contaminants [*31*].

The major impediment to development of LFERs for reactions with reducing minerals is the difficulty in obtaining reliable mineral redox potentials under environmental conditions. Conventional electrode potential measurements of oxidation-reduction potential (ORP) are easily performed on mineral suspensions, but these are mixed potentials and are highly sensitive to factors such as mass transport, aggregation, and secondary redox-active species [*5, 81, 82*]. The "formal" reduction potentials for iron oxide/Fe(II) couples that appear in some literature [*83*] are based on calculations using thermodynamic data from calorimetry, and therefore may not be representative of the mineral phases present in heterogeneous environmental media (aquifers, sediments, and soils). Mineral reduction potentials of Fe(II) sorbed to iron oxides have also been estimated with LFERs developed for aqueous Fe(II)-ligand complexes, but the calculated potentials vary substantially with the contaminants used in the training data set for LFER development [*84*].

Recent efforts to measure the reduction potentials of iron minerals have employed redox-mediator or "shuttle" compounds to provide an intermediate redox couple that rapidly and reversibly equilibrates between redox active minerals and the surface of a working electrode [*85*]. Alternatively, if the speciation of the mediator can be determined spectrophotometrically (provided negligible sorption of the mediator to mineral surfaces), these data can be used in the Nernst equation to calculate redox potentials of the medium [*72, 86*]. Various redox indicators have been used to characterize the redox processes of biogeochemical systems, including iron oxides [*87-89*], soil suspensions [*90*], and anaerobic sediment [*29, 30*]. However, the power of this approach for quantification of specific mineral redox properties (potentials, kinetics, and capacities) has not been systematically developed.

In this study, spectrophotometric measurement of redox indicator speciation was used to characterize the redox properties of a range of reducing iron minerals containing Fe(II). The calculated mineral redox potentials were compared with those obtained by potentiometry, and used as a descriptor variable in correlation analysis with kinetic data for the reduction of (model) contaminants by the minerals. Based on their functions, the redox indicators and model contaminants are referred to as the thermodynamic and kinetic chemical reactivity probes (CRPs), respectively. The broader implications of these results for contaminant fate and remediation are explored by extending the correlation analysis to include literature data for a wider range of contaminants, reducing iron minerals, and conditions. The results provide a semi-quantitative framework for understanding the relative reactivity of important contaminants with common minerals.

## 10.2.2. Experimental

**Materials and Common Methods.** All chemical regents were ACS reagent grade and used as received without further purification. Resorufin (RSF) was acquired from Sigma Aldrich as sodium salt with 98% purity. Indigo-5,5'-disulfonate (I2S) and 9,10-anthraquinone-2-sulfonate

(AQS) were purchased from TCI America (Portland, OR), as disodium salts with greater than 95% purity. 9,10-anthraquinone-2,6-disulfonate (AQDS) was purchased as disodium salt with 98% purity (Combi-Blocks, San Diego, CA). Anaerobic conditions were maintained for all operations involving Fe(II) and CRPs inside an anaerobic chamber (100% $N_2$, $O_2$ < 1 ppm), unless otherwise mentioned.

**Preparation of Mineral Suspensions.** Goethite (GT), hematite (HT), and lepidocrocite (LP) were acquired from Bayferrox (Burgettstown, PA). These materials have been used in many prior studies of redox reactions involving iron oxide [*74, 82, 91-93*]. A detailed analysis of the specific surface area of these samples is provided as Supporting Information (Table 3). Magnetite (MT) and green rust chloride (GR-Cl) were synthesized by co-precipitation methods adapted or modified from prior studies [*72, 94*]. To prepare Fe(II) sorbed onto the three commercial iron oxides and synthetic magnetite, various quantities of Fe(II) stock solution (~100 mM) were added to the anoxic mineral suspensions with pH adjusted to 7.2 (or as noted) by 10 mM HEPES. The suspensions were transferred to amber bottles, which were then crimp sealed and placed on an end-over-end rotator for equilibration (~20 h). Additional details on the synthesis and preparation of suspensions of the iron oxides are described below, in a section of supporting information.

**CRP Assay for Mineral Reduction Potential.** The thermodynamic CRPs were selected to (*i*) encompass the range of relevant redox potentials and (*ii*) be compatible with subsurface solid matrix (so that they can eventually be applied to characterize natural porous media). The latter criterion excluded a group of common redox indicators that are positively charged, because they tend to sorb strongly to negatively charged aquifer and sediment solids [*30*]. The four redox indicators selected are RSF, I2S, AQDS, and AQS. All probes except RSF are negatively charged due to one or more sulfonate groups, while RSF is neutral but relatively hydrophobic (e.g., log $P$ = 1.77 predicted by chemicalize.org). The standard reduction potentials of these CRPs at pH 7 range from −46 mV to −229 mV (Table 4). Other properties of the CRPs, such as maximum absorption wavelength, molar absorptivity, and $pK_a$ are also given in Table 4.

The reactions of the CRPs with the mineral suspensions were evaluated vs. mineral loading and dose of added Fe(II). For each combination of CRP and mineral, the reaction was carried out in a 10-mL amber serum vial to avoid photo reactions involving the CRP or aqueous Fe(II). Aliquots of deoxygenated CRP stock solutions (~1 mM) were added to 5 mL mineral suspensions, giving an initial concentration of ~20 µM for RSF and I2S and ~90 µM for AQDS and AQS. The reaction vial was crimp sealed with a 20 mm Viton septum (Sigma Aldrich) and placed on an end-over-end rotator overnight to reach equilibrium (45 rpm). Sample aliquots of 5 mL were then filtered by 0.2 µm nylon filters (Fisher). The first mL of filtrate was discarded and the rest was collected in a glass (for RSF and I2S) or quartz (for AQS and AQDS) cuvette (1 cm path length), which was then sealed by screw cap with a 4 mm Viton lining. The sealed cuvette was removed from the anaerobic chamber and the absorbance spectra of the reduced CRPs were immediately measured with a UV-vis spectrophotometer. The reduced CRP was then reoxidized by briefly exposing to ambient air, which served to determine how much of the CRP was adsorbed to the solids.

**Potentiometric Measurements.** Open circuit potential (OCP) measurements were performed following the protocol developed in our previous study with suspensions of nano zerovalent iron (nZVI) [*5*]. A two-electrode system was used with a 3 mm Pt rotating disc

electrode (RDE) as the working electrode and an Ag/AgCl electrode (3 M KCl filling) as the reference electrode. Before each set of experiments, the Pt electrode was polished with 0.05 μm alumina and sonicated to avoid electrode fouling or memory effects, which are common causes for inconsistent results with commercial ORP electrodes. The experiments were carried out in a 20-mL electrochemical cell that was purged with Ar gas for at least 10 minutes before the mineral suspension was introduced. Aliquots of the suspension were withdrawn with a 10-mL syringe, taken out of the anaerobic chamber, and immediately injected into the electrochemical cell. The Pt electrode was immersed into the suspension and rotated at 2000 rpm to maintain mixing. The OCP data was recorded using an Autolab PGSTAT30 (EcoChemie, Utrecht, The Netherlands) for 30 minutes, during which the headspace was continuously purged with Ar to maintain anoxic conditions. In selected experiments, the effects of CRPs on OCP were assessed by adding aliquots of appropriate CRPs into the cell during OCP measurement.

**Reduction of Kinetic CRPs**. Three kinetic CRPs were selected for batch experiments: carbon tetrachloride (CT), 4-chloronitrobenzene (4Cl-NB), and 2-chloroacetophenone (2-CAP). These compounds represent three classes of model organic contaminants that are relatively labile to abiotic reduction: perchlorinated alkanes [*75, 95*], nitro aromatics [*80, 96*], and α–haloketones [*23, 97*]. For CT, an aliquot of stock solution was added into a ~19 mL mineral suspension in a 20-mL serum vial to an initial concentration of ~10 μM with minimum headspace. The vial was immediately crimp sealed with a Viton septum, transferred out of the anaerobic chamber, and placed on an end-over-end rotator at 125 rpm in the dark at 23ºC. At each sampling point, 0.25 mL mineral suspension was withdrawn after injecting 0.3 mL $N_2$ into the vial using a gas-tight glass syringe. The mineral suspension was injected into a headspace vial containing 2 mL deionized water. After brief vortex mixing, the CT concentration in headspace was measured by gas chromatography with an electron capture detector.

For 4Cl-NB and 2-CAP, the reactions were carried out in 60 mL amber serum bottles, crimp sealed with Viton septa, containing an initial concentration of ~10 μM and ~50 μM, respectively. The reactors were mixed on the end-over-end rotator at 125 rpm at 23ºC. At each sampling time point, 2.5 mL aliquot was withdrawn and filtered by a 0.20 μm filter. For the combination of goethite and 4Cl-NB, the reactions were carried out in 10 mL syringes inside the anaerobic chamber due to rapid reaction. The samples were analyzed for disappearance of parent compounds by a high-performance liquid chromatography (HPLC) with a photodiode detector.

### 10.2.3. Results and Discussion

**Reduction by Fe(II) containing minerals.** Preliminary experiments showed that 1 mM aqueous Fe(II) reduced RSF completely and I2S partially, but did not reduce AQDS or AQS (data not shown). This result is consistent with aqueous Fe(II) being a weak reductant that only reduces the CRPs with relatively high redox potentials (Table 4). The same trend in CRP reduction was observed with Fe(II) in suspensions of the minerals. Using lepidocrocite and 0.5 mM Fe(II) as an example, Figure 18 shows complete reduction of RSF, significant reduction of I2S, little reduction of AQDS, and no reduction of AQS. The extent of CRP reduction was used to select appropriate CRPs for calculating mineral redox potentials (described later).

The reduction of the CRPs varied with mineral type and loading and Fe(II) concentration (Figure 12). The absorbance spectra in Figure 12A show that the degree of AQDS reduction after 20 hr of exposure to suspensions of ~50 $m^2$/L iron oxide and 1.0 mM Fe(II) ranged from no

reduction for hematite, to partial reduction for lepidocrocite and magnetite, and to complete reduction for goethite. Lowering the goethite loading from 2.2 g/L to 0.3 g/L (in Figure 12B)—with constant Fe(II) dose—decreased the extent of AQDS reduction about 10-fold. Figure 12C and Figure 12D show increasing reduction of AQS with increasing Fe(II) concentration for magnetite and goethite, respectively. The observed effects of these variables on the redox speciation of CRPs has not been reported previously (in the limited number of prior studies that used this approach), but it resembles the effects on contaminant reduction by sorbed Fe(II) that have been identified in many prior studies. These studies have shown that reduction rates of various contaminants vary with mineral type, loading, and Fe(II) concentrations [*70, 74, 84, 98*]. The similarity between this work and previous work formed the basis for our attempts to correlate the results obtained with thermodynamic and kinetic CRPs, which is discussed later.

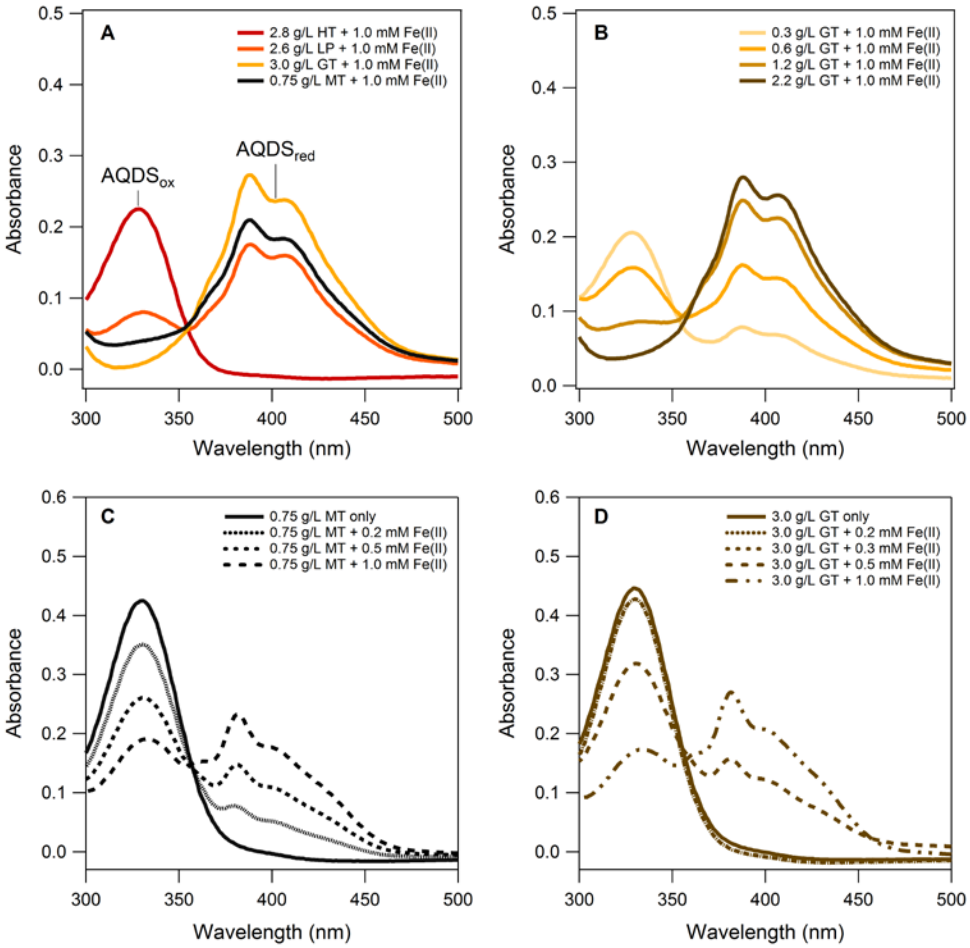


Figure 12. The effects of (A) oxide type, (B) goethite loading, (C) Fe(II) loading with magnetite, and (D) Fe(II) loading with goethite on reduction of CRPs by Fe(II) + iron oxide suspensions. The CRP was AQDS for (A) and (B) and AQS for (C) and (D). All spectra were taken after 20 hr of exposure to the mineral suspensions.

**Reduction Potentials of Minerals Determined with Thermodynamic CRPs.** For each mineral suspension, CRPs were selected that did not give too much (e.g., Figure 18A) or too little (e.g., Figure 18D) reduction (defined as <95% and >5%, respectively). The matches

between CRP and reductant that we deemed suitable are identified in Table 5. Using the selected CRP, the amount of CRP reduction was quantified using the difference in absorbance at $\lambda_{max}$ of the oxidized form (Table 4) before and after reoxidation, a protocol adapted from Orsetti et al. [*86*] In most cases, adsorption of the CRP was found to be negligible (because the absorbance after reoxidation was similar to the control). Interference from Fe(III) (due to oxidation of aqueous Fe(II)) was also minimal, because reoxidation of the reduced CRPs is much faster (complete in a few seconds) than Fe(II) oxidation at neutral pH ($t_{1/2}$ = ~3 min). Assuming that equilibrium was reached between the CRP and the mineral suspension, the mineral reduction potentials were calculated from the CRP data ($E_{CRP}$), using the Nernst equation for a two-electron redox couple with two relevant pKa's for the reduced CRP (eq 1):

$$E_{\mathrm{CRP}} = E^0 + \frac{\mathrm{R}T}{2\mathrm{F}} \ln\left(\left[\mathrm{H}^+\right]^2 + K_{\mathrm{r1}}\left[\mathrm{H}^+\right] + K_{\mathrm{r1}}K_{\mathrm{r2}}\right) + \frac{\mathrm{R}T}{2\mathrm{F}} \ln\left(\frac{\left[\mathrm{CRP_{ox}}\right]}{\left[\mathrm{CRP_{red}}\right]}\right) \qquad (1)$$

where $E^0$ is the standard reduction potential of the CRP (Table 4), R is the gas constant, $T$ is temperature, F is the Faraday constant, and $[CRP_{ox}]$ and $[CRP_{red}]$ are the concentrations of oxidized and reduced forms of the CRP after reduction. Additional pH effects due to other pKa's are minimal near neutral pH [*86, 99*] and therefore were neglected. For the conditions and assumptions that apply to this work, eq 1 can be further simplified to eq 2:

$$E_{\mathrm{CRP}} = E^0_{\mathrm{pH}} + \frac{\mathrm{R}T}{2\mathrm{F}} \ln\left(\frac{\left[\mathrm{CRP}_{ox}\right]}{\left[\mathrm{CRP}_{red}\right]}\right) \qquad (2)$$

where $E^0_{\mathrm{pH}}$ is the formal reduction potential of the CRP at pH 7.2 used in the assay.

The mineral reduction potentials ($E_{CRP}$) calculated using eq 2 are given in Table 5 and summarized in Figure 13. In Figure 13, each type of mineral tested is represented as a category (column), which contains several sub columns. Each sub column includes a series of $E_{CRP}$ values (horizontal markers) determined as a function of the variable (e.g., Fe(II) dose, mineral loading) that is indicated by the bold label above the corresponding sub column. At the lowest Fe(II) concentration tested (0.2 mM), reduction potentials were not obtained for hematite, lepidocrocite, and goethite because no CRP reduction occurred, suggesting that the reduction potentials of these oxides under these conditions are out of the range of potentials that are accessible by the CRPs used in this study. With increasing Fe(II), the calculated reduction potentials became more negative, as expected, for all oxides (Figure 13), but goethite gave a much wider range of potentials than hematite and lepidocrocite. Magnetite (0.75 g/L) without Fe(II) gave a negative potential around −180 mV because of structural Fe(II), but only dropped ~30 mV as aqueous Fe(II) increased from 0.2 to 1.0 mM. The different sensitivities of $E_{CRP}$ to the Fe(II) concentration for different minerals is likely attributed to the intrinsic difference of mineral properties (e.g., bulk crystal conductivity [*100*]).

Other notable trends shown in Figure 13 include *(i)* increasing $E_{CRP}$ with increasing addition of natural organic matter (NOM) for goethite, which is consistent with the consensus that NOM decreases the reductant reactivity [*29, 101*], (*ii*) decreasing $E_{CRP}$ with increasing mineral loading for MT (with no added Fe(II)), which simply shows the correlation between $E_{CRP}$ and the amount of structural Fe(II), and (*iii*) a bimodal pattern of $E_{CRP}$ with increasing

mineral loading at 1 mM Fe(II) for GT and LP, which is also shown in Figure 19. The latter result—which is discussed in more detail as supporting information below—may prove to be analogous to the effect reported in several recent studies of Fe(II) adsorption onto iron oxides, wherein removal of excess aqueous Fe(II) was found to significantly lower rates of contaminant reduction by Fe(III) oxides with adsorbed Fe(II) [*70*, *76*].

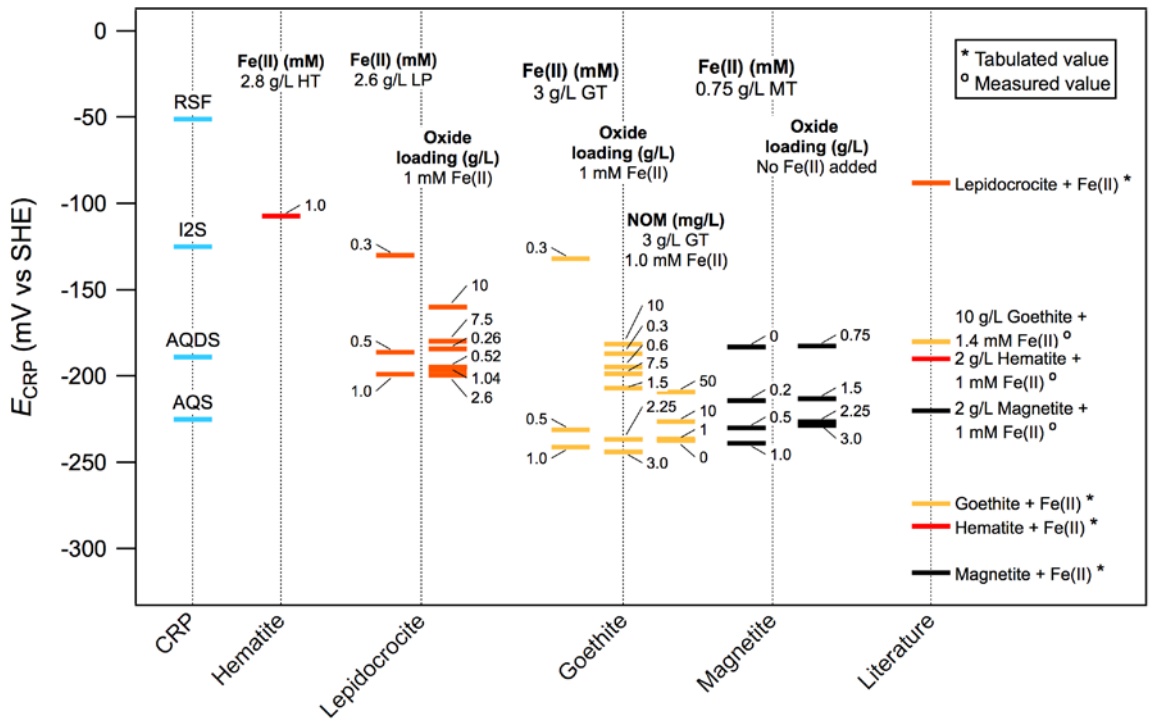


Figure 13. Summary of the $E_{CRP}$ values determined for different reducing iron minerals under various conditions. Each marker is labeled with the specific value of the varied parameter (bold labels). The plain text annotation above each subcolumn indicates the experimental parameter that was constant in that series of experiments. For reference, reduction potentials of the four CRPs at pH = 7 ($E_H$') are plotted in the far left column for reference. For comparison, formal reduction potentials reported in prior studies are plotted in the far right column. Tabulated values are from Stumm [*102*] and measured values are based on Orsetti et al. [*86*] and Gorski et al. [*72*].

The calculated mineral reduction potentials were further compared to previously measured or tabulated values for Fe(II) containing minerals, which are summarized in the far right column of Figure 13. The measured potentials for Fe(II) sorbed onto goethite reported by Orsetti et al. [*86*] and for Fe(II) sorbed to synthetic hematite and magnetite reported by Gorski [*72*] are of particular relevance because (*i*) both studies used thermodynamic CRPs (i.e., redox indicators) to calculate the mineral reduction potentials and (*ii*) the origins of minerals used in those studies are the same as some of the minerals used here.

In general, the $E_{CRP}$ values agree well with the literature data. The reduction potential for 10 g/L goethite suspension with 1.4 mM Fe(II) determined by AQDS at pH 6.7 ranged from −180 to −160 mV [*86*], which agrees well with −181 mV, measured in this study for 10 g/L goethite with 1 mM Fe(II) at pH 7.2 (Figure 13). The measured reduction potential of

stoichiometric magnetite at pH 7.4 [*103*] also falls into the range of magnetite reported here. In contrast, the synthetic hematite used by Gorski showed a much lower reduction potential than the Bayferrox hematite used in this study [*72*]. The reason for this discrepancy is unclear, but it is consistent with other work showing that synthetic hematite is generally more reactive with contaminants than the Bayferrox hematite [*84*].

**Comparison with Electrochemically Measured Potentials.** $E_{Pt}$ (i.e., OCP referenced to SHE) was measured on suspensions of hematite, lepidocrocite, goethite, and magnetite with a range of initial Fe(II) concentrations. In selected experiments, CRPs were added during the $E_{Pt}$ measurement to serve as electron transfer mediators to improve the electrode response to the redox active minerals [*85*]. Sample chronopotentiograms (CPs) are shown in Figure 14A for goethite and hematite suspensions with 1 mM aqueous Fe(II) (after 20 h pre-equilibrium). Initially, the $E_{Pt}$ for the goethite suspension was only ~20 mV below the $E_{Pt}$ for the hematite suspension (Figure 14A), which is much less than their difference in $E_{CRP}$ shown in Figure 13.

However, adding small concentrations (~12 μM) of a CRP during the CP measurement resulted in a sharp drop in $E_{Pt}$. The decrease of $E_{Pt}$ in the presence of CRP is evidence that the CRPs served as mediators of electron transfer between the mineral surfaces and the electrode surface, thereby improving electrode response to minerals. However, this effect was only seen with AQS on the goethite suspension and I2S on the hematite suspension, and not with AQDS on the hematite suspension (Figure 14A). The absence of an $E_{Pt}$ decrease with AQDS in the hematite suspension is because the standard reduction potential of AQDS is substantially lower than the mineral reduction potential, which also explains the lack of AQDS reduction by hematite with 1 mM Fe(II) shown in Figure 12A. Based on constraints defined by the Nernst equation, Sanders et al. concluded that for a mediator to be effective in transfering electrons between mineral and electrode, the difference between the standard reduction potentials of mineral and mediator should be less than 120 mV [*85*]. The results shown here suggest that the operational threshold for this type of mediator effect might be even lower.

CP experiments such as those shown in Figure 14A were performed with other oxides and oxide loadings, and the plateau values of $E_{Pt}$ are shown in Figure 14 as a correlation with the corresponding $E_{CRP}$ data (from Figure 13 and Table 3). All of the $E_{Pt}$ data obtained without added CRPs were significantly more positive than their $E_{CRP}$ counterparts, but addition of CRPs resulted in lower values of $E_{Pt}$ that agree well with $E_{CRP}$. These results demonstrate that the potentials obtained by equilibration of CRPs with mineral suspensions are consistent regardless of whether the potential is determined potentiometrically or spectrophotometrically.

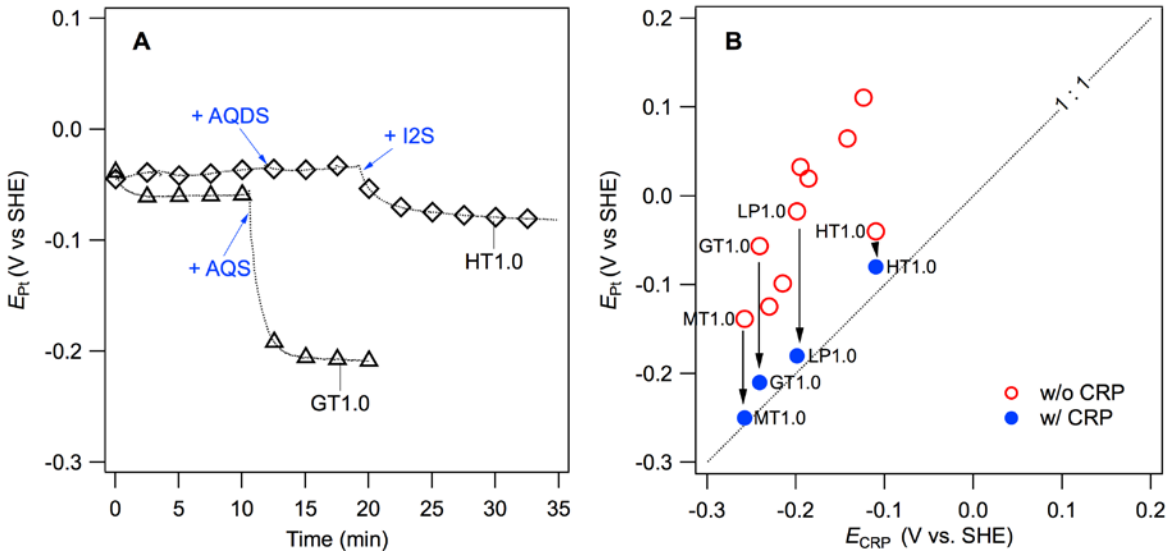


Figure 14. (A) The $E_{Pt}$ of mineral suspension as a function of time measured by a 3 mm Pt electrode (rotated at 2000 rpm) and a Ag/AgCl reference electrode under Ar headspace (arrows indicate the time aliquots of thermodynamic CRPs were added); (B) Potentiometrically measured $E_{Pt}$ vs. $E_{CRP}$ shown in Figure 13.

**Kinetic CRP Measurements and Links to $E_{CRP}$.** To explore the kinetic aspect of reduction by minerals, we used three model contaminants (4Cl-NB, 2-CAP, and CT) that are labile to abiotic degradation as kinetic CRPs in batch experiments with various doses of iron oxide and aqueous Fe(II). No effort was made to quantify the reaction products as they have been investigated in detail by prior studies [*23, 71, 74*]. All of the data fit pseudo first order kinetics well, and the resulting values of $k_{obs}$ were used to calculate the mass- and surface-area normalized rate contants ($k_M$ and $k_{SA}$, respectively) (Table 6). All three probes gave good correlations to values of $E_{CRP}$ determined under equivalent conditions, but only the correlation to $k_{SA}$ is shown (Figure 14) because it gave fewer outliers and should have the most generality. For all three kinetic CRPs, the increase in $k_{SA}$ with decreasing $E_{CRP}$ of the mineral suspension appears to be linear, so the trends were fit by linear regression. The slopes of these correlations—which reflect the sensitivity of the reaction to mineral reduction potential—are similar for the two dechlorination reactions (CT and 2-CAP) and roughly 2-fold less than for the nitro reduction reaction (2-Cl-NB). Overall, the rate constants for nitro reduction are consistently greater than for dechlorination (by 1-4 orders of magnitude).

The linear correlations between log $k_{SA}$ and $E_{CRP}$ (Figure 15**)** resemble the (L)FERs developed in previous studies formed between second-order rate constants for contaminant reduction and one electron-reduction potentials of aqueous Fe(II)–ligand complexes [*79, 104*]. However, the mechanistic significance of the LFERs reported here is less clear because both the response ($k_{SA}$) and descriptor ($E_{CRP}$) variables used are confounded with effects for which there still is no practical method of normalization. For $k_{SA}$, the main issue is that normalization to total surface area may not reflect variations in reactive surface area (e.g., surface coverage of reactive sites) [*105*]. For $E_{CRP}$, the apparent dependence on dose of mineral and Fe(II) (Figure 13) suggests that this is an operationally-defined measure of effective reduction potential (rather than an ideal thermodynamic property of the materials). This is expected because there are many factors that make reduction potentials difficult to define for sorbed Fe(II) as Fe(II) sorption is

proved to be a dynamic and complex process. [*76*, *77*, *106*, *107*] However, the relative success of the LFERs based on $E_{CRP}$ in Figure 15 could also be evidence that the value of this descriptor variable reflects actual differences in the material properties of each preparation.

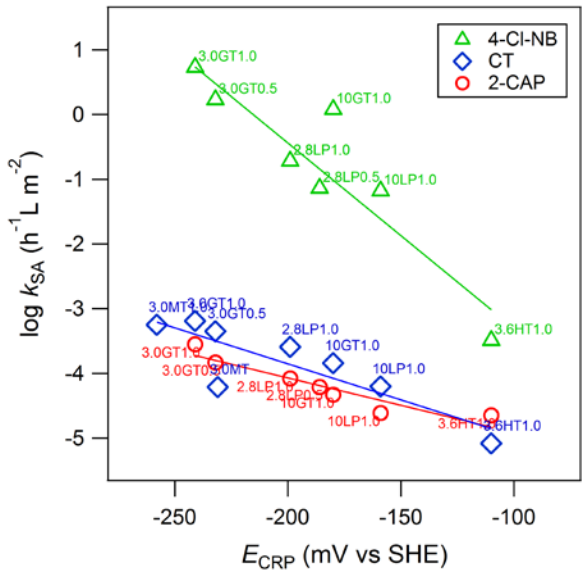


Figure 15. Pseudo-first order rate constants (log $k_{SA}$) for reduction of 4Cl-NB, 2-CAP, and CT by iron minerals versus mineral reduction potentials determined by chemical reactivity probes ($E_{CRP}$) Fitting results (slope, intercept, $r^2$) are −0.029±0.005, −6±1, 0.839; −0.008±0.001, −5.8±0.3, 0.885; and −0.011±0.003, −6.1±0.6, 0.738 for 4-Cl-NB, 2-CAP, and CT, respectively. (Oxide loading (g/L), type, and Fe(II) concentration (mM) for each data point are annotated next to the marker).

To explore the generality of the correlations between mineral reduction potential and contaminant reduction kinetics, we compiled kinetic data from previous studies on the abiotic reduction of three classes of contaminants by Fe(II) containing oxides and sulfides (summarized in Table 7 to Table 10). In addition to nitroaromatics (represented by NB and 4Cl-NB), and chlorinated alkanes (represented by CT and HCA), we also included chlorinated ethenes (represented by TCE and PCE) in order to examine whether the approach developed in this study can be extended to those environmentally-relevant and highly-recalcitrant contaminants. The literature data ($k_{obs}$) were normalized to mineral mass loading ($k_M$) instead of $k_{SA}$, as surface area data were not provided in all studies. The results are summarized in Figure 16 by plotting log $k_M$ (from the literature and this study) versus a semi-quantitative ranking of the reduction potential of abiotic iron oxide and sulfide based minerals. The position of each mineral included in this study (magnetite, goethite, lepidocrocite, and hematite) on the x-axis was assigned to the corresponding value of $E_{CRP}$ measured at 1 mM Fe(II) in this study. For green rust and iron sulfide, their reduction potentials were more negative than could be characterized with the thermodynamic CRPs that we have tested so far (data not shown), so they were assigned potentials slightly below the limit of the most strongly reducing CRP tested (AQS). FeS was assigned a lower potential than green rust as FeS is generally considered to be more reactive, but the difference between these two potentials was arbitrary.

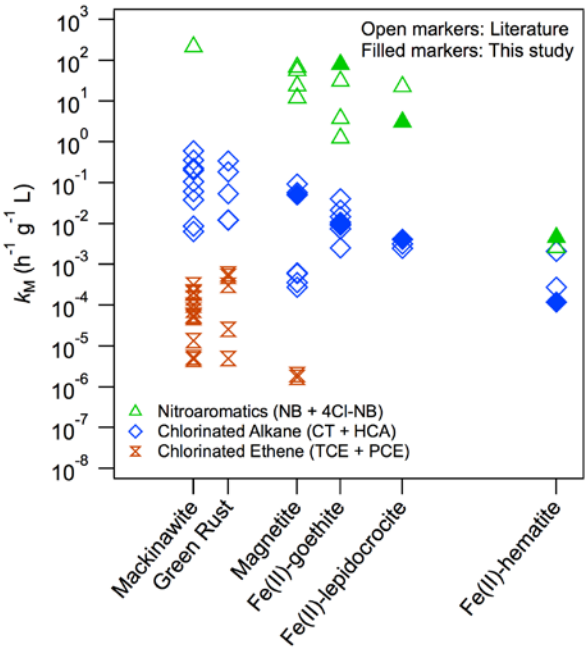


Figure 16. Mass-normalized reduction rate constants ($k_M$) of kinetic CRPs (including nitroaromatics and chlorinated alkanes) and chlorinated ethenes with various reducing iron minerals (open symbols: values reported in literature; solid symbols: value determined in this study). Literature data used in this plot are summarized in Table 7 to Table 10.

Figure 5 shows variable, sometimes substantial, degrees of scatter, some of which is undoubtedly because the values of $E_{CRP}$ used to define the descriptor axis do not fully represent all of the operational factors that vary within and among the experiments summarized (Table 7 to Table 10). For example, the variation in $k_M$ for CT reduction by magnetite appears to be related to differences in synthesis methods (Table 7), and $k_M$ for reduction of chlorinated compounds by FeS appears to be affected by whether freeze drying is used during mineral preparation (Table 7). However, despite the variability in $k_M$ that is not described by the representative values of $E_{CRP}$ used to make Figure 16, the kinetic data for the three classes of contaminants do form clusters and trends that offer potentially useful insights into aspects of abiotic contaminant degradation by reducing minerals. The relative rates of the three classes of contaminant reduction processes (nitro aromatics > chlorinated alkanes > chlorinate alkenes) is consistent with other evidence (e.g., Figure 16 and Elsner [*74*]). Similarly, the decrease in reduction rates with less strongly reducing minerals that is evident for nitro aromatics and chlorinated alkanes is consistent with expectations (e.g., Figure 15), but the available data are insufficient to demonstrate if this trend holds for reduction of chlorinated ethenes by weakly reducing mineral phases. Nevertheless, assuming a slope similar to the other two classes of contaminants, extrapolation from the available data for chlorinated ethenes to the less reactive oxides suggests rate constants on the order of $10^{-6}$ hr$^{-1}$ ($t_{1/2} \approx 8$ yr). Such slow rates would be very difficult to measure in laboratory batch experiments (which undoubtedly is part of the reason for the absence of literature data), but they could still be environmentally-significant in the context of abiotic NA in the field.

**Implications for Assessing Abiotic NA.** Characterization of abiotic NA of recalcitrant contaminants, such as TCE, in the subsurface is challenging mainly because the absolute degradation rates are slow under most field conditions. These challenges might be overcome by

characterization using kinetic and thermodynamic CRP methods developed in this study. However, extension of this approach to previously reported kinetic data from laboratory studies of abiotic contaminant reduction by reducing minerals confirmed that there is considerable variability in reactivity within classes of minerals (presumably due to operational factors ranging from accessibility of reactive surface area to electronic effects of mineral stoichiometry). Much of this variability may be reduced by in situ measurements with thermodynamic CRPs, but the overall behavior of the thermodynamic CRPs when applied to real environmental samples may be affected by factors that were not addressed in this study: sorption to natural organic matter or non-reactive mineral surfaces, non-uniform permeability and transport, etc. Controlled characterization of these effects probably is best done with column experiments (e.g. with aquifer material collected from field sites), but the ultimate goal of this study is to develop CRP-based assays that can be used as reactive tracers in push-pull tests for in situ characterization of field conditions. Preliminary results suggest that the thermodynamic CRP assays developed in this study are effective in push-pull tests performed on laboratory columns, and these CRPs are compounds that should be suitable for field-scale applications, in terms of cost, toxicity, etc.

## 10.2.4. Supporting Information for Fan et al. 2016 [*108*]

### 10.2.4.1. Experimental Details

**Preparation of Iron Oxide Suspension.** Iron oxide suspensions were prepared by agitating powders in deionized water (DIW) overnight, vacuum filtered and resuspended in DIW. The suspensions were then deoxygenated by sparging with $N_2$ for 2 hours and stored in a $N_2$ filled anaerobic chamber (100% $N_2$, $O_2$ < 1 ppm). Magnetite and chloride green rust (GR-Cl) were synthesized inside the anaerobic chamber using well-established co-precipitation protocols adapted or modified from prior studies (see below). The resulting suspensions of the synthesized particles were centrifuged under $N_2$ atmosphere, washed with deoxygenated DIW (DO/DIW) at least three times, and resuspended in DO/DIW for batch experiments.

**Mineral Synthesis.** Stoichiometric magnetite was synthesized based on the procedure described by Gorksi and Scherer [*72*]. A 1:2 Fe(II):Fe(III) mixture was prepared from $FeCl_2 \cdot 6H_2O$ and $FeCl_3 \cdot 6H_2O$ in 200 mL DO/DI water in the anaerobic chamber with a total iron concentration of 0.19 M. The mixture was titrated with 10 M NaOH (prepared with DI/DO water) to above pH 10. The brownish mineral suspension was sealed under $N_2$ atmosphere and placed on an end-over-end rotator overnight. The black suspension was centrifuged, washed and resuspended in DO/DI water for probe experiments.

The chloride green rust was prepared inside the anaerobic chamber following the coprecipitation procedure described by Refait et al. [*94*]. 2.52 g $FeCl_2$ and 0.84 g $FeCl_3 \cdot 6H_2O$ were dissolved in 60 mL DO/DI water. 4 g NaOH was dissolved in 40 mL DO/DI water. The two aqueous solutions were mixed, resulting a ratio of [Fe(II) + Fe(III)]/[NaOH] = 0.6 and a ratio of Fe(II) to Fe(III) of 3. The concentration of resulted green rust suspension is 150 mM, which equals to ~60 g/L if we assume the chemical formula of chloride green rust is $Fe(II)_3Fe(III)(OH)_8Cl \cdot 2H_2O$. The co-precipitation protocol was selected over partial oxidation methods—another commonly used approach to prepare green rust—for controlling Fe(II) to Fe(III) ratio to be exact.

### 10.2.4.2. Characterization of Iron Oxides

**Specific Surface Area (SSA)**. To provide a reliable set of specific surface areas for the iron oxides from Bayferrox, we made multiple measurements over the range of conditions commonly used in BET gas adsorption on metal oxide powders. Sample preparation temperature was applied for 60 min while continuously purging with $N_2$. The results are shown in Figure 17.

Above 200 °C, the lepidocrocite color transformed from orange to dark red, and goethite transformed from yellow to bright red. Below 200 °C, all four oxides showed a small increase in SSA with preparation temperature (Figure 17A). Lacking a mechanistic explanation for this effect on which to select a single representative value for each oxide, we chose to fit the data by linear regression and used the predicted value of SSA at 120 °C, which is near where the confidence interval about the regression (dashed lines in Figure 17B) is narrowest. The resulting, recommended values of SSA are given in Table 3.

Table 3. Results of fitting SSA data in Figure S1 for Bayferrox iron oxides

| | Intercept | Slope | Chi Square | N | SSA at 120 °C |
|---|---|---|---|---|---|
| Goethite | 13.7 ± 1.0 | 0.0107 ± 0.0075 | 5.4835 | 8 | 14.9 |
| Hematite | 13.8 ± 0.3 | 0.0030 ± 0.0020 | 0.3199 | 7 | 14.2 |
| Lepidocrocite | 15.4 ± 0.5 | 0.0070 ± 0.0037 | 1.0569 | 7 | 16.2 |
| Magnetite | 88 .2± 1.8 | 0.0099 ± 0.0015 | 0.1793 | 7 | 11.6 |

Using the protocol based on the results obtained with Bayferrox iron oxides (above), we measured the BET SSA of magnetite prepared by the method used for experiments with CRPs that are described in this study. Triplicate measurements done with sample preparation at 120 °C gave 86.2±3.5 $m^2/g$.

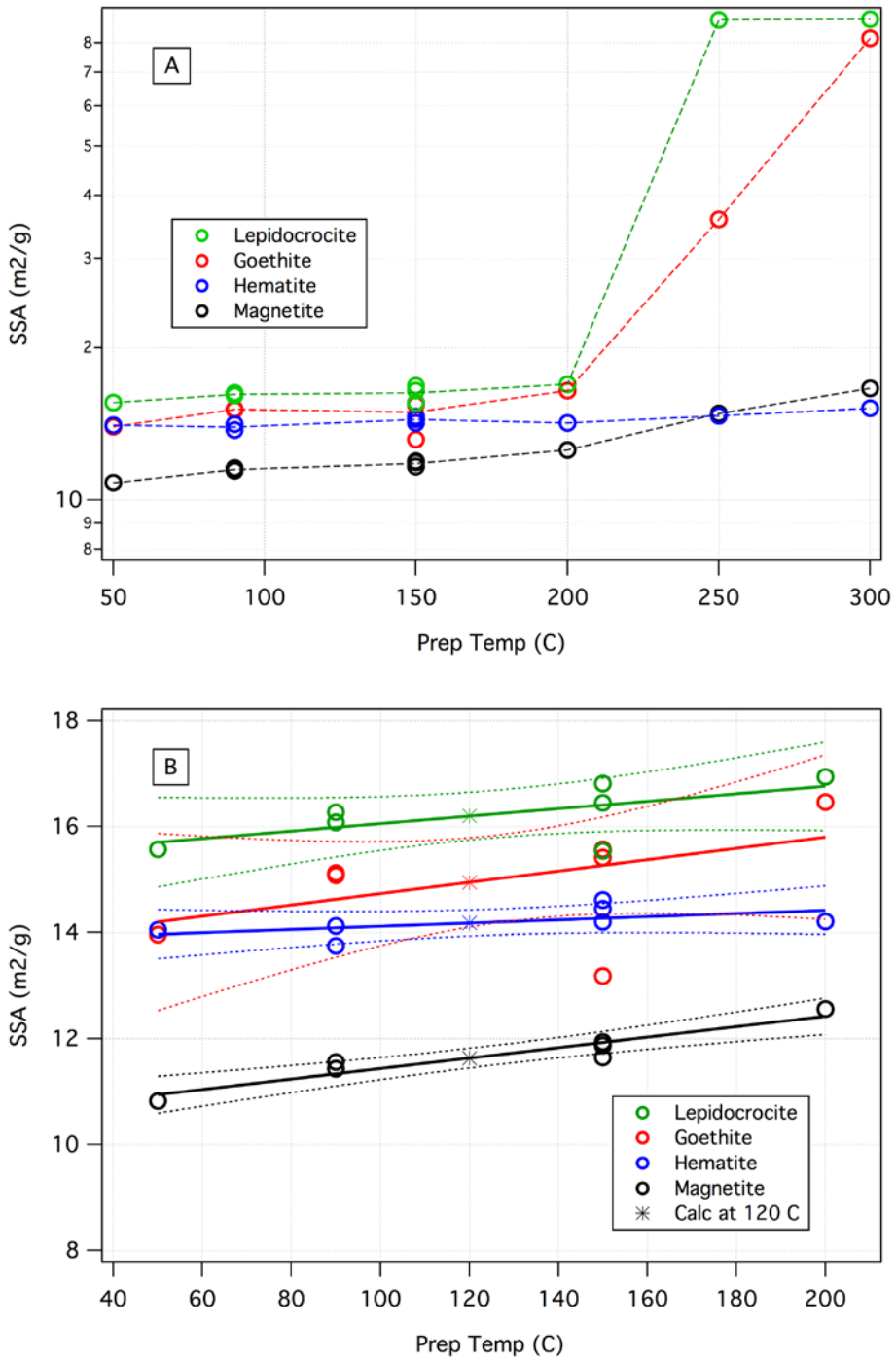


Figure 17. Specific surface areas of Bayferrox iron oxides determined by $N_2$ gas adsorption by the BET method. Open symbols represent independent replicate measurements, starting with 0.7 to 1.0 g of fresh sample each time. The instrument (Micromeritics Gemini V Surface Area & Pore size Analyzer) had recently received manufacturer maintenance and verification. The absolute accuracy of the instrument was determined to be within 3.5% using a carbon black standard.

Table 4. Nomenclature and Properties of Thermodynamic Chemical Reactivity Probes (CRPs).

| Oxidized Form | | | | | Reduced Form | | | | | Couple | |
|---|---|---|---|---|---|---|---|---|---|---|---|
| Names | Color [a] | $\lambda_{Max}$ [b] | ε [c] | $pK_a$ | Names | Color [a] | $\lambda_{Max}$ [b] | ε [c] | $pK_a$ | $E_0'$ [d] | $E_m^7$ [d] |
| 2,6-Dichloro-indophenol (DCIP) | blue | 601 | 17.4[e] | 8.1 | | leuco | 256 | N/A | 9.4, 10.6 | +0.668 | 0.228 |
| Resazurin (Alamar Blue)(RSZ) | purple | 600 | 40.1[e] | 6.93 | Resorufin (RSF) | pink | 569 | 93.1 | NA | N/A | N/A |
| Indigo tetrasulfonate (I4S) | blue | 589 | 18.5[e] | 11.9, 12.9 | | yellow | 433 | | 7.2, 12.1 | 0.365 | −0.046 |
| Resorufin (RSF) | pink | 569 | 93.1[f] | 6.93 | Dihydroresorufin | leuco | 293 | | 9.26, 10.00 | 0.380 | −0.051 |
| Indigo trisulfonate (I3S) | blue | 600 | 14.6[e] | 11.7, 12.8 | | yellow | 421 | | 7.4, 12.1 | 0.332 | −0.081 |
| 5,5'-Indigo disulfonate (Indigo Carmine)(I2S) | blue | 610 | 19.6[f] | 12.3, 12.8 | | yellow | 407 | N/A | 9.3, 10.0 | 0.291 | −0.125 |
| 9,10-Anthraquinone-2,6-disulfonate (AQDS) | leuco | 328 | 2.81[f] | N/A | | Pale yellow | 386 | 7.0 [g] | 8.10, 10.5 | 0.228 | −0.184 |
| 9,10-Anthraquinone-2-sulfonate (AQS) | leuco | 328 | 5.33 [f] | N/A | | Pale yellow | 386 | N/A | N/A | 0.187 | −0.225 |

[a] At circum-neutral pH. [b] Absorbance maximum at pH 7 (nm). [c] Extinction coefficient ($mM^{-1}$ $cm^{-1}$). [d] Formal potentials at pH 0 and 7 (mV vs SHE). [e] ref [*29*]. [f] measured based on calibration. [g] estimated based on ref [*88*].

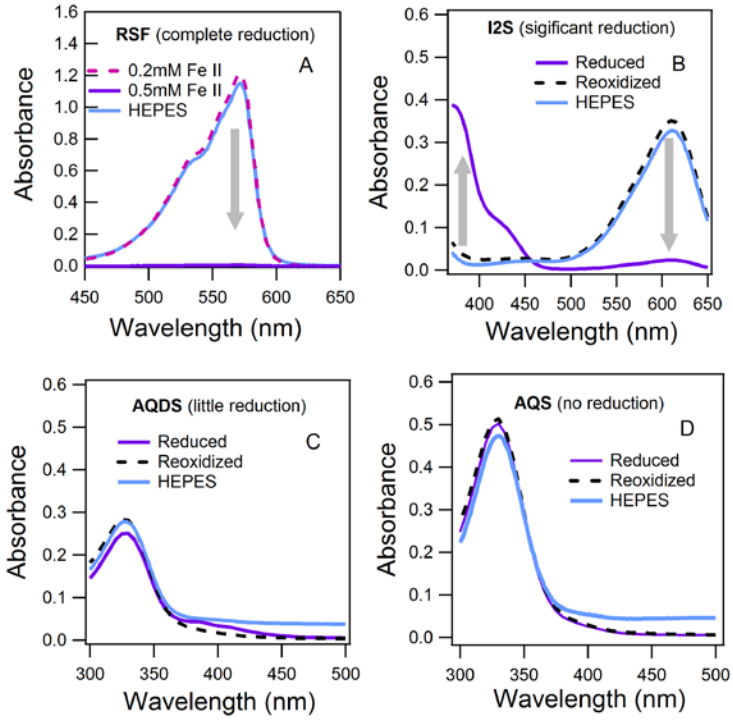


Figure 18. Absorbance spectra of (A) RSF, (B) I2S, (C) AQDS, and (D) AQS after reduction by lepidocrocite + 0.5 mM Fe(II) (solid line) and after exposing to ambient air (dash line)

Typical absorbance spectra measured are presented in Figure 18 using lepidocrocite (LP) and 0.5 mM Fe(II) as an example. Each panel (except Panel A) shows three spectra for each probe: (*i*) before reoxidation, (*ii*) after reoxidation, and (*iii*) without oxide and Fe(II) (i.e., the buffer only control). In this case, adsorption of the probe was found to be significant only for RSF, because the absorbance spectrum after reoxidation of the reduced RSF was not different from the reduced spectrum. Our protocol cannot identify the redox states of sorbed RSF, but we believe that the adsorbed RSF is in the reduced form because no RSF disappearance was found with LP + 0.2 mM Fe(II) compared to HEPES only (Figure 18A). If we consider RSF is completely reduced by LP + 0.5 mM Fe(II), the pattern is then clear that the extent of probe reduction followed the order of RSF > I2S > AQDS > AQS (Figure 18B–Figure 18D), which is consistent with the order of reduction potentials of these four probes (cf., Table 3).

Table 5. Summary of the experimental conditions, the CRPs selected for calculating the $E_{CRP}$ of each iron minerals, the calculated $E_{CRP}$, and measured $E_{Pt}$ under each condition

| Iron Minerals | Mineral dose (g/L) | Fe(II) (mM) | CRPs | $E_{CRP}$ (V vs SHE) | $E_{Pt}$ (V vs SHE) | $E_{Pt}$ w/CRP (V vs SHE) |
|---|---|---|---|---|---|---|
| Goethite | 3.0 | 0.2 | N/A | N/A | N/A | N/A |
| Goethite | 3.0 | 0.3 | I2S | −0.124 | 0.1105 | N/A |
| Goethite | 3.0 | 0.5 | AQDS | −0.232 | 0.0325 | N/A |
| Goethite | 3.0 | 1.0 | AQS | −0.241 | −0.0565 | −0.21 |
| Goethite | 3.0 | 1.0 | AQS | −0.244 | N/A | N/A |
| Goethite | 2.25 | 1.0 | AQS | −0.237 | N/A | N/A |
| Goethite | 1.2 | 1.0 | AQDS | −0.207 | N/A | N/A |
| Goethite | 0.6 | 1.0 | AQDS | −0.195 | N/A | N/A |
| Goethite | 0.3 | 1.0 | AQDS (I2S)[a] | −0.187 (−0.178)[b] | N/A | N/A |
| Goethite | 7.5 | 1.0 | AQDS | −0.198 | N/A | N/A |
| Goethite | 10 | 1.0 | AQDS | −0.181 | N/A | N/A |
| Goethite | 3.0 | 1.0 | AQS | −0.237 | N/A | N/A |
| Goethite + 1 mg/L NOM | 3.0 | 1.0 | AQS | −0.236 | N/A | N/A |
| Goethite + 10 mg/L NOM | 3.0 | 1.0 | AQS | −0.227 | N/A | N/A |
| Goethite + 50 mg/L NOM | 3.0 | 1.0 | AQS | −0.209 | N/A | N/A |
| Lepidocrocite | 2.6 | 0.2 | N/A | N/A | N/A | N/A |
| Lepidocrocite | 2.6 | 0.3 | I2S | −0.142 | 0.0645 | N/A |
| Lepidocrocite | 2.6 | 0.5 | AQDS | −0.186 | 0.0195 | N/A |
| Lepidocrocite | 2.6 | 1.0 | AQDS | −0.199 | −0.0175 | −0.18 |
| Lepidocrocite | 2.6 | 1.0 | AQDS | −0.199 | N/A | N/A |
| Lepidocrocite | 1.04 | 1.0 | AQDS | −0.197 | N/A | N/A |
| Lepidocrocite | 0.52 | 1.0 | AQDS | −0.195 | N/A | N/A |
| Lepidocrocite | 0.26 | 1.0 | AQDS | −184 | N/A | N/A |
| Lepidocrocite | 7.5 | 1.0 | AQDS | −180 | N/A | N/A |
| Lepidocrocite | 10 | 1.0 | AQDS | −160 | N/A | N/A |
| Hematite | 3.6 | 0.2 | N/A | N/A | 0.1305 | N/A |
| Hematite | 3.6 | 0.3 | N/A | N/A | 0.1075 | N/A |
| Hematite | 3.6 | 0.5 | N/A | N/A | 0.0665 | N/A |
| Hematite | 3.6 | 1.0 | I2S | −0.110 | 0.0345 | −0.08 |
| Magnetite | 075 | 0.3 | AQS (AQDS) | −0.215 (−0.212) | −0.099 | N/A |
| Magnetite | 0.75 | 0.5 | AQS (AQDS) | −0.229 (−0.225) | −0.125 | N/A |
| Magnetite | 0.75 | 1.0 | AQS (AQDS) | −0.239 (−0.234) | −0.139 | N/A |
| Magnetite | 0.75 | 0 | AQDS | −0.182 | N/A | N/A |
| Magnetite | 1.5 | 0 | AQS | −0.213 | N/A | N/A |
| Magnetite | 2.25 | 0 | AQS | −0.226 | N/A | N/A |
| Magnetite | 3 | 0 | AQS | −0.238 | N/A | N/A |
| Magnetite | 3 | 1.0 | AQS | −0.258 | N/A | −0.25 |

[a] Measurement performed with another CRP; [b] $E_{CRP}$ determined by the corresponding CRP.

.

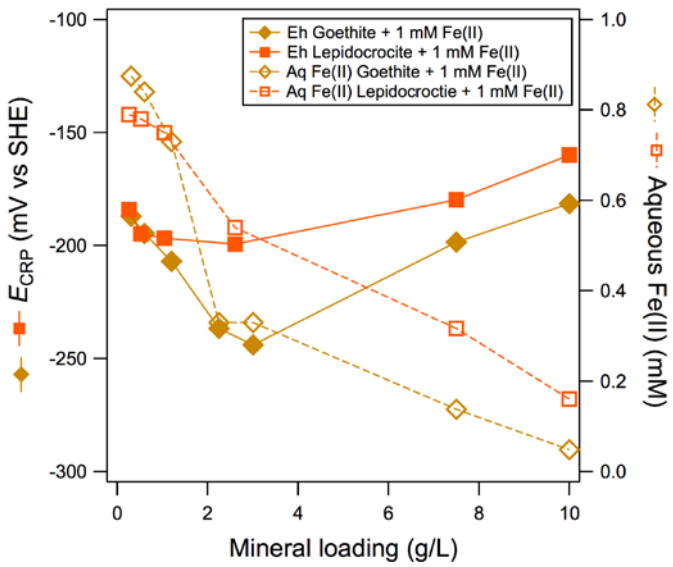


Figure 19. Mineral reduction potential ($E_{CRP}$) and aqueous Fe(II) concentration measured before probe addition for goethite and lepidocrocite at different mineral loadings with 1 mM initial Fe(II) concentration.

A notable trend in $E_{CRP}$ was obtained by varying the mineral loading for lepidocrocite and goethite with 1 mM initial Fe(II) concentration (Figure 19). The $E_{CRP}$ (left axis), along with aqueous Fe(II) measured immediately before adding the CRP (right axis), is plotted as a function of mineral loading. Preparing these experiments with constant initial Fe(II) allows differentiation of the effects of aqueous and solid Fe(II) on $E_{CRP}$. Aqueous Fe(II), as expected, showed monotonic decrease as mineral loading increased (Figure 19). By contrast, the trend in $E_{CRP}$ is bimodal with minima at about 3 g/L for goethite and 2.7 g/L for lepidocrocite. The front part shows decreasing $E_{CRP}$ with increasing mineral loading, which can be attributed to increasing sorbed Fe(II) [*84*, *98*]. But a reverse trend is shown with higher oxide loading, which cannot be explained by the changes in quantity of sorbed Fe(II) because it was monotonic with Fe(II) dose. A closer look at the sorbed Fe(II) data shows a break point for both goethite and lepidocrocite, where the slope changes. The change of slope occurs concurrently with the reversed trend in $E_{CRP}$, suggesting possible correlation between the two events. This might be related to different Fe(II) adsorption sites exhibiting different reactivity [*109*]. With increasing oxide loading, the contributions from different adsorption sites might change, causing the reverse in $E_{CRP}$.

Table 6. Observed reduction rate constants ($k_{obs}$) for three contaminants

| Mineral Phase | Loading (g/L) | Fe(II) (mM) | $k_{obs}$ ($h^{-1}$) | log $k_{obs}$ | log $k_M$ | log $k_{SA}$ |
|---|---|---|---|---|---|---|
| **4-Chloronitrobenzene (4Cl-NB)** | | | | | | |
| Goethite | 3 | 0.5 | 75.19 | 1.88 | 1.40 | 0.23 |
| Goethite | 3 | 1.0 | 240 | 2.38 | 1.90 | 0.73 |
| Goethite | 10 | 1.0 | 180.62 | 2.26 | 1.26 | 0.084 |
| Lepidocrocite | 2.7 | 0.5 | 3.11 | 0.49 | 0.06 | -1.15 |
| Lepidocrocite | 2.7 | 1.0 | 8.3 | 0.92 | 0.49 | -0.72 |
| Lepidocrocite | 10 | 1.0 | 10.78 | 1.03 | 0.03 | -1.18 |
| Hematite | 2.8 | 1.0 | 0.016 | −1.79 | -2.34 | -3.49 |
| **Carbon Tetrachloride (CT)** | | | | | | |
| Goethite | 3 | 0.5 | 0.0196 | −1.71 | -2.18 | -3.36 |
| Goethite | 3 | 1.0 | 0.0289 | −1.54 | -2.02 | -3.19 |
| Goethite | 10 | 1.0 | 0.0215 | −1.67 | -2.67 | -3.84 |
| Lepidocrocite | 2.7 | 1.0 | 0.0112 | −1.95 | -2.38 | -3.59 |
| Lepidocrocite | 10 | 1.0 | 0.0102 | −1.99 | -2.99 | -4.20 |
| Magnetite | 3 | 0 | 0.0167 | −1.78 | -2.25 | -4.21 |
| Magnetite | 3 | 1.0 | 0.151 | -0.82 | -1.30 | -3.25 |
| Hematite | 2.8 | 1.0 | 4.2e-4 | -3.38 | -3.93 | -5.09 |
| **2-Chloroacetophenone (2-CAP)** | | | | | | |
| Goethite | 3 | 0.5 | 0.0125 | −1.90 | -2.38 | -3.55 |
| Goethite | 3 | 1.0 | 6.6e-3 | -2.18 | -2.66 | -3.83 |
| Goethite | 10 | 1.0 | 6.9e-3 | -2.16 | -3.16 | -4.33 |
| Lepidocrocite | 2.7 | 0.5 | 2.7e-3 | -2.57 | -3.00 | -4.21 |
| Lepidocrocite | 2.7 | 1.0 | 3.6e-3 | -2.44 | -2.88 | -4.08 |
| Lepidocrocite | 10 | 1.0 | 3.9e-3 | -2.41 | -3.41 | -4.62 |
| Hematite | 2.8 | 1.0 | 1.1e-3 | -2.95 | -3.51 | -4.66 |

Table 7. Published reduction rate constants of nitrobenzene (including 4Cl-nitrobenzene), carbon tetrachloride, and trichloroethene (and tetrachloroethene) by magnetite.

| Label and Reference | Mineral Dose (g/L) | Chloroethenes $k_{obs}$ ($h^{-1}$), $k_M$ ($h^{-1}$ $g^{-1}$ L) | | Chloromethanes $k_{obs}$ ($h^{-1}$), $k_M$ ($h^{-1}$ $g^{-1}$ L) | | Nitrobenzenes $k_{obs}$ ($h^{-1}$), $k_M$ ($h^{-1}$ $g^{-1}$ L) | | Notes |
|---|---|---|---|---|---|---|---|---|
| Zwank05 [*92*] | 2.6 | | | 0.245 | 0.094 | | | w/ Fe(II)[a] |
| Vikesland07 [*110*] | 5 | | | 0.29 | 0.058 | | | w/o Fe(II)[a] |
| Vikesland07 [*110*] | 5 | | | 3e-3 | 6e-4 | | | w/o Fe(II)[b] |
| Danielsen04 [*111*] | 25 | | | 9e-3 | 3.6e-4 | | | w/o Fe(II)[b] |
| McComick04 [*112*] | 3.6 | | | 1e-3 | 2.8e-4 | | | Biogenic w/ Fe(II) |
| Lee02 [*60*] | 63 | 1.27e-4 | 2.02e-06 | | | | | w/o Fe(II)[c,d] |
| Lee02 [*60*] | 63 | 1.08e-4 | 1.71e-06 | | | | | w/o Fe(II)[c,d] |
| Gorski09 [*72*] | 1 | | | | | 12 | 12 | w/o Fe(II)[a] |
| Elsner04 [*113*] | 1.27 | | | 7.9e-4 | 6.2e-4 | 30 | 23.62 | w/ Fe(II)[a] |
| Klausen95 [*109*] | 0.2 | | | | | 11.22 | 56.1 | w/ Fe(II)[c] |
| Klausen95 [*109*] | 0.2 | | | | | 13.68 | 68.4 | w/ Fe(II)[c] |

[a] Chemical precipitation that mixes predetermined amount of Fe(II) and Fe(III) solutions together at high pH. [b] Adapted from [*114*]. [c] Adapted from [*115*]. [d] Freeze dried.

Table 8. Published reduction rate constants of nitrobenzene (including 4Cl-nitrobenzene), carbon tetrachloride, and trichloroethene (and tetrachloroethene) by Fe(II) sorbed onto Fe(III) oxide.

| Label and Reference | Mineral Dose (g/L) | Chloroethenes $k_{obs}$ ($h^{-1}$), $k_M$ ($h^{-1}$ $g^{-1}$ L) | | Chloromethanes $k_{obs}$ ($h^{-1}$), $k_M$ ($h^{-1}$ $g^{-1}$ L) | | Nitrobenzenes $k_{obs}$ ($h^{-1}$), $k_M$ ($h^{-1}$ $g^{-1}$ L) | | Notes |
|---|---|---|---|---|---|---|---|---|
| Zwank05 [*92*] | 3.1 | | | 0.023 | 7.4e-3 | | | Goethite[a] |
| Zwank05 [*92*] | 3.1 | | | 0.028 | 9.0e-3 | | | Goethite[a] |
| Elsner04 [*113*] | 3 | | | 7.6e-3 | 2.5e-3 | | | Goethite[a] |
| Amonette00 [*70*] | 5 | | | 0.108 | 0.0216 | | | Goethite[b] |
| Pecher02 [*116*] | 1.47 | | | 0.016 | 0.0108 | | | Goethite[a] |
| Kenneke03 [*117*] | 6.9 | | | 0.052 | 7.5e-3 | | | Goethite[a] |
| Maithreepala04 [*118*] | 0.89 | | | 0.036 | 0.0404 | | | Goethite[b] |
| Shao07 [*119*] | | | | | | | | Goethite[b] |
| Elsner04 [*113*] | 1.54 | | | 0.0227 | 0.0147 | 47.5 | 30.84 | Goethite[a] |
| Hoffstetter [*71*] | 0.64 | | | | | 0.792 | 1.24 | Goethite[a] |
| Rugg98 [*32*] | 0.64 | | | | | 2.4 | 3.75 | Goethite[a] |
| Elsner04 [*113*] | 1.42 | | | | | 32.5 | 22.89 | Lepidocrocite[a] |
| Elsner04 [*113*] | 1.42 | | | 4.5e-3 | 3.2e-3 | | | Lepidocrocite[a] |
| Elsner04 [*113*] | 1.82 | | | | | 4.75e-3 | 2.6e-3 | Hematite[a] |
| Elsner04 [*113*] | 1.82 | | | 3.75e-3 | 2.06e-3 | | | Hematite[a] |
| Zwank05 [*92*] | 2.8 | | | 6.9e-3 | 2.46e-3 | | | Lepidocrocite[a] |
| Zwank05 [*92*] | 3.6 | | | 1.0e-3 | 2.8e-4 | | | Hematite[a] |

[a] Acquired from Bayferrox. [b] Laboratory synthesized based on established methods.

Table 9. Published reduction rate constants of nitrobenzene (including 4Cl-nitrobenzene), carbon tetrachloride, and trichloroethene (and tetrachloroethene) by green rust

| Label and Reference | Mineral Dose (g/L) | Chloroethenes $k_{obs}$ ($h^{-1}$), $k_M$ ($h^{-1}$ $g^{-1}$ L) | | Chloromethanes $k_{obs}$ ($h^{-1}$), $k_M$ ($h^{-1}$ $g^{-1}$ L) | | Nitrobenzenes $k_{obs}$ ($h^{-1}$), $k_M$ ($h^{-1}$ $g^{-1}$ L) | | Notes |
|---|---|---|---|---|---|---|---|---|
| Maithreepala05 [*120*] | 15 | 7.58e-4 | 5.05e-05 | 0.0808 | 5.4e-3 | | | GR-Cl, pH 7.2 |
| O'Loughlin03 [*121*] | 5 | | | 0.0612 | 0.012 | | | GR-$SO_4$, pH 7.2 |
| Liang10 [*122*] | 10 | | | 11.837 | 1.18 | | | GR-Cl pH 8.0 |
| Liang09 [*62*] | 10 | 4.9e-5 | 4.9e-6 | | | | | GR-Cl, pH 8.0 |
| Liang09 [*62*] | 10 | 2.56e-4 | 2.56e-5 | | | | | GR-Cl, pH 8.0 |
| Lee02 [*60*] | 7 | 0.004 | 5.7e-4 | | | | | GR-$SO_4$, pH 8.1 |
| Lee02 [*61*] | 7 | 0.0021 | 3.0e-4 | | | | | GR-$SO_4$, pH 8.1 |
| O'Loughlin04 [*123*] | 5 | | | 0.060 | 0.012 | | | GR-$SO_4$, pH 7.0 |
| Elsner04 [*113*] | 0.55 | | | 0.18 | 0.33 | | | GR-$SO_4$, pH 7.0 |

Table 10. Published reduction rate constants of nitrobenzene (including 4Cl-nitrobenzene), carbon tetrachloride, and trichloroethene (and tetrachloroethene) by mackinawite

| Label and Reference | Mineral Dose (g/L) | Chloroethenes $k_{obs}$ ($h^{-1}$), $k_M$ ($h^{-1}$ $g^{-1}$ L) | | Chloromethanes $k_{obs}$ ($h^{-1}$), $k_M$ ($h^{-1}$ $g^{-1}$ L) | | Nitrobenzenes $k_{obs}$ ($h^{-1}$), $k_M$ ($h^{-1}$ $g^{-1}$ L) | | Notes |
|---|---|---|---|---|---|---|---|---|
| Zwank05 [*92*] | 4 | | | 2.43 | 0.609 | | | Not freeze dried |
| Zwank05 [*92*] | 0.6 | | | 0.063 | 0.106 | | | Not freeze dried |
| Butler00 [*124*] | 10 | | | 0.064 | 6.4e-3 | | | Freeze dried |
| Lipczynska94 [*125*] | 200 | | | 1.73 | 8.7e-3 | | | |
| Assaf-Anid02 [*126*] | 18 | | | 4.04 | 0.224 | | | |
| Kennneke03 [*117*] | 44 | | | 15.63 | 0.36 | | | Sigma Aldrich |
| Choi09 [*127*] | 33 | | | 1.24 | 0.038 | | | Not freeze dried |
| Devlin99 [*128*] | 0.73 | | | 0.045 | 0.061 | | | |
| AmirLee12 [*129*] | 4.17 | 1.3e-3 | 3.1e-4 | | | | | |
| Butler99 [*130*] | 10 | 5.7e-4 | 5.7e-5 | | | | | Freeze dried |
| Jeong07 [*131*] | 10 | 7.6e-4 | 7.6e-5 | | | | | Freeze dried |
| Liang07 [*132*] | 10 | 5.27e-5 | 5.3e-6 | | | | | |
| Butler99 [*130*] | 10 | 1.49e-3 | 1.5e-4 | | | | | |
| Butler01 [*133*] | 10 | 5.0e-4 | 5.0e-5 | | | | | Freeze dried |
| Butler01 [*133*] | 10 | 2.0e-3 | 2.0e-4 | | | | | Freeze dried |
| Liang07 [*132*] | 10 | 1.35e-5 | 1.4e-5 | | | | | |
| Liang07 [*132*] | 10 | 5.36e-4 | 5.4e-5 | | | | | |
| Jeong07 [*131*] | 10 | 2.12e-4 | 2.12e-5 | | | | | Freeze dried |
| He10 [*134*] | 63 | 6.3e-3 | 1.0e-4 | | | | | Not freeze dried |
| He10 [*134*] | 63 | 2.99e-4 | 4.75e-6 | | | | | Freeze dried |
| Elsner04 [*113*] | 1.98 | | | 0.4 | 0.202 | 425 | 214.6 | Not freeze dried |

## 10.3. Objective 2(B)—Bench Scale Applications to nZVI

Additional results from Objective 2 were published in Fan et al. (2015), the content of which is summarized in this section.

Fan, D., S. Chen, R. L. Johnson, and P. G. Tratnyek. 2015. **Field deployable chemical redox probe for quantitative characterization of carboxymethylcellulose modified nano zerovalent iron**. *Environ. Sci. Technol.* 49(17): 10589-10597. [DOI: 10.1021/acs.est.5b02804].

Nano zerovalent iron synthesized with carboxymethylcelluose (CMC-nZVI) is among the leading formulations of nZVI currently used for in-situ groundwater remediation. The main advantage of CMC-nZVI is that it forms stable suspensions, which are relatively mobile in porous media. Rapid contaminant reduction by CMC-nZVI is well documented, but the fate of the CMC-nZVI (including "aging" and "reductant demand") is less well characterized. Improved understanding of CMC-nZVI fate requires methods with greater specificity for Fe(0), less vulnerability to sampling/recovery artifacts, and more practical application in the field. These criteria can be met with a simple and specific colorimetric approach using indigo-2,6-disulfonate (I2S) as a chemical redox probe (CRP). The measured stoichiometric ratio for reaction between I2S and nZVI is 1.45±0.03, suggesting complete oxidation of nZVI to Fe(III) species. However, near pH 7, reduction of I2S is diagnostic for Fe(0), because aqueous Fe(II) reduces I2S much more slowly than Fe(0). At that pH, adding Fe(II) increased I2S reduction rates by Fe(0), consistent with depassivation of nZVI, but did not affect the stoichiometry. Using the I2S assay to quantify changes in the Fe(0) content of CMC-nZVI, the rate of Fe(0) oxidation by water was found to be orders of magnitude faster than previously reported values for other types of nZVI.

### 10.3.1. Introduction

Biogeochemical transformations of engineered nanomaterials (ENMs) significantly affect their fate, transport, and reactivity in environment [*135-138*]. Nano zerovalent iron (nZVI) is unique among ENMs in that it is deliberately released into the environment under conditions that take advantage of its high reactivity for degradation of contaminants in groundwater [*139-142*]. However, the high reactivity of nZVI with contaminants also applies to reaction with other groundwater constituents and aquifer materials, resulting in substantial "reductant demand" in the short term [*58, 143*], "aging" in the medium term [*144-146*], and stimulation/inhibition of various biogeochemical processes over the long term [*147-150*]. For example, detailed studies of aging products formed from RNIP—one of the first commercial nZVI products used for remediation—showed significant loss of Fe(0) and formation of other iron mineral phases after one month exposure to anoxic water [*144, 151, 152*] and common groundwater constituents [*146*]. Using another commonly studied type of nZVI (synthesized with borohydride [*153-155*]), we showed that sulfidic groundwater conditions result in formation to iron sulfides, which changes the sequestration pathway for technetium [*156, 157*]. However, these and most other studies of nZVI transformation (or aging) have been conducted in batch systems without the stabilizers used to make nZVI useful in field applications, which leaves considerable uncertainty regarding the transformation of stabilized formulations of nZVI under field conditions.

Many methods for improving the stability of nZVI suspensions have been investigated [*152, 158-161*], but one of the most widely used for field-scale groundwater remediation applications involves nZVI synthesized in the presence of carboxymethylcellulose (CMC) [*143, 160, 162-165*]. Despite extensive characterization of the physical properties of CMC-nZVI, and its reactivity *with* contaminants, less is known about the chemical transformation *of* CMC-nZVI, especially after emplacement under field conditions. This is partly because the small size (~10 nm) and dispersion of the nZVI on the CMC polymer matrix results in stable solutions, from which the nZVI can not be recovered by conventional methods (filtration, centrifugation, etc. [*166*]). Without recovered solids, characterization of the nZVI using standard methods for nanomaterials (transmission electron microscopy, X-ray absorption spectroscopy, and X-ray diffraction [*167*]) is generally not feasible. Instead, characterization of the fate of CMC-nZVI—in both lab and field studies—has been based mainly on methods that provide bulk analyses of solution samples.

The bulk analyses that have been used to characterize CMC-nZVI include methods that respond directly to nZVI and those that are indirect in that they respond to the products of reaction between nZVI and the medium [*81*]. The *direct* methods include spectrophotometry at 800 nm (where nZVI should be the only species with significant absorbance) [*81, 143*], or digestion followed by colorimetry for ferrozine complexed total iron [*81*]. *Indirect* methods that have been used to detect CMC-nZVI impacted fluids include measurement of changes in dissolved $O_2$, $H_2$, Fe(II), pH, and oxidation-reduction potential (ORP) [*5, 81*]. However, none of these bulk analysis methods are entirely specific for Fe(0) and the degree to which they are influenced by other reducing species (e.g., ferrous iron oxides and sulfides) is often uncertain. One assay that should be specific for Fe(0) involves acidification of samples and then measurement of $H_2$ from reduction of $H^+$, which has proven useful in laboratory [*151*] and field [*164*] studies, but aggressive digestion provides total Fe(0) and little information about the availability of that Fe(0) for reactions under environmentally relevant conditions. From a practical perspective, the most relevant way to characterize nZVI reactivity is by measuring the transformation kinetics and products of target (or model/probe) contaminants, but adding real contaminants for this purpose usually can only be done in laboratory studies and previously described "reactive tracer" compounds (e.g., trichlorofluoroethene, TCFE [*25*]) have not been evaluated for their behavior in ZVI containing systems.

In this study, we describe a simple, yet powerful, field-deployable method for characterizing nZVI reactivity and transformations using indigo-5,5′-disulfonate (I2S) as a reactive tracer or "chemical redox probe" (CRP). Although I2S and other redox active indicators have long been used in characterizing the redox properties of geochemical systems [*24, 29, 87, 168-170*], most of these studies have been focused on using indicator equilibrium to describe the thermodynamic conditions of the systems. In nZVI-containing systems, characterizing thermodynamic conditions is less useful because (*i*) the relevant species (Fe(0), Fe(II), Fe(III), $H_2$, etc.) are far from equilibrium with each other, and (*ii*) any Fe(0) containing system has more than enough thermodynamic potential to affect the reduction of most contaminants. Instead, kinetic and capacity considerations are more relevant for characterizing nZVI exposed to media because these aspects are what controls the rate and extent of contaminant degradation. In the present study, we designed

the experiments in such a way that I2S (which usually is used as a thermodynamic probe) serves mainly as a CRP for kinetic and capacity aspects of CMC-nZVI transformation and reactivity. The results suggest a practical method for characterizing nZVI that is deployable in the field as well as providing new insights into the factors that control the reactivity of nZVI in water.

## 10.3.2. Experimental

**Chemical Reagents.** All chemical regents except indigo-5,5′-disulfonate (indigo carmine, I2S) were ACS reagent grade and used as received without further purification. I2S was purchased from TCI America (Portland, OR), as the disodium salt, with 95% purity. Deoxygenated deionized (DO/DI) water was prepared by sparging with $N_2$ for 1 hr and used to prepare deoxygenated stock solutions in an anoxic glove box (100% $N_2$, $O_2$ < 0.8 ppm). Fresh CMC-nZVI suspension was prepared daily based on modified protocol adapted from He et al. [*159*], which is detailed below as Supporting Information to this section. The freshly-prepared CMC-nZVI was determined to be 100% Fe(0) based on $H_2$ produced by acidification [*151*].

**CMC-nZVI Incubations.** Several experimental variables—including CMC-nZVI concentration, pH, aging time, and presence of Fe(II) and various anions—were chosen to simulate a range of conditions that are likely to result in transformation of CMC-nZVI during its transport in the subsurface. Accordingly, the stock CMC-nZVI suspension (1 g/L) was diluted to the target concentration with deoxygenated 10 mM HEPES at pH = 7.2 or 8.5 into 12 mL serum vials and crimp sealed with butyl rubber septa. The exposure time varied up to 24 h, which was chosen to cover the initial time period of rapid reactions after CMC-nZVI is first introduced into the subsurface (based on the results of the pilot injection we described in Johnson et al. [*143*]).

**Probe Assay.** At each sampling point, the incubated CMC-nZVI suspension was further diluted with DO/DI to give 2–10 mg/L total iron with a final volume of 3.8 mL in a 1 cm cuvette. Dilution to low concentrations of nZVI was necessary to (*i*) give an initial rate of I2S reduction that is slow enough to measure accurately and (*ii*) make absorbance from CMC-nZVI negligible compared with I2S. The solution was buffered with 10 mM HEPES at pH 7.2 to avoid pH effects on probe reduction rate and absorbtivity of the probe. The cuvette was sealed with a Viton-lined screw cap and then transferred out of the anaerobic chamber. Because the oxidized form of I2S has maximum absorbance wavelength ($\lambda_{max}$) at 610 nm (Figure 25), the initial absorbance at 610 nm contributed by CMC-nZVI ($Abs_{ini}$) was measured (Perkin-Elmer, Lambda 20 UV-vis spectrophotometer). Aliquots of ~3.5 mM deoxygenated I2S stock solution (~0.17 mL) were then injected into the cuvette through the septum to make an initial I2S concentration around 140 µM. The cuvette was mixed by hand for 5 sec and placed into the UV-Vis spectrophotometer. The decrease in absorbance at 610 nm ($Abs_{610}$) was continuously recorded as a function of time. After the reaction was complete, the solution was reoxidized by opening the cuvette, allowing ~5 s exposure to ambient air, and then absorbance ($Abs_{reox}$) was remeasured to determine the exact initial concentration of I2S in solution.

## 10.3.3. Results and Discussion

**Probe Properties.** The oxidized quinoid form of I2S ($I2S_{ox}$) is bright blue ($\lambda_{max}$ = 610 nm) and the reduced dihydro form ($I2S_{red}$) is pale yellow ($\lambda_{max}$ = 407 nm) at circum-neutral pH [*29*]. At the concentrations used in this study (~140 µM), the reduction of I2S is easily detected by the visible change of solution color from blue to yellow. We have shown previously that the sulfonated indigo redox indicators do not adsorb significantly to most relevant, environmental materials (ZVI, iron oxides, sediments, etc.) [*29, 30*].

**Scheme 1**. Two-electron reduction half-reaction of indigo-5,5'-disulfonate.

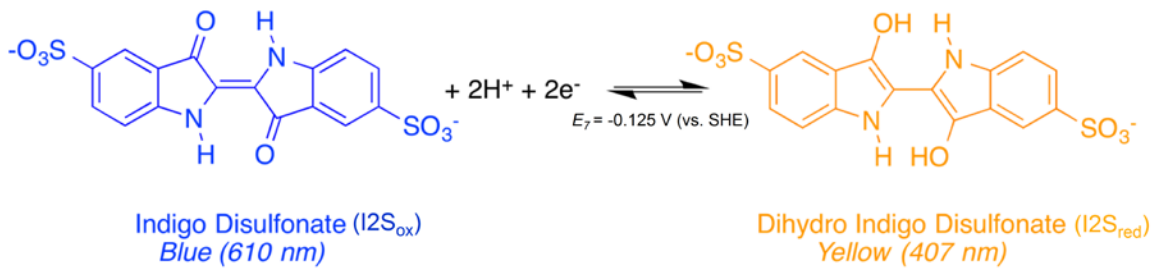


The overall half-reaction between $I2S_{ox}$ and $I2S_{red}$ (**Scheme 1**) has been studied thoroughly by potentiometric titration, and found to give Nernstian response with a formal reduction potential of +0.291 V vs. SHE at pH 0 ($E_0'$) and –0.125 V at pH 7 ($E_7$) [*99, 171*]. The semiquinone intermediate is not expected to be significant below pH 9 [*99*], and no evidence (e.g., red color) for it was noted. $I2S_{red}$ has one environmentally relevant $pK_a$ at 7.4 (for the first hydroxyl moiety) [*29, 99*], but there is no acid-base speciation of $I2S_{ox}$ to affect its absorbance spectrum. The speciation of I2S is summarized in the Eh-pH diagram shown in Figure 24. Superimposing the most relevant stability fields for the iron system reveals that reduction of I2S by Fe(0) is thermodynamically favorable by >17 kcal at all pH's, whereas reduction by Fe(II) phases, such as $Fe_3O_4$, is only marginally favorable (~3 kcal) around neutral pHs.

**Determining Apparent Stoichiometry.** The half-reaction for the reduction of $I2S_{ox}$ to the $I2S_{red}$ involves addition of two-electrons and two protons (Scheme 1). If Fe(II) is the end product of nZVI oxidation, then a 1-to-1 stoichiometric ratio between I2S reduced and CMC-nZVI oxidized is expected. To experimentally determine the reaction stoichiometry, we reduced ~140 µM $I2S_{ox}$ with freshly-synthesized nZVI at concentrations ranging from 2 to 10 mg/L (defined by the total iron)—corresponding to molar ratios of 0.25 to 1.25—and monitored the reaction by measuring $Abs_{610}$. The results (Figure 20A) show that the highest concentrations of nZVI (10 mg/L) gave a rapid decrease in absorbance, due to reduction of $I2S_{ox}$, followed by a well-defined plateau. At nZVI concentrations below 5 mg/L, the absorbance decreased more slowly and leveled out later at higher plateaus. The yellow color that developed in the aqueous phase of the high nZVI dose experiments indicates that there was complete reduction of $I2S_{ox}$ to $I2S_{red}$, and therefore the plateau absorbance was due to excess nZVI. At lower nZVI doses (2 and 4 mg/L), the aqueous phase was still blue at the end of the experiments, indicating that $I2S_{ox}$ was in excess, which contributes to the absorbance plateau.

To calculate the concentrations of I2S and nZVI based on absorbance spectra shown in Figure 20A, four species that could contribute to $Abs_{610}$ were considered, including $I2S_{ox}$, $I2S_{red}$, $nZVI_{red}$ (fully reduce material, as originally synthesized), and $nZVI_{ox}$ (fully oxidized material). The full absorbance spectra of individual species (Figure 25)—obtained independently, but at relevant concentrations—show that $I2S_{ox}$ contributed >90% of $Abs_{610}$, $nZVI_{red}$ contributed less than 10%, and neither $I2S_{red}$ nor $nZVI_{ox}$ (obtained by exposing fresh CMC-nZVI to air) contribute significantly. Using a calibration curve for $I2S_{ox}$ obtained at 610 nm (

Figure 26), the amount of I2S reduction was calculated from the difference in absorbance of (*i*) the fully reoxidized sample ($Abs_{reox}$) and (*ii*) the final, plateau absorbance ($Abs_{end}$) if I2S was in excess, or simply $Abs_{reox}$ if nZVI was in excess. Likewise, using the calibration curve for nZVI (

Figure 26), the amount of nZVI oxidation was determined from (*i*) the initial absorbance of the suspension before I2S addition ($Abs_{ini}$) if nZVI was completely oxidized, or (*ii*) the difference between $Abs_{ini}$ and $Abs_{end}$ (because $I2S_{red}$ showed little absorbance at 610 nm) if nZVI was in excess. The majority of the experiments were conducted with $I2S_{ox}$ in excess because the larger absorptivity of $I2S_{ox}$ gave more reliable measurements.

Plotting the amount of I2S reduction against the amount of nZVI oxidation for all experiments (Figure 20B), shows that the quantity of reacted I2S and nZVI give a strong linear correlation, for both fresh and aged nZVI. Regression on the correlation in Figure 20B gives a slope of 1.45±0.03, which is the experimental stoichiometry for reaction between I2S and nZVI, and is significantly greater than the 1:1 stoichiometry that would be expected if Fe(II) was the oxidation end point.

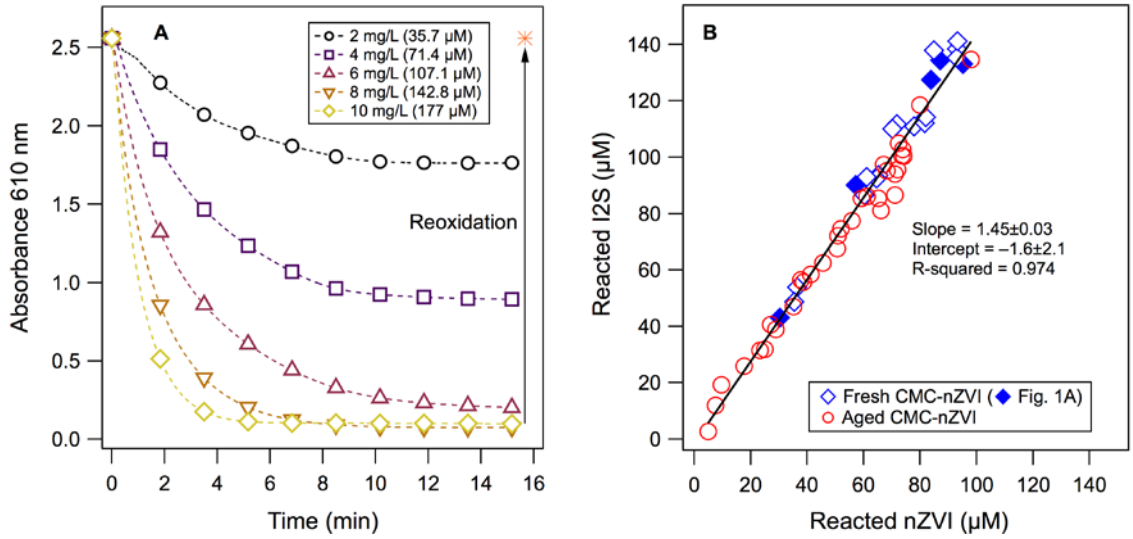


Figure 20. Determination of the apparent stoichiometry of I2S reaction with nZVI: (A) decrease in aqueous absorbance at 610 nm due to reduction of $I2S_{ox}$ by freshly-prepared CMC-nZVI diluted to the specified initial concentrations. The asterisk represents $Abs_{610}$ measured after sample reoxidation. (Data was recorded continuously, but markers are only shown every 1000 data points.) (B) Correlation between the

amount of I2S reduction and nZVI oxidation for fresh and aged CMC-nZVI (each data point is derived from an individual I2S reduction curve, including the examples in A, shown by solid diamonds. The solid line corresponds to the linear regression coefficients given in the graph).

The "excess" stoichiometry was not due to loss of $I2S_{ox}$ by adsorption to nZVI surfaces because reoxidation of the aqueous suspension at the end of the experiments immediately gave complete recovery of the initial absorbance at 610 nm (Figure 20A, asterisk). Alternatively, the excess could be due to reactions with reductants other than nZVI, such as residual borohydride from nZVI synthesis, or Fe(II) species (aqueous or solid) generated from nZVI oxidation by $I2S_{ox}$. However, residual borohydride should be negligible because the synthesis was performed with borohydride and Fe(II) at concentrations that exactly match the expected 2:1 stoichiometry of the Fe(0) formation reaction [*172*]. Reduction of I2S by aqueous Fe(II) at pH 7.2 was excluded, as well, because control experiments with aqueous Fe(II) gave negligible I2S reduction (Figure 27). The remaining candidate is solid phase Fe(II)—e.g., Fe(II) minerals or sorbed Fe(II)—which has been shown (as stronger reductants than aqueous Fe(II)) to reduce a variety of organic compounds, including redox mediators that are analogous to I2S [*86, 173*]. Complete oxidation of solid Fe(II) results in Fe(III) oxyhyroxide, which suggests the following overall reaction between Fe(0) and $I2S_{ox}$.

$$2\ Fe(0) + 3\ [I2S_{ox}] + 6\ H_2O \rightarrow 2\ Fe(III) + 3\ [I2S_{red}] + 6\ OH^- \quad (3)$$

Equation 3 suggests a stoichiometric ratio between $I2S_{ox}$ and Fe(0) of 1.5, which is consistent with the calculated ratio of 1.45±0.03, obtained from Figure 20B.

Note that the calculated stoichiometry is slightly less than the theoretical value of 1.5. This difference could be due to the parallel reaction between nZVI and water (i.e., anaerobic corrosion). Control experiments to characterize the rate of this reaction were performed by measuring the decrease in $Abs_{610}$ in DO/DI water, under the same conditions as probe assay but without I2S. The results (Figure 27) show that at pH 7.2, the reactions were slower compared to oxidation by I2S, but still caused 5─10% of Fe(0) loss over the time frame of probe assay. The Fe(0) loss was less at pH 8.5, but Figure 27 showed appreciable I2S reduction by aqueous Fe(II) only at this pH. Therefore, conducting the I2S assay at high pH might overestimate the quantity of Fe(0), especially under field conditions, where significant Fe(II) is likely to be present as a result of Fe(0) corrosion. Although the rates of nZVI reaction with water in the presence of $I2S_{ox}$ might be different than measured in Figure 28 due to competitive reaction with $I2S_{ox}$, these results are consistent with stoichiometric ratio of 1.45 being due to a small fraction of nZVI oxidation by $H_2O$ rather than by I2S.

**Fitting Second Order Kinetics.** In all experiments reported in this study, neither nZVI nor I2S were in significant excess, so the requirement for application of pseudo first-order kinetics was not met [*174, 175*]. Instead, the data were fit to a second order kinetic model adapted from a previous study on a system with some similar characteristics: reduction of lepidocrocite by reduced anthraquinone disulfonate ($AH_2DS$) [*88*]. To implement this model, several simplifying assumptions were made: (*i*) Fe(0) and all Fe(II)-containing solid phases were modeled as a single reducing species ), and (*ii*) the

reaction rate was first order with respect to the individual reactants nZVI and I2S. The reaction rate ($r$) for eq. 3 is given by eq. 4:

$$r = \frac{d\left[\mathrm{I2S_{ox}}\right]}{dt} = k''\left[\mathrm{I2S_{ox}}\right]\left[\mathrm{nZVI}_{red}\right] \tag{4}$$

where $[\mathrm{I2S_{ox}}]$ is the concentration of oxidized I2S (μM), $k''$ is the second-order reaction rate constant ($\mu M^{-1}\ min^{-1}$), [nZVI] is the concentration of nZVI. Solving eq 4 for of $\mathrm{I2S_{ox}}$ versus time (following the treatment by Shi et al. [*88*]) gave eq 5:

$$\left[\mathrm{I2S_{ox}}\right]_t = \left[\mathrm{I2S_{ox}}\right]_0 - \frac{1.5 \times \left[\mathrm{I2S_{ox}}\right] \times \left[\mathrm{nZVI}_{red}\right]_0 \times \left(e^{\left[\mathrm{nZVI}\right]_0 kt} - e^{2/3\left[\mathrm{I2S_{ox}}\right]_0 kt}\right)}{1.5 \times \left[\mathrm{nZVI}_{red}\right]_0 \times e^{\left[\mathrm{nZVI}\right]_0 kt} - \left[\mathrm{I2S_{ox}}\right] \times e^{2/3\left[\mathrm{I2S_{ox}}\right] kt}} \tag{5}$$

where $[\mathrm{I2S_{ox}}]_0$ is the initial $\mathrm{I2S_{ox}}$ concentration, $[\mathrm{nZVI}]_0$ is the initial nZVI concentration, and $k''$ is the second order reaction constant. The latter two parameters were determined by fitting eq 5 to $[\mathrm{I2S_{ox}}]$ vs. time data.

As can be seen from examples in Figure 21A, this approach fit the data very well, indicating that the second-order kinetic model (eq. 2) is appropriate for describing the kinetics of I2S reduction by CMC-nZVI under the conditions of this study. At relatively high nZVI/I2S ratios, a small but consistent degree of tailing was observed (e.g., 4 mg/L in Figure 21A), which may be due to (*i*) small contributions of nZVI (< 5%) to the overall absorbance (cf. Figure 25), which was not included when calculating I2S concentrations, or (*ii*) the inclusion of solid Fe(II) with Fe(0) in the term for [nZVI], which would not fully describe the I2S reduction kinetics if there was substantial variations in the contributions of Fe(0) and solid Fe(II). The model was fit only to the data where nZVI was completely consumed (2 and 4 mg/L total iron) because the quantity of I2S reduction can be more accurately determined than the amount of nZVI oxidation (due to high absorptivity of $\mathrm{I2S_{ox}}$, as noted above).

Another way to examine the kinetic modeling results is to compare the molar concentration of oxidized nZVI obtained from the fit to eq. 3 against those calculated from the $Abs_{610}$ measured before addition of I2S. The resulting correlation shown in Figure 21B (for all the conditions tested, not just the examples shown in Figure 21A) suggests good agreement between fitted and measured value for reacted nZVI as all the data points follow the 1:1 line with no bias and little scatter. Similar to Figure 20B, both fresh and aged samples were well described (Figure 21B), demonstrating that the model is sufficiently robust to be used in characterization of the range of subsurface media conditions created by the impacts of nZVI emplacement.

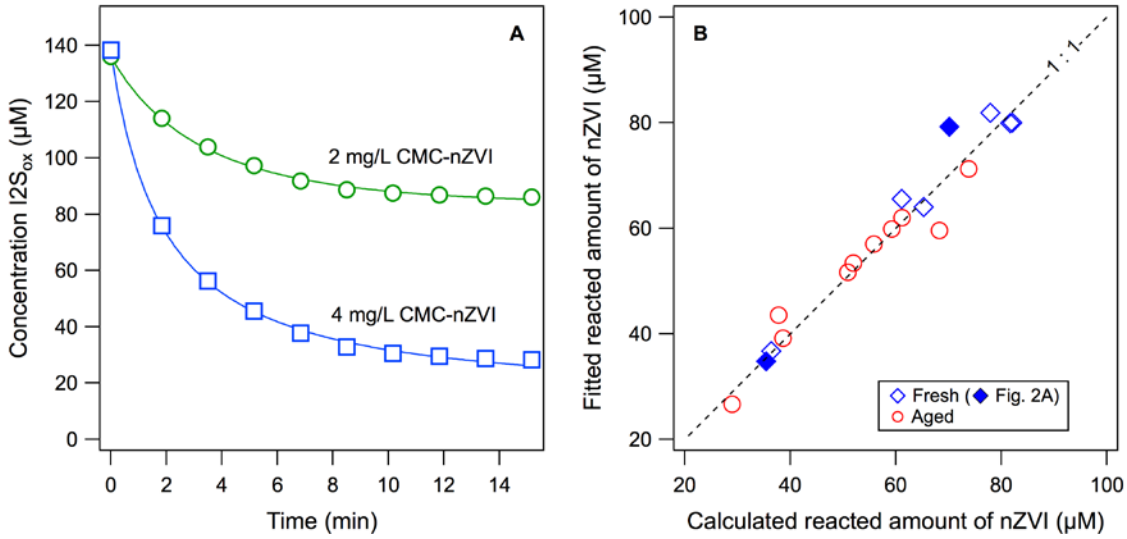


Figure 21. Second-order kinetic modeling: (A) Fitting of representative data for I2S reduction by freshly-prepared CMC-nZVI diluted to 2 and 4 mg/L in pH 7.2 HEPES buffer (the concentration was calculated based on the absorbance data shown in Figure 1A), (B) Correlation between oxidized nZVI determined by fitting and oxidized nZVI determined by absorbance.

**Distinguishing Fe(II) from Fe(0).** The negligible rate of I2S reduction by aqueous Fe(II) alone at pH 7.2 (Figure 27) suggests that I2S could be useful as a CRP to distinguish aqueous Fe(II) from Fe(0), such as to quantify the Fe(0) (as opposed to total iron) in groundwater samples used to characterize the distribution of nZVI after injection into the subsurface. Because aqueous Fe(II) would coexist with Fe(0) in field, we measured the rates of I2S reduction in mixtures of aqueous Fe(II) and CMC-nZVI, with Fe(0)/Fe(II) ratio varied from 0.25 to 4, but constant 10 mg/L total iron, at pH 7.2. These data are shown in Figure 22A, together with data for the corresponding nZVI dose without added Fe(II). With and without added Fe(II), the higher Fe(0) concentrations gave more complete reduction of I2S (similar to the results seen in Figure 20A and Figure 21A). The primary effect of added Fe(II) was to increase the rate at which the limiting I2S concentration was reached, but the Fe(II) does not appear to provide additional capacity for I2S reduction (because the limiting I2S$_{ox}$ concentrations are nearly the same with and without added Fe(II)). The quantity of I2S reduced at the plateau values is approximately 1.5 times the amount of nZVI oxidation in these experiments, which is consistent with the reaction stoichiometry determined above (eq 3), and further evidence that aqueous Fe(II) is not directly responsible for reduction of I2S.

The increased rate of I2S reduction caused by addition of Fe(II) to CMC-nZVI (shown in Figure 22A) was further investigated at 4 mg/L nZVI by systematically varying added Fe(II) from 0 to 15 mg/L (Figure 22B). The data were again fitted using eq 3 and the resulting rate constants ($k''$) are plotted against aqueous Fe(II) in Figure 22C (left axis). Increasing aqueous Fe(II) produced a monotonic, and nearly linear, increase in $k''$, whereas the plateau concentration of I2S decreased non-linearly with Fe(II) (right axis in Figure 22C). The difference between the two trends in Figure 22C could be because Fe(II) increases the rate of nZVI reaction with water as well, resulting in less Fe(0) to

reduce I2S. This effect would be consistent with several recent studies that have concluded that adsorption of Fe(II) to the oxide film on Fe(0) results in depassivation, accelerated corrosion of Fe(0), and concomitant enhancement of the reduction rate of target contaminants [*176, 177*]. Under the strictly anoxic conditions of this study, there should be little if any Fe(III) oxide on the unreacted nZVI. This suggests that the effect of aqueous Fe(II) on rates of probes/contaminant reduction might apply in non-aged (n)ZVI systems as well any system where the ZVI is passivated by significant quantities of Fe(III) oxides.

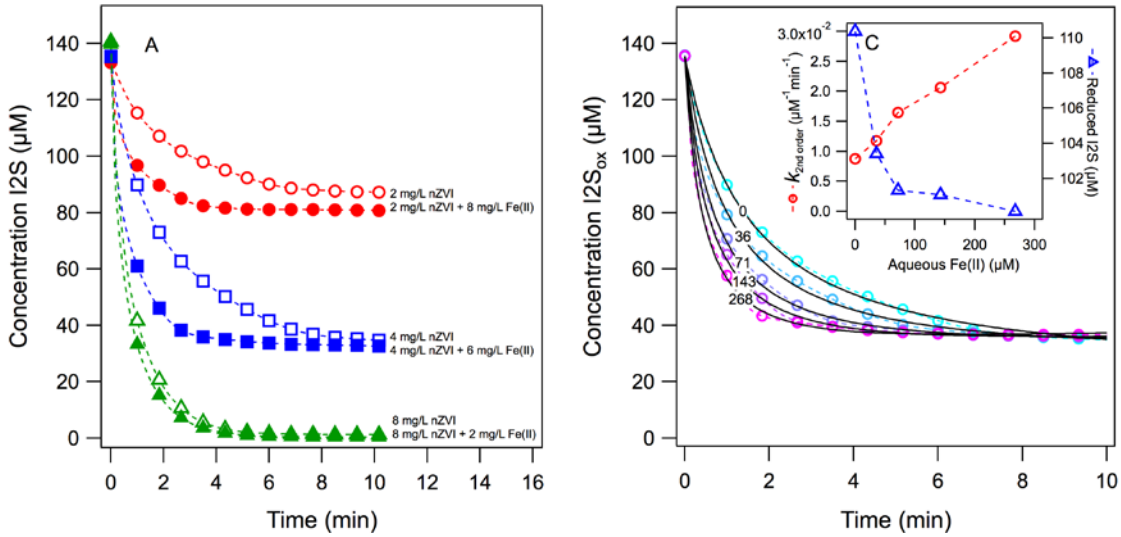


Figure 22. Effect of Fe(II) on I2S reduction by Fe(0): (**A**) I2S reduction by mixtures of Fe(II) and nZVI with the total iron concentration of 10 mg/L and equal concentrations of nZVI without Fe(II). (**B**) I2S reduction by 4 mg/L nZVI with aqueous Fe(II) concentrations from 0 to 15 mg/L (open symbols are experimental data, and solid lines are second-order kinetic fits). (C) Second-order rate constant (left axis) and amount of I2S reduction (right axis) extracted from fitting the data in Figure 21B.

Quantifying the Lifetime of nZVI in Water. An extension and application of using I2S as a CRP is for the quantification of nZVI transformation in the presence of background "reductant demand (i.e., oxidation by reaction with water). Previous studies that have addressed this issue have relied mainly on measurement of $H_2$ that is formed from reduction of water by Fe(0). This assay has been performed by measuring the volume or pressure of $H_2$ gas produced [*178, 179*], or concentration of dissolved $H_2$ by gas chromatography [*151, 180*], but the former requires large sample volumes and has low sensitivity and the latter requires special sample handling and relatively-specialized instrumentation. Even more specialized methods of determining Fe(0) include fitting of XRD and Mössbauer data [*144, 152, 181*]. In contrast, reduction of I2S provides an assay that is selective for Fe(0), requires only small sample volumes (<1 mL), provides immediate results, and can easily be implemented in the field.

To test the applicability of I2S for quantifying Fe(0) reaction with water, the I2S assay was applied to determine molar Fe(0) content (i.e., Fe(0)/$Fe_{total}$ [*144, 152*]) as function of time on CMC-nZVI suspensions with a range of initial nZVI concentrations

and pH's (chosen to represent the degree of nZVI dilution [*143*] and range of pH [*182*] that have been observed during injection and transport of CMC-nZVI in field). The initial portion of the resulting data (Figure 23) were fit by pseudo-first order kinetics, giving $k_{obs}$ ranging from 0.02 to 0.26 $hr^{-1}$ ($t_{1/2} \approx$ 3–33 hr). These rate constants are 2–3 orders of magnitude greater than previously reported rates for several conventional types of nZVI (determined by measuring $H_2$ evolution), which include 6 x $10^{-3}$ $d^{-1}$ for RNIP [*151*] and 2.72 x $10^{-2}$ $d^{-1}$ for NANOFER [*181*] (another widely used formulation of commercially available nZVI). The reaction rate of background reductant demand with CMC-nZVI is expected to be greater than other types of nZVI, because of the smaller size and greater dispersion of the primary particles in CMC-nZVI (Figure 31), but the large degree to which this process is accelerated with CMC-nZVI is another way (in addition to forming true solutions) in which this material is qualitatively different than the other Fe(0)-based reductants that are widely used.

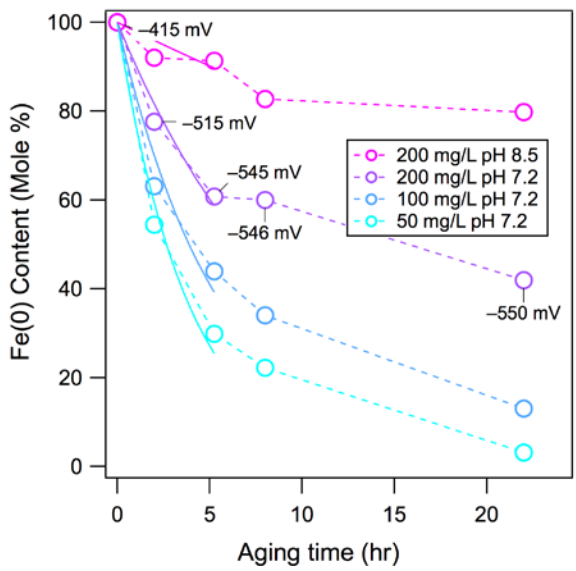


Figure 23. Quantifying the lifetime of nZVI in DO/DI water: Kinetics of Fe(0) oxidation by water with 50, 100, and 200 mg/L initial nZVI concentrations (in 10 mM HEPES buffer at pH 7.2) and 200 mg/L initial nZVI concentration (in 10 mM HEPES buffer of pH 8.5). Each data point was determined by I2S reduction in subsamples of the nZVI suspension). Labels are ORP measured with a Pt electrode and reported vs. SHE.

The half-lives that correspond to the kinetics shown in Figure 23 are on the order of hours, which matches the time-frame of typical laboratory column or field transport studies of nZVI. In most of these studies, the implications of Fe(0) oxidation by reaction with water—although occasionally reported [*182*]—are not fully evaluated. The results presented here suggest that the decrease in Fe(0) content of CMC-nZVI may be great enough to influence the kinetics of contaminant degradation measured in batch experiments with contaminants such as the chlorinated ethenes (TCE, etc.) because they react more slowly than water with CMC-nZVI. Over longer time-periods, such as during full-scale field applications, the conversion of Fe(0) to Fe(II) by background reductant demand processes is certain to have a large effect on net rates of contaminant reduction (given that most contaminants are reduced much more rapidly by Fe(0) than Fe(II) in any

form) [*46, 183*]. Therefore, characterization of nZVI delivery in field applications should be based mainly on assays that can distinguish Fe(0) from other iron species, and this could be done efficiently with the I2S described here.

The results (Figure 23) show that the rate of Fe(0) loss (normalized to the initial nZVI dose)—due to reductant demand from reaction with water—is mostly affected by two parameters that vary significantly under field conditions: pH and the concentration of nZVI (except for phosphate, adding 0.5 mM of various anions had minimal effects (Figure 30). The data in Figure 23 suggests that the Fe(0) loss rate was greatest at lower initial Fe(0) concentrations, which implies that the dilution of nZVI (e.g., downgradient from an injection point) will cause the reaction rate with reductant demand to increase. Note that the concentrations used in prior studies on nZVI dissolution rates were at least one order of magnitude higher than the concentrations tested here, which are more representative of the field conditions. Therefore, the expected dissolution rates of those types of nZVI in field (if applicable at all) might be higher than the reported values.

With respect to pH, for 200 mg/L CMC-nZVI, Fe(0) loss was significantly slower at pH 8.5 than at 7.2. Loss of Fe(0) was also relatively slow in the freshly prepared CMC-nZVI suspension (without dilution in HEPES buffer), which had high concentration (1 g/L) and high pH, and for 200 mg/L nZVI aged in DO/DI water without buffer (Figure 29). It is worth noting that for the latter experiment, initial Fe(0) loss was still fast (slope similar to 200 mg/L nZVI in pH 7.2 buffer) but tailing becomes evident after about 5 hr, possibly due to the increase in pH (up to ~9) driven by reaction of Fe(0) with water. These results are consistent with a previous study that showed $H_2$ production for RNIP was inhibited at high pH [*151*]. In that study, the formation of iron oxides (such as $Fe_3O_4$ or green rust) was invoked as a potential explanation for suppressing $H_2$ production. While $Fe_3O_4$ formation was plausible (e.g., by the Shickorr reaction [*181*]), it is not certain that the same mechanism applies under the conditions of this study. One argument against significant passivation of CMC-nZVI by coating Fe(0) with $Fe_3O_4$ is that reduction of I2S dominated by $Fe_3O_4$ should produce a stoichiometry of 1:2 (based on electron equivalence calculations similar to those described), but the observed I2S/Fe(0) stoichiometric ratio remained about 1.4 throughout the experiments shown in Figure 4 (data not shown). Nevertheless, the possibility of forming a thin/conductive layer of $Fe_3O_4$—which might not affect the apparent overall stoichiometry—cannot be excluded. Detailed characterization of surface layer mineralogy would be needed to address this issue, but only the TEM given in Supporting Information (Figure 31) was performed as part of this study.

Oxidation reduction potential (ORP) was measured using a combination (Pt) ORP electrode on the samples from the experiment with 200 mg/L nZVI at pH 7.2. The results—given as annotations in Figure 23—show that the ORP became more negative as Fe(0) content decreased (due to reaction with water). This trend is opposite to the relationship between ORP and Fe(0) that is commonly assumed when ORP is used as an indicator for nZVI in studies of emplacement and transport [*81*]. However, several effects that complicate the interpretation of ORP measurement in the presence of nZVI have been identified [*5, 81*], and the ORP data in Figure 4 apparently reflect those effects. For example, the sensitivity of Pt ORP electrodes to dissolved $H_2$ probably explains why the measured ORP decreased from −415 mV to −550 mV during the first 2 hr, whereas the

Fe(0) content (determined by the I2S assay) decreased 20%. Later, the decrease in measured ORP appears to have leveled out to a greater degree than the decrease in Fe(0) content, which again is consistent with the Nernstian response of the Pt electrode in a system that is accumulating high concentrations of $H_2$. These complications in interpretation of the ORP data are further evidence for why ORP measured with a conventional Pt electrode is not a straight-forward indicator of the presence of nZVI and probably only should be used in conjunction with complementary methods [*81*] including I2S as a CRP for Fe(0).

**Implications for Field Applications and nZVI Improvement.** The selectivity of I2S for Fe(0) could make this assay especially beneficial for field applications of nZVI, where the abundance of co-existing redox active species and complex water chemistry greatly complicates the ability of conventional methods (e.g., ORP) to detect Fe(0) impacted zones. A simple and robust protocol for field deployment would be to inject a known volume of water sample containing nZVI into a deoxygenated and buffered solution with known concentration of I2S in a sealed vial (prepared in advance in the laboratory). After injection, the absorbance change at 610 nm can easily be recorded over time with a portable spectrophotometer. The concentration range of nZVI should be diluted to less than half of the initial I2S concentration used, to ensure complete consumption of nZVI (based on the stoichiometric ratio of reaction between nZVI and I2S calculated from Figure 20**B**). The required dilution factor can be pre-determined by estimating the nZVI concentration in the water samples with a total iron or absorbance measurement. Although measuring the initial absorbance of nZVI suspension without I2S can be used in quantifying nZVI concentration in laboratory (Figure 25**)**, it will likely be less reliable in field applications because of interference from background turbidity or absorbance in natural groundwater samples. The CRP approach, on the other hand, is not subject to interference by background absorbance because the change in absorbance is used for calculating nZVI concentration.

Current field scale applications of nZVI are limited primarily by two factors: transport and longevity. Many approaches have been proposed to overcome the transport or longevity limitations of nZVI, but many solutions for one limitation are contradictory to solutions to the other limitation. These contractions are especially evident for CMC-nZVI, which has enhanced mobility, but orders of magnitude shorter lifetime in groundwater than most other types of nZVI. Refining nZVI formulation to achieve balance between these two aspects should be the focus of the next phase nZVI development. During this process, the reactions with I2S (and potentially other CRPs) could serve as an easy and quick assay to more efficiently evaluate the reactive transformations of nZVI and their effects on nZVI lifetime and provide guidance on improved design of nZVI to achieve field applicability. In addition, data on the rates of probe compound reduction might facilitate “higher order” use of CRP data, such as developing correlations with the relatively slow kinetics of contaminant reduction to allow rapid screening of the reactivity of nZVI to target contaminants.

## 10.3.4. Supporting Information for Fan et al. 2015 [*184*]

### 10.3.4.1. Method Details

**Synthesis of CMC-nZVI.** CMC-stabilized nZVI suspensions were synthesized with the same procedure we used in Johnson et al. [*143*] which was based on the method developed by He et al. [*159*] The suspension was prepared in 50 mL batches in a 120 mL serum bottle, while purging the suspension with $N_2$ throughout the synthesis process. Starting with a CMC solution (0.5% w/w) prepared in 40 mL DO/DI water, 0.89 mM $FeSO_4 \cdot 7H_2O$ was added to give an Fe(II) concentration of 1 g/L. The solution was mixed for 10 min to allow Fe(II)–CMC complex development. Then, a 10-mL solution containing 0.0675 g of $NaBH_4$ (twice the stoichiometric amount needed to completely reduce Fe(II) to Fe(0)) was added, dropwise, to the Fe(II)–CMC mixture, dropwise, with continuous swirling by hand. After all the $NaBH_4$ was added, the reaction was allowed 10 min for $H_2$ evolution to subside. The bottle containing the nZVI suspension was then crimp sealed and moved into the anoxic glove box. The suspension was prepared daily and used immediately.

The Fe(0) content of the freshly-prepared CMC-nZVI was determined at by acidification of samples. measurement of the $H_2$ produced by gas chromatography (with an Supelco Carboxen-1010 column and thermoconductivity detection), and calculation assuming 1:1 stoichiometry for $H_2$ production from corrosion of Fe(0) [*151*]. Transmission electron microscopy (TEM) was used to confirm that the composition of the CMC-nZVI synthesized was consistent with prior work on with the material (Figure 31).

**Transmission Electron Microscopy.** Samples for TEM were prepared by applying a 5 µL drop of CMC-nZVI suspension onto a Cu-carbon grid and letting it dry overnight in the anaerobic chamber on a filter paper. The samples were then sealed under $N_2$ and transported to the imaging facility. During the sample loading, there was approximately 1 min exposure to the ambient atmosphere. The TEM images were taken by FEI Tecnai F-20 TEM.

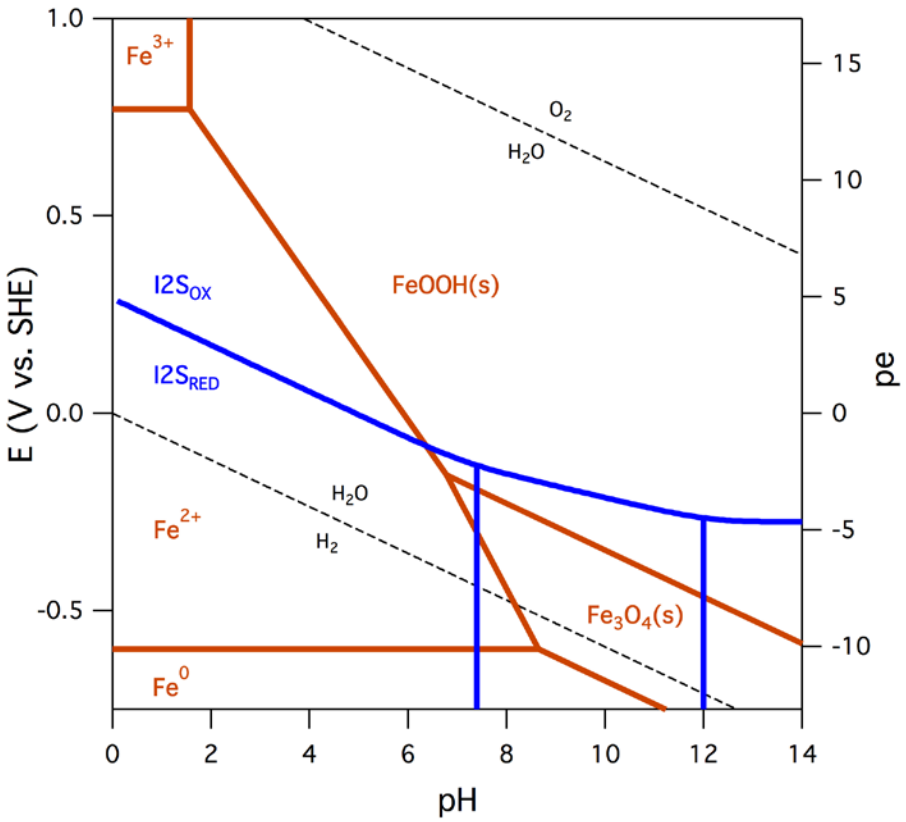


Figure 24. Eh-pH diagram for species of I2S and iron (Fe(II) = 4 mg/L; Temperature = 298 K; Suppressed iron phases: hematite). Speciation modeling for iron performed using the Geochemist's Workbench modeling package (RockWare Inc., Golden, CO). Thermodynamic data for I2S from references [*99, 171*]. The vertical lines in blue separate the fully protonated, monoanionic, and dianionic species of $I2S_{RED}$ (respectively from left to right).

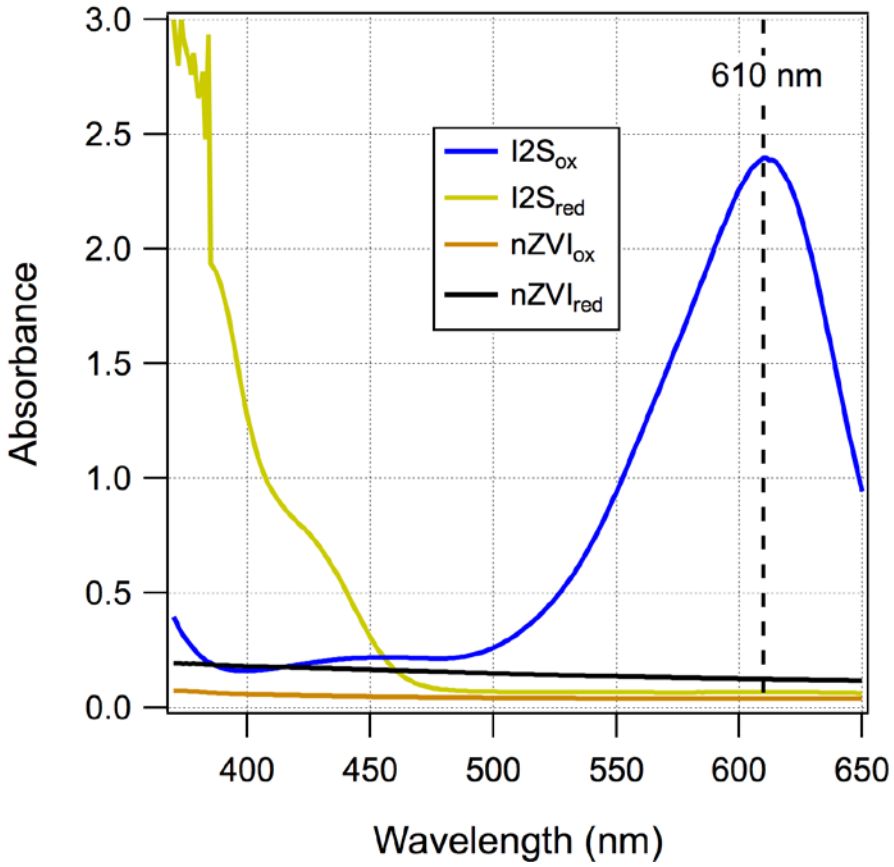


Figure 25. Absorbance spectra of ~140 µM I2S$_{ox}$ and I2S$_{red}$ and 4 mg/L nZVI$_{ox}$ and nZVI$_{red}$ in deoxygenated 10 mM HEPES buffer at pH 7.2. (I2S$_{red}$ was prepared by adding 1 drop of freshly-prepared 1 M sodium dithionite into the I2S$_{ox}$ solution; nZVI$_{ox}$ was prepared by exposing the nZVI$_{red}$ suspension to ambient air).

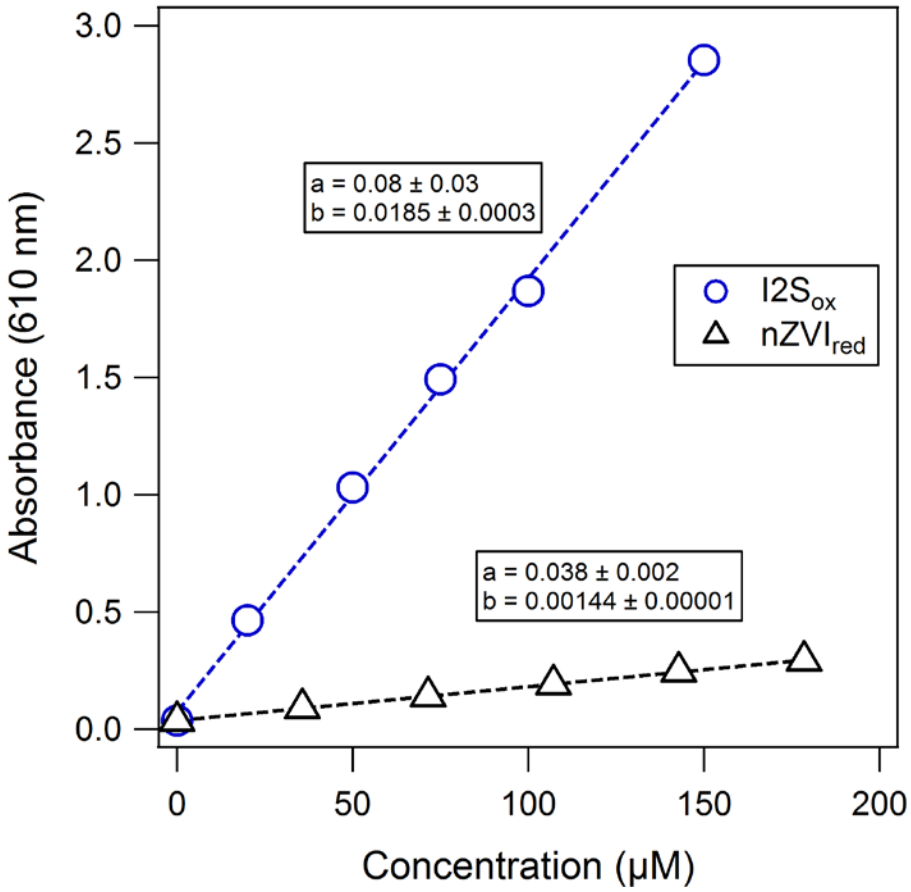


Figure 26. Calibration curves ($y = ax + b$) for absorbance at 610 nm for $I2S_{ox}$ and freshly-prepared CMC-nZVI ($nZVI_{red}$), both in 10 mM HEPES buffer at pH 7.2. Spectrophotometry performed in a screw-cap sealed optical glass cuvette with 1-cm path length.

The calibration curve for $I2S_{ox}$ corresponds to an extinction coefficient of 18.5 $mM^{-1}$ $cm^{-1}$ which is comparable to the previously reported value for DI water (20.0 $mM^{-1}$ $cm^{-1}$) [*29*]. The calibration for $nZVI_{red}$ is unique to the conditions of this study, but analogous examples and discussion of the rational for this assay have been reported previously [*81*, *143*].

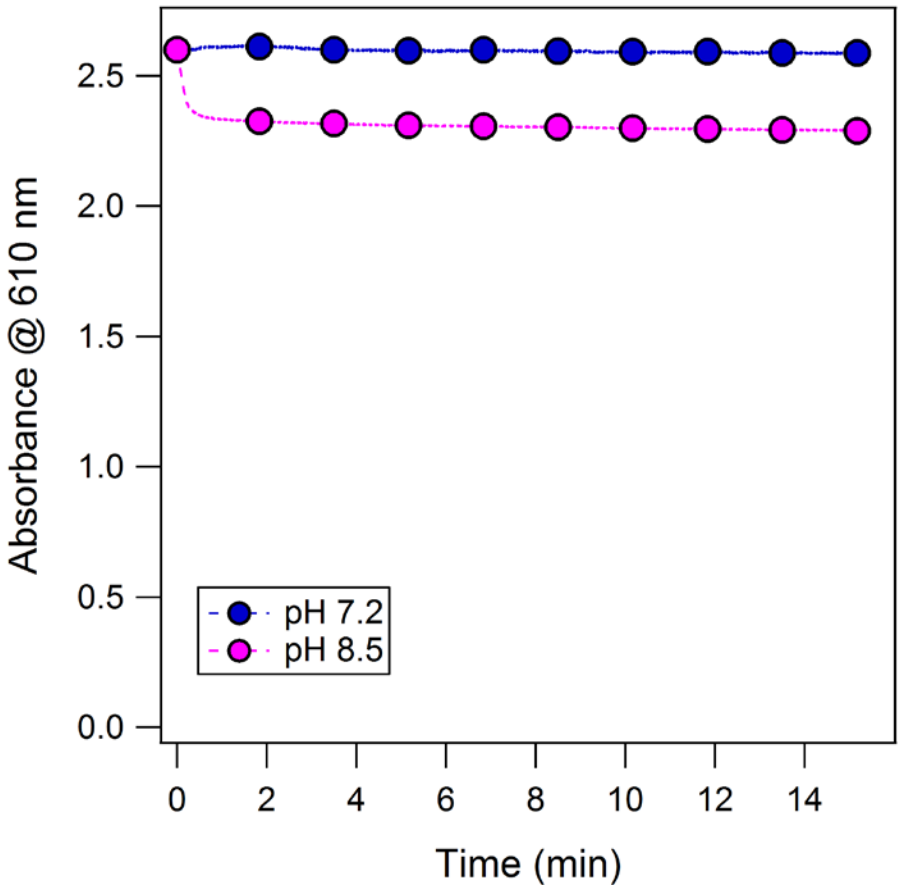


Figure 27. Change in $Abs_{610}$ due to reduction of I2S by 10 mg/L aqueous Fe(II) (without nZVI) at pH 7.2 and 8.5 with 10 mM HEPES buffer. The initial concentration of I2S was ~140 µM.

**Figure S4** shows that reduction of I2S by divalent iron was negligible at pH 7.2 and about 10% at pH 8.5. The greater reduction at pH 8.5 is consistent with the more favorable free energy of this reaction at higher pHs (see Figure 24). At pH 8.5, $Abs_{610}$ rapidly dropped in the first 30 s and then reached a plateau. Based on the difference between plateau and initial absorbance, the amount of I2S reduction is ~17 µM. By contrast, the total Fe(II) concentration is ~170 µM, which in theory should give 85 µM I2S reduction if the reaction is capacity limited. The much less I2S reduction indicates that the reaction is limited by thermodynamics rather than capacity. The fast initial reduction is consistent with the rapid reduction of redox mediators by other iron based reductants [*78, 86*].

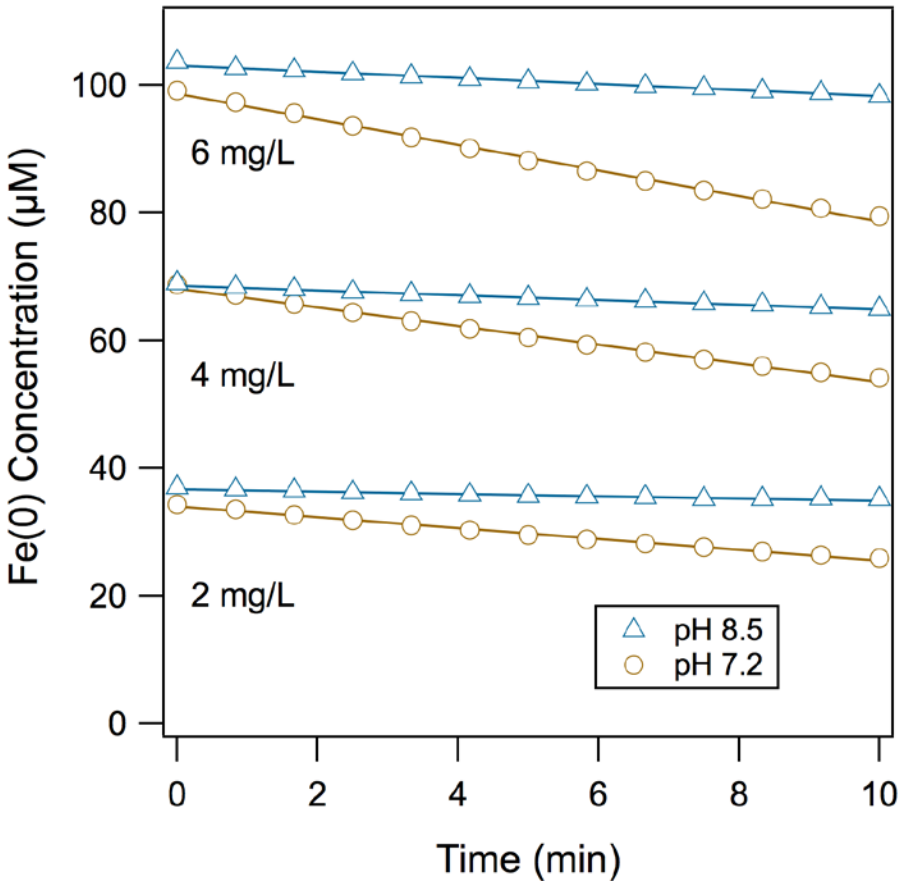


Figure 28. Change in Fe(0) concentration due to reaction with water only (without I2S) in 10 mM HEPES buffer at pH 7.2 and 8.5. Initial concentrations of CMC-nZVI were 2, 4, and 6 mg/L. Fe(0) concentrations are calculated by the $Abs_{610}$ using the calibration curve of $nZVI_{red}$ shown in Figure 26.

Prior work on the stability of nZVI suspensions has noted decreases in absorbance (usually at 508 nm) that were attributed to aggregation and settling/sedimentation of the nZVI [*143, 158, 185*]. With the materials and methods used in this study, we also found there is a gradual decrease in absorbance at 610 nm (Figure 28), but ultrasonication of the suspension did not bring the absorbance back to the initial values. Therefore, the decrease in absorbance shown in Figure 27 was not primarily due to particle aggregation/settling, and instead must be due to oxidation of nZVI by water. Although aggregation/settling is more rapid at the higher nZVI concentrations that are typically used for characterizing physical stability, decolorization of CMC-nZVI suspensions due to oxidation with water should also be considered, especially over longer time periods (as shown in Figure 23).

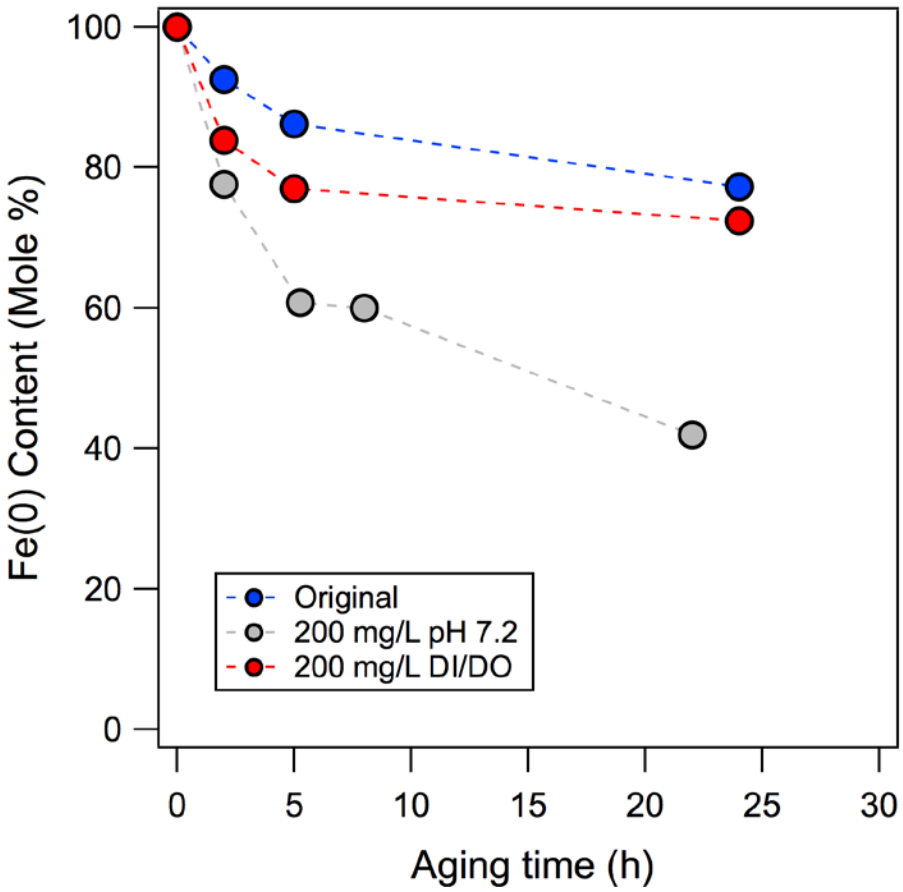


Figure 29. Decrease in Fe(0) content over time (due to oxidation in water, etc.) for the freshly-synthesized CMC-nZVI stock solutions and solutions of nZVI diluted to 200 mg/L nZVI in DI/DO and in pH 7.2 10 mM HEPES buffer. The latter data (gray symbols) are also shown in Figure 4 of the main text.

The data in Figure S6 provide control data (without HEPES buffer) for comparison with the results in Figure 4 (main text). The initial rate of Fe(0) oxidation is fastest for the sample buffered at pH 7.2 (grey), whereas the other two samples appear to oxidize more slowly. However, the dissolution rate for 200 mg/L nZVI in DO/DI water was initially similar to that for 200 mg/L nZVI buffered at pH 7.2, but gradually decreased, suggesting that pH increase over time in DO/DI water due to corrosion of Fe(0) might result in slower Fe(0) loss.

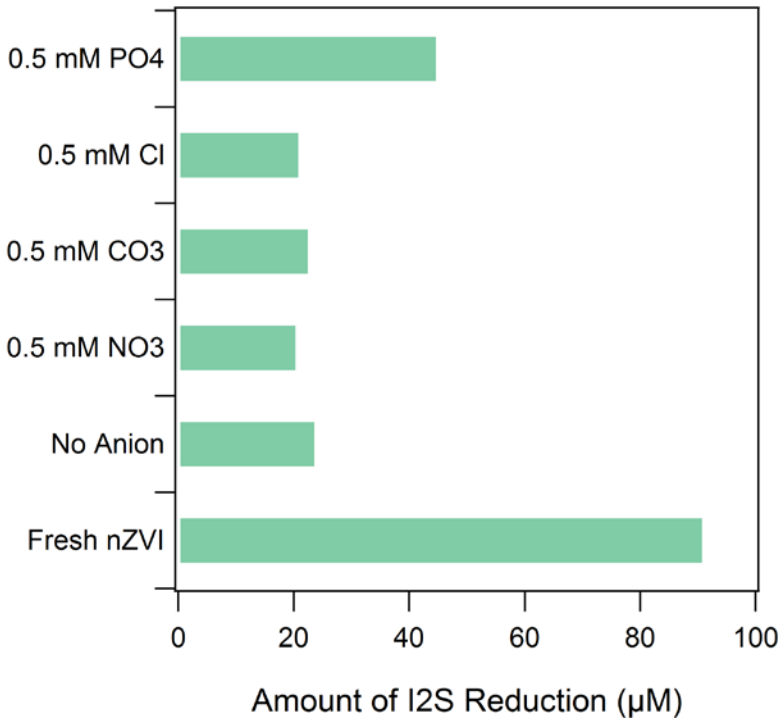


Figure 30. Effects of anions on the reduction capacity of Fe(0), represented by the amount of I2S reduction by nZVI suspension after 24 h exposure ([anion] = 0.5 mM, [nZVI] = 200 mg/L, pH = 7.2. For I2S reduction, 200 mg/L nZVI was further diluted to 4 mg/L in 10 mM HEPES buffer at pH 7.2).

The effects of common groundwater anions on reduction of I2S by CMC-nZVI are shown in Figure 30. The amount of I2S reduction was measured after reacting freshly prepared CMC-nZVI (diluted to 200 mg/L) with different anions of 0.5 mM concentration for 24 h at pH 7.2. The results showed that I2S reduction in the presence of chloride, carbonate, and nitrate did not differ significantly from the control (with no anions added), which exhibited more than 70% loss of I2S reduction capacity compared to fresh nZVI.

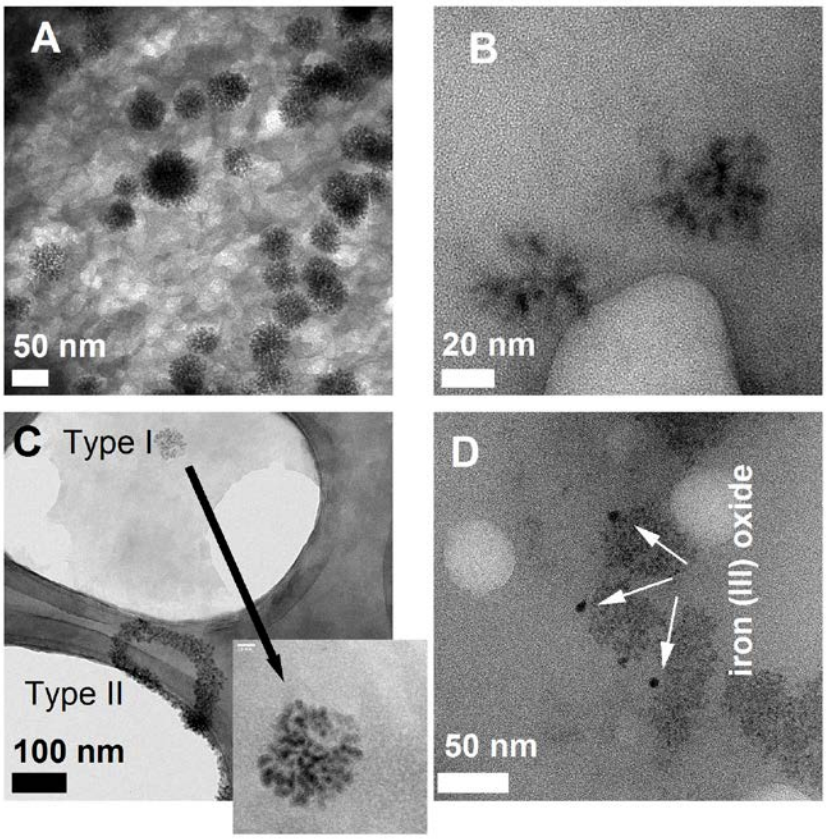


Figure 31. Transmission electron micrographs of (**A**) original CMC-nZVI aged for 24 h, (**B**) 200 mg/L CMC-nZVI aged for 24 h in DO/DI water, (**C**) 200 mg/L CMC-nZVI aged for 24 h in pH 7.2 HEPES buffer, and (**D**) 100 mg/L CMC-nZVI after complete oxidation by I2S.

TEM images of selected samples were obtained, in order to provide microscopic evidence to support the interpretations made based on the probe results. The probe data shown in Figure 23 and Figure 29 indicated after 24-h aging, the original CMC-nZVI and 200 mg/L CMC-nZVI in DO/DI water had significantly less Fe(0) loss than 200 mg/L CMC-nZVI in pH 7.2 HEPES buffer due to high pH. Here, we compared TEMs obtained for these three conditions. Figure 31A shows that despite 24-h aging, the morphology of the original CMC-nZVI particles was consistent with that reported by prior literature [*182*]. The individual particles are dark spheres with the diameter ranging from 20 to 60 nm (Figure 31A). For 200 mg/L nZVI aged in DO/DI water for 24 hr, however, the integrity of individual particles substantially degraded (Figure 31B). Given similar pHs (above 9) between original CMC-nZVI and 200 mg/L CMC-nZVI in DO/DI water, the remaining factor that could favor this morphological change is the concentration of nZVI. However, in a previous field study, little morphological change was found between injected CMC-nZVI and CMC-nZVI recovered from adjacent monitoring well after 5 hr injection [*143*], and the explanation for the discrepancy between these two studies was not further investigated.

For nZVI aged in pH 7.2 buffer, two types of structures are observed. Type I showed similar morphology to the original nZVI but the interior was less well defined (Inset in Figure 31C). Type II structure in HEPES buffer at pH 7.2 is the chain-like aggregate composed of very fine particles (<5 nm). It remains unclear whether this structure originated from the suspension or precipitated on the grid during the drying process. We speculate the latter might be the case as formation of ferrous hydroxide is not favored at this pH even when 200 mg/L Fe(0) is completely converted to Fe(II). The absence of this type of structure in prior two samples further suggested this fine structure might indeed result from artifacts of dissolved Fe(II), which is not favored at high pH. This supports our interpretation that fast corrosion at neutral pH produces dissolved Fe(II), which further causes loss of I2S reduction capacity (Figure 29). In the last sample, where 100 mg/L nZVI was completely consumed by adding high dose of I2S (Figure 31D), the original nZVI structure was not observed at all. Instead, <10 nm particles were prevalent, presumably as the iron(III) oxide particles.

## 10.4. Objective 3—Column-Pilot Scale Demonstration

The major results of Objective 3 will be published the following journal article, and the results that follow is mostly summarized from that article.

Johnson, R. L., C. M. Kocur, G. O'Brien Johnson, and P. G. Tratnyek. 2017. In situ thermodynamic and kinetic redox measurements using single-well: "Pull-push-pull" tests and chemical reactivity probes. Environ. Sci. Technol. in preparation.

A method for improved in situ thermodynamic redox and abiotic kinetic measurements is presented. The method involves injecting groundwater containing the oxidized form of a redox-sensitive dye (indigo disulfonate or anthraquinone sulfonate) into porous media where it is reversibly reduced by abiotic reactions. Tests can be used to determine reduction potential by allowing the dye to equilibrate in the medium, then extracting and measuring the ratio of oxidized to reduced forms of the dye and applying the Nernst equation. Alternately, the tests can be applied in "continuous flow" mode in which the dye is injected for a period of time, and then continuously extracted to spectrophotometrically measure the decrease in the oxidized form (and increase in the reduced form) as a function of time to yield a reduction rate constant. Results from laboratory column studies under iron- and sulfate-reducing conditions show good thermodynamic agreement between the CRP method and a conventional platinum electrode (with electron shuttle). Kinetic measurements show greater reactivity in the sulfate-reducing column as well as a decrease in reactivity down the 0.5m-long columns after more than one year of operation. The data suggest that measurement of kinetic rate in addition to reduction potential is necessary to understand in situ reactions. The methods can be performed in the field under conditions very similar to those described here and represent a practical alternative to conventional field redox measurements.

### 10.4.1. Introduction

Abiotic reduction of chemicals in groundwater can play an important role in restoration of complex contamination sites. This is the case, in part, because those reactions can occur in portions of sites where our inability to deliver reactants makes enhanced

remediation difficult (e.g., within low-permeability zones). At the same time, those areas can contain mineral phases that are sufficiently reducing to degrade chlorinated solvents, explosives and other contaminants. The rates of these mineral reactions are generally quite slow (e.g., half-lives of 1 year or greater) and, as a consequence, they can be difficult to quantify.

In earlier laboratory work we demonstrated that chemical reactivity probes (CRPs), including redox-sensitive dyes, could be used to improve measurement of reduction potential [*108*]. In addition, those same CRPs were used in batch kinetic experiments to demonstrate reduction rates on a variety of mineral surfaces [*108, 184*]. The focus of the work described here was to examine if those same approaches could be used to make measurements in situ in laboratory columns and, by extension, field measurements in the subsurface.

The application of redox-sensitive dyes to measure oxidation/reduction potential using UV/Vis spectrophotometry is well documented [*10, 29, 30, 186, 187*]. Basically, the equilibrium ratio between the oxidized and reduced forms of the dye is determined by changes in absorption and the potential is calculated based on that ratio is used along with the standard reduction potential for the dye in the Nernst equation.

In situ measurement of reduction potential has been shown to be important because the surface of mineral phases (rather than the extracted solution phase) plays a controlling role in determining reduction potential. As a consequence, a “probe” which can directly access the surface will provide a more-accurate measure of potential than, for example, a platinum electrode measuring only the water phase. In the work reported here, we have developed a methodology for measuring in situ reduction potential using “pull-push-pull” tests. These tests, often called “single-well injection-withdrawal” or “push-pull” test, have been extensively used to measure microbiological reactions in the subsurface (e.g., sulfate and iron reduction) and have been summarized by Istok [*188*].

To our knowledge, abiotic reactions (and in particular, abiotic contaminant degradation reactions, have not been examined using push-pull tests. This is due, at least in part, to the much-slower rates of those reactions (e.g., half-lives of months to years). Here we use CRPs as a proxy for abiotic reactivity. While this approach may not allow estimation of absolute abiotic reaction rates, it likely provides a good measure of relative rates, and it allows measurement of reactivity over time frames of minutes to hours, rather than years.

## 10.4.2. Methods

### 10.4.2.1. Column setup

For these experiments, two laboratory columns were operated for more than one year. They consist of 2 inch O.D. polycarbonate with flanges on each end (Figure 37). Each column was ~50 cm long and was filled with medium beach sand from the Columbia River. One percent by weight magnetite sand was added to both columns. The flow system for the columns is shown schematically in Figure 37. Water flow to each column is provided by a dedicated ceramic piston pump running at 1 mL/min. The source of the

water is a stock solution containing 10 mM lactate and 6.4 mM $Na_2CO_3$. Prior to being pumped into the columns, oxygen is stripped from the water using a counter-current stripper and UHP nitrogen gas. The pH of the column influent is ~7.2. For the sulfate column, a computer-controlled syringe pump delivers a 10.4 mM sulfate solution at 0.025 mL/min to the water just downstream from the ceramic-piston pump.

A suite of chemical measurements were made on the influent solution and column ports. Depending on the column, these included pH, iron (total and ferrous), lactate, sulfate and sulfide.

#### 10.4.2.2. Thermodynamic measurements

#### 10.4.2.3. Selection of appropriate redox dye

A number of redox-sensitive dyes are available for the kinds of measurements proposed here (see Figure 38 for a partial list). Each dye has a useful reduction potential range of ~+/-100 mV. We have used two sulfonate dyes, indigo disulfonate (I2S) and anthraquinone sulfonate (AQS). I2S has a reduction potential at neutral pH of -0.125 volts and AQS has a value of -0.225 V, so taken together they have a range appropriate for the iron and sulfate reducing conditions anticipated in the columns.

#### 10.4.2.4. Design of the pull-push-pull tests

As discussed above, push-pull tests have been widely used to measure biologic processes. We have chosen to designate these tests as pull-push-pull test to emphasize the importance of the injection solution used in the test. In both the laboratory and field contexts, it is important that the geochemistry of the injection solution be as close as possible to the groundwater. As a consequence, the injection solution was prepared by diluting a small quantity of dye stock solution with water carefully removed from the porous medium (i.e., without exposure to the atmosphere). Approximately 20 mL of the dye solution was then injected back into the porous medium over a ~10 minute period. The system was then allowed to sit for one hour, which was determined in previous experiments to be sufficiently long to allow equilibrium to be achieved in the oxidation-reduction reaction of the dye.

Following equilibration of the dye, a series of 2.5 mL sub-samples was extracted from the column and analyzed by UV-vis spectrophotometry. These measurements were initially problematic because of re-oxidation of the dye during the sample handling process. As a consequence, the sample-handling portion of the experiments was conducted in an anaerobic chamber by running a 1/16th inch stainless steel tube from the column into a glove box. Once subsamples were sealed in screw-top cuvettes, they were removed from the glove box and analyzed.

Concurrent with sub-sampling, reduction potential was measured with a flow-through micro platinum electrode (with AgCl reference electrode, both from Microelectrodes, Inc.). The electrode was also located in the glove box. Measured reductions potentials were corrected to standard hydrogen electrode conditions (i.e., by

adding +0.21 volts to the value measured with a Pt electrode and AgCl reference electrode).

### 10.4.2.5. Calculation of ECRP

Calculation of reduction potential using equilibrium speciation of the CRPs is accomplished using the Nernst equation, which can be expressed in simplified form at circum-neutral pH as Fan et al., 2016 [*108*]:

$$E_{\mathrm{CRP}} = E^{0}_{\mathrm{pH}} + \frac{\mathrm{R}T}{2\mathrm{F}}\ln\left(\frac{[\mathrm{CRP}_{ox}]}{[\mathrm{CRP}_{red}]}\right)$$

where $E^{0}_{pH}$ is the formal reduction potential of the CRP at pH ~7, R is the ideal gas constant (8.314 J/(Mole), T is the absolute temperature (298 °K), and F is the Faraday constant (96485 J/(Voile)).

As discussed above, the ratio of oxidized to reduced forms of the CRP were determined by first measuring the concentration of the oxidized form of the dye remaining in solution. The cuvette was then opened to expose the solution to oxygen, which resulted in rapid oxidation of the reduced form of the dye. The cuvette was then re-analyzed to determine the total amount of dye present in the solution and the concentration of the reduced form of the dye was determined by difference. (This approach removes the need to correct for differences in extinction coefficient of the oxidized and reduced forms of the dye and also takes into account any interferences in the measurement (e.g., turbidity).

### 10.4.2.6. Kinetic measurements

To conduct kinetic measurements, we used an approach similar to the thermodynamic measurements, except that rather than waiting for equilibrium to occur in the medium, the dye was continuously extracted and analyzed using a flow-through optical system to track the shift from oxidized to reduced forms. This was done to eliminate the need for sample handling, and thereby avoid the need to an anoxic chamber (i.e., to prevent oxidation of the dye).

The experimental configuration is shown schematically in Figure 32. As with the thermodynamic measurements, introduction of the dye into the column was accomplished by first diluting the dye with water extracted from the column. The diluted mixture is then injected into the column using a computer-controlled syringe pump. Because of the limited volume of the columns, during injection a second computer-controlled syringe pump removed an equivalent amount of water from the column. To monitor this process and insure water balance during the process a water manometer was placed on the top of the column

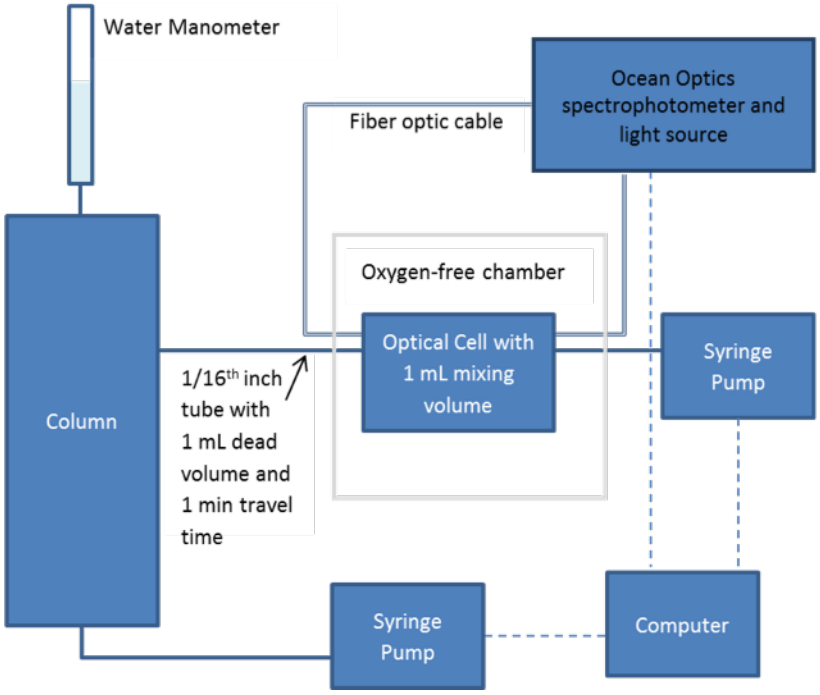


Figure 32. Schematic drawing of the experimental setup for the abiotic kinetic experiments.

Because of the extreme sensitivity of the dyes to re-oxidation, the flow-through approach again proved initially problematic due to oxygen diffusion through and out of porous materials in the flow-through optical cell. To overcome this, the cell was placed in a portable oxygen-free chamber (Figure 39). The combination of the chamber and all stainless steel tubing allowed samples from the column to be accurately measured by the spectrophotometer. In this case, the re-oxidation approach used for speciation in the thermodynamic measurements was not practical, and we relied instead on absorption of the reduced form of the dye (350 nm) as well as the oxidized form (610 nm) in water extracted from the column.

Because thermodynamic equilibrium was not necessary for the kinetic measurements, we were able to use a single dye (I2S) for all of the measurements (i.e., as long as the $E^0_{pH}$ was greater than the measured reduction potential, reduction of the dye could be tracked even if the final concentration of the oxidized form approached zero).

### 10.4.2.7. Determination of rate constants

While the flow-through cell provides a direct measure of oxidized and reduced dye, the size of the columns limits the flow rate to the optical cell to ~1 mL/min. Since the volume of the cell is approximately 0.8 mL, and the contents of the cell are generally well mixed during flow, the time required for the concentration in the cell to match the concentration coming out of the column is approximately 2.5 minutes. (i.e., assuming perfect exponential mixing the time required to reach 95% of the influent concentration within the cell is ~2.9 minutes). In addition, there is approximately a 1-minute delay during transport from the column to the optical cell. To reconstruct the concentration *in the*

*column*, data from the optical cell was processed using a simple compartmental flow model.

Using this approach, values of the reduction and oxidation rate constants in the column for the dye were adjusted to match the observed data. The flow model was calibrated by pumping dye from a constant-concentration source through the tubing and optical cell at the same flow rate used in the experiments. These data were used to calibrate the flow model and are shown in Figure 38.

### 10.4.3. Results

#### 10.4.3.1. Thermodynamic measurements

As described above, after equilibration of the dyes for one hour, 2.5-mL subsamples were extracted from the columns, placed in a screw-top cuvette and removed from the glove box. The ratio of oxidized to reduced dye concentration was then determined and the CRP-based reduction potential ($E_{CRP}$) calculated. Data for subsamples from each port on the two columns are shown in Figure 33. As the data indicate, the reduction potential values remained relatively constant throughout the sub-sampling process.

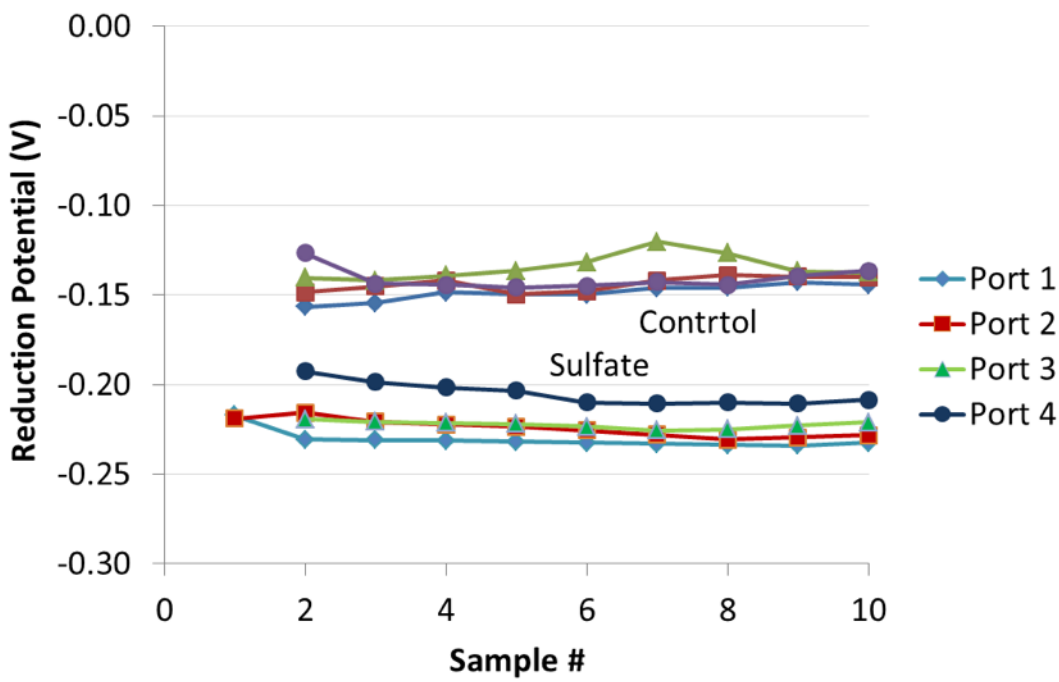


Figure 33. $E_{CRP}$ values for sub-samples taken from all sample ports on the control and sulfate columns.

Figure 34 shows the average reduction potential for each port on both columns measured by the CRP method and using the platinum electrode (corrected to the standard hydrogen electrode potential to make them consistent with the $E_{CRP}$ data.) The data suggest that reduction potentials are fairly consistent down the column. An important

note should be made here regarding platinum electrode measurements. Namely, the quality of the electrode measurements presented here was dramatically improved (and made more accurate) because of the presence of the CRP in the extracted water. As discussed by Fan et al. [*108*], the CRP acts as an electron shuttle that "allows" the external electrode to sense conditions on the surfaces of the minerals in the column.

Based on ancillary data from the columns (see supporting information, below, Section 10.4.4.5), the control column was operating under iron reducing conditions, while the sulfate column was operating under sulfate reducing conditions. This is consistent with the measured reduction potentials for the two columns.

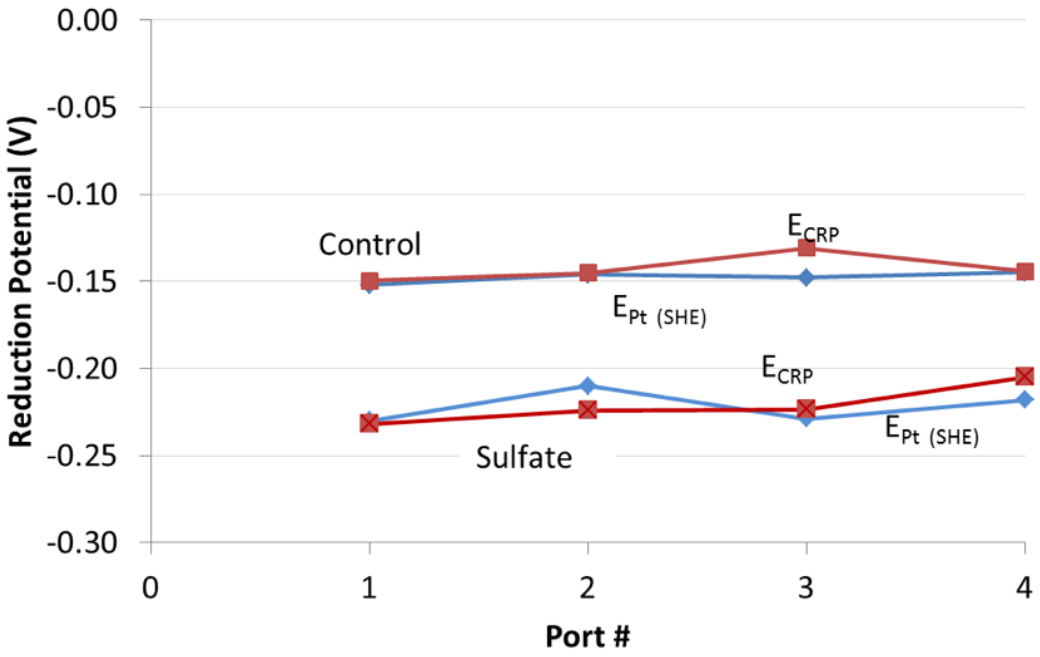


Figure 34. Average reduction potential values for all ports on both columns. Values were determined by chemical reactivity probe and by platinum electrode corrected to the standard hydrogen electrode.

### 10.4.3.2. Kinetic measurements

As described above, to provide a methodology that eliminated sample handling, and thus facilitated application in field settings, a continuous flow approach was used for the kinetic measurements. As with the thermodynamic measurements, the injection solution was created by diluting a small volume of I2S stock solution (1 mM) with pore water carefully extracted to preclude introduction of oxygen. For the kinetic measurements, controlled injection of 30 mL of the solution (at 1 mL/min) was accomplished using a syringe pump, while a corresponding amount was withdrawn from the influent end of the column. Immediately upon completion of injection, extraction from the sample port was initiated (again at 1 mL/min.)

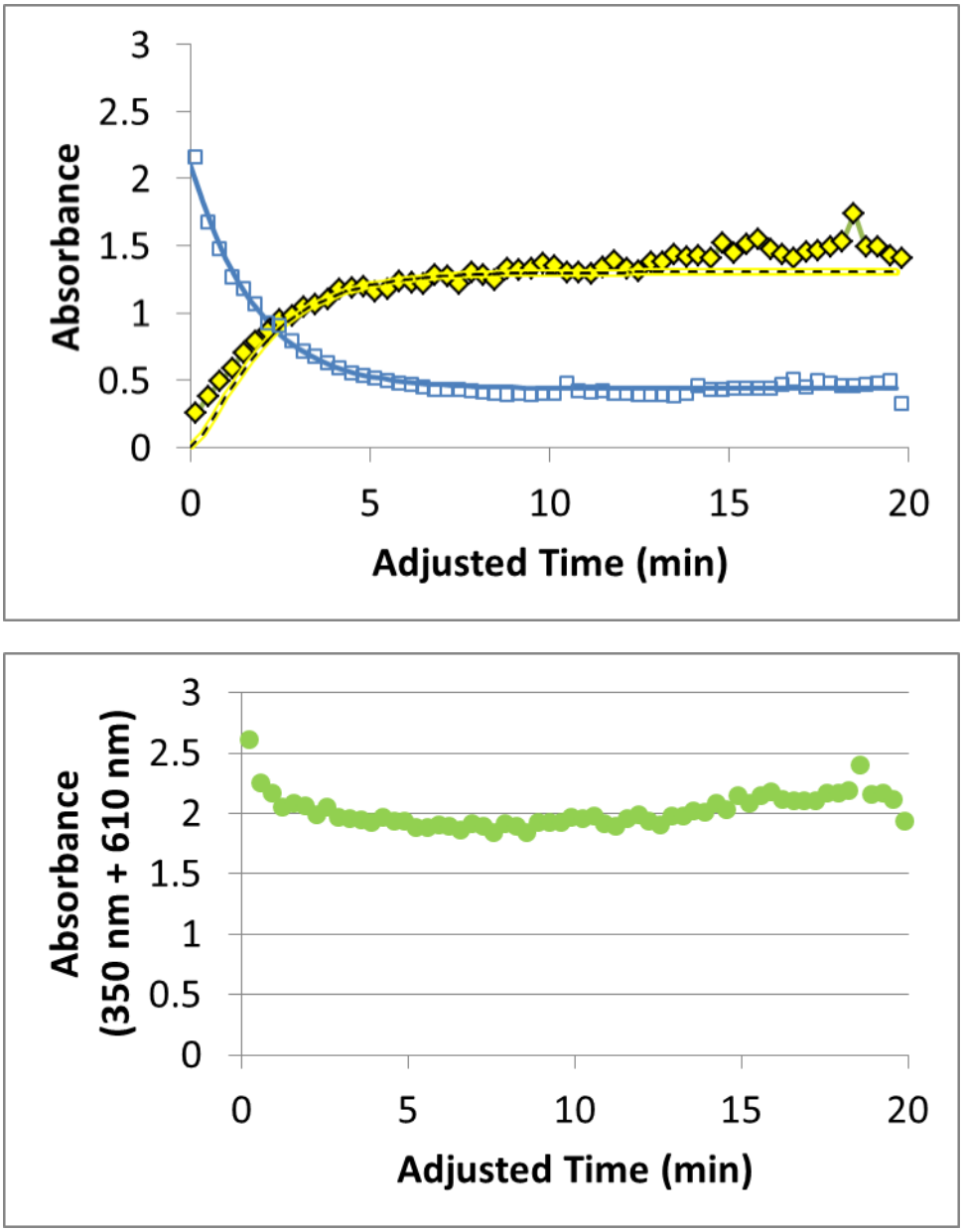


Figure 35. (A) example of absorbance data from the continuous-flow tests. This example is for Port 1 of the sulfate column. Other data are shown as supporting information, below, in Section 1.7.4.6. (B) mass balance (represented as the sum of the absorbances) for Port 1 on the sulfate column

An example of the absorbance at 350 and 610 nm for port 1 from the sulfate column is shown as symbols Figure 35. (All of the kinetic data are shown below as supporting information, Section 10.4.4.6). The yellow/black symbols correspond to the 350 nm data, which is characteristic of the reduced (yellow) form of the dye. The blue symbols are the 610 nm data and represent the oxidized (blue) form of the dye. Due to the dead volume within the optical cell and the tube connecting the cell to the column, the time of the experiments has been adjusted. Furthermore, since the residence time in the column is assumed to be twice the extraction time, the time values on the x-axis have

been further adjusted by doubling the extraction time. (I.e., we have assumed that the residence time is the sum of the time since that parcel of water was injected into the column and the time after start of extraction when that parcel of water reaches the optical cell. It is implicit in this assumption that the travel time of a parcel of water into the porous medium is exactly the same as the travel time for removal of that same parcel. This ignores dispersion and is a complicating factor in interpreting injection/withdrawal tests.)

The absorbance data in Figure 35A were fit to a first-order reversible reaction model. A global fitting approach using Monte Carlo simulation was used to determine the reduction and oxidation rate constants that minimized the sum of the squares of the differences between the experimental and model values. The blue and yellow/black lines represent the model fits for the data and indicate that a first-order analysis was appropriate.

Figure 35B presents mass balance data for the experiment. Since the molar extinction coefficients at 350 and 610 nm are virtually the same, we can use the sum of oxidized plus reduced absorbances to track the total concentration of dye in the samples. In this example, and all other tests (data not shown), there was good mass balance throughout the experiments.

#### 10.4.3.3. Comparison of thermodynamic and kinetic data for the columns

Kinetic experiments using I2S were conducted on each port for both columns and the first-order rate constants for reduction are shown in Figure 36. As the data indicate, reduction was approximately twice as fast in the sulfate column as in the control. In addition, the rates decreased significantly as one moves downgradient in the column. The result was initially surprising since the reduction potentials along the column were consistent in both cases. However, the observed result is consistent with the idea that, while the thermodynamic measurement describes the nature of the reducing species, it is an intensive property of the medium. In contrast, the rate constants are extensive properties. While this result is an interesting one, the underlying reasons for the apparent decrease are beyond the scope of the current work.

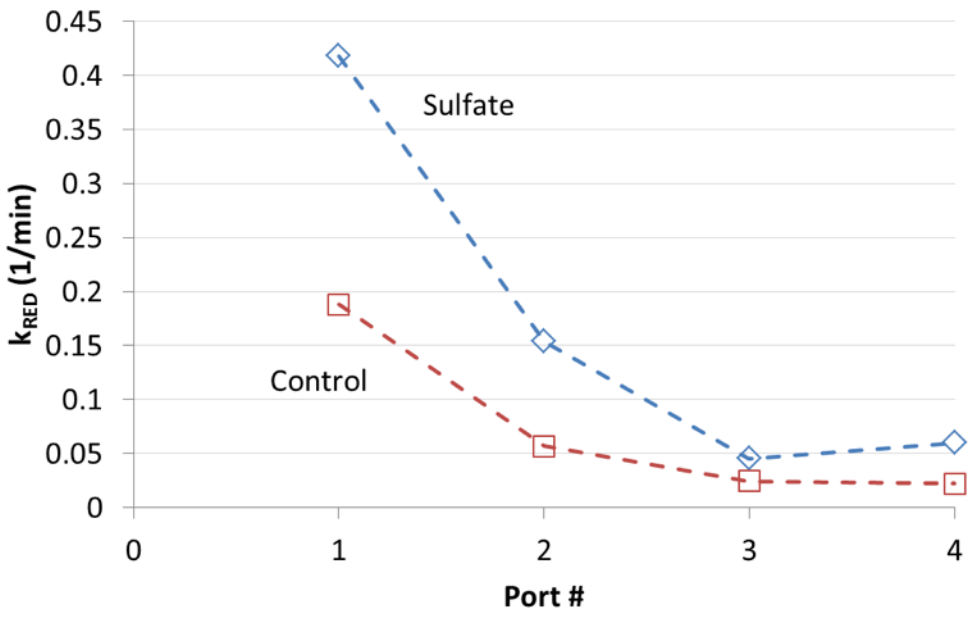


Figure 36. First order reduction rate constants for the control and sulfate columns measured at the four ports on the columns.

### 10.4.3.4. Strengths and weaknesses of CRP pull-push-pull tests

The use of CRPs allows kinetic measurements possible in the time frames appropriate for injection-withdrawal tests (e.g., less than 24 hours). Importantly, this approach facilitates direct contact between the probe and the medium, which allows the reduction potentials of mineral surfaces to be actively assessed. However, interpretation of injection-withdrawal tests can be complicated due to a variety of factors. For example, mixed redox conditions may occur in a well due to mixing of different waters in contact with the well screen. This can be at least partially addressed using small-diameter, low-dead volume piezometers, rather than conventional wells. A second potential challenge associated with all well-based approaches is that it is difficult to test lower-permeability zones because of lack of flow in homogeneous low-permeability media or preferential flow in heterogeneous media.

An alternate approach is to collect high-quality, well-preserved core and make kinetic measurements in the lab. CRPs represent a useful tool in this approach as well, allowing kinetic measurements to rapidly made under well-controlled (e.g., glove box) conditions. This approach is currently being examined as part of SERDP ER-2621.

### 10.4.4. Supporting Information for Johnson et al. 2017 [*189*]

10.4.4.1. Flow system for the columns

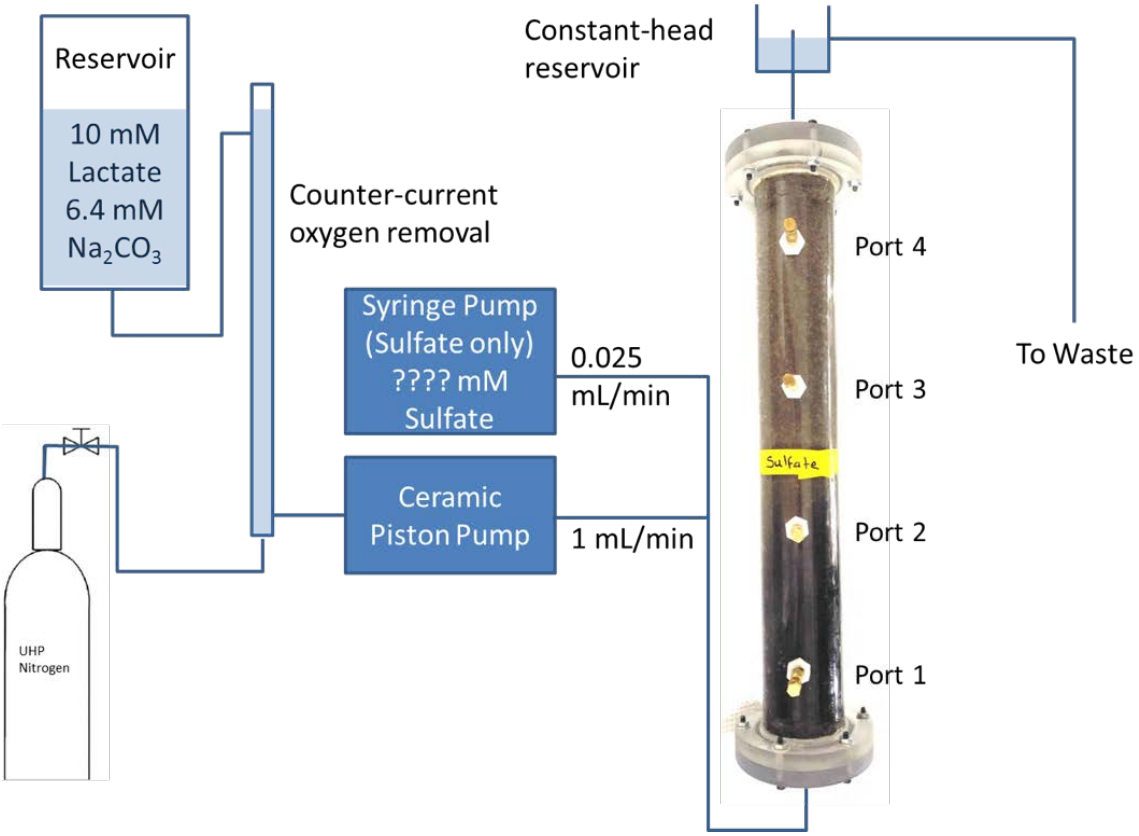


Figure 37. Flow system for the columns

## 10.4.4.2. Chemical reactivity probes

| Oxidized Form | | | | | Reduced Form | | | | | Couple | |
|---|---|---|---|---|---|---|---|---|---|---|---|
| Names | Color [a] | $\lambda_{Max}$ [b] | ε [c] | $pK_a$ | Names | Color [a] | $\lambda_{Max}$ [b] | ε [c] | $pK_a$ | $E_0'$ [d] | $E_m^7$ [d] |
| 2,6-Dichloro-indophenol (DCIP) | blue | 601 | 17.4[e] | 8.1 | | leuco | 256 | N/A | 9.4, 10.6 | +0.668 | 0.228 |
| Resazurin (Alamar Blue)(RSZ) | purple | 600 | 40.1[e] | 6.93 | Resorufin (RSF) | pink | 569 | 93.1 | NA | N/A | N/A |
| Indigo tetrasulfonate (I4S) | blue | 589 | 18.5[e] | 11.9, 12.9 | | yellow | 433 | | 7.2, 12.1 | 0.365 | −0.046 |
| Resorufin (RSF) | pink | 569 | 93.1[f] | 6.93 | Dihydroresorufin | leuco | 293 | | 9.26, 10.00 | 0.380 | −0.051 |
| Indigo trisulfonate (I3S) | blue | 600 | 14.6[e] | 11.7, 12.8 | | yellow | 421 | | 7.4, 12.1 | 0.332 | −0.081 |
| 5,5′-Indigo disulfonate (Indigo Carmine)(I2S) | blue | 610 | 19.6[f] | 12.3, 12.8 | | yellow | 407 | N/A | 9.3, 10.0 | 0.291 | −0.125 |
| 9,10-Anthraquinone-2,6-disulfonate (AQDS) | leuco | 328 | 2.81[f] | N/A | | Pale yellow | 386 | 7.0 [g] | 8.10, 10.5 | 0.228 | −0.184 |
| 9,10-Anthraquinone-2-sulfonate (AQS) | leuco | 328 | 5.33 [f] | N/A | | Pale yellow | 386 | N/A | N/A | 0.187 | −0.225 |

[a] At circum-neutral pH. [b] Absorbance maximum at pH 7 (nm). [c] Extinction coefficient ($mM^{-1}$ $cm^{-1}$). [d] Formal potentials at pH 0 and 7 (mV vs SHE). [e] ref [*29*]. [f] measured based on calibration. [g] estimated based on ref [*88*].

Figure 38. Summary of nomenclature and properties of thermodynamic chemical reactivity probes (CRPs). (Same as Table 4)

10.4.4.3. Experimental setup for the flow-through columns.

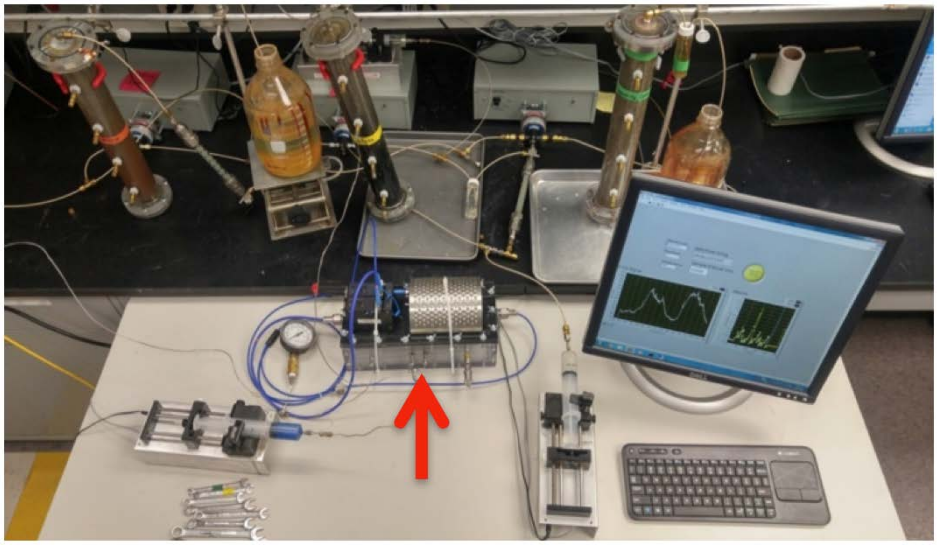

Figure 39. Experimental setup for the flow-through columns. Ceramic piston pumps for the eluent in the back, syringe pumps for CRPs in the foreground. The oxygen-free chamber containing the flow cell is shown above the red arrow.

10.4.4.4. Flow Modeling

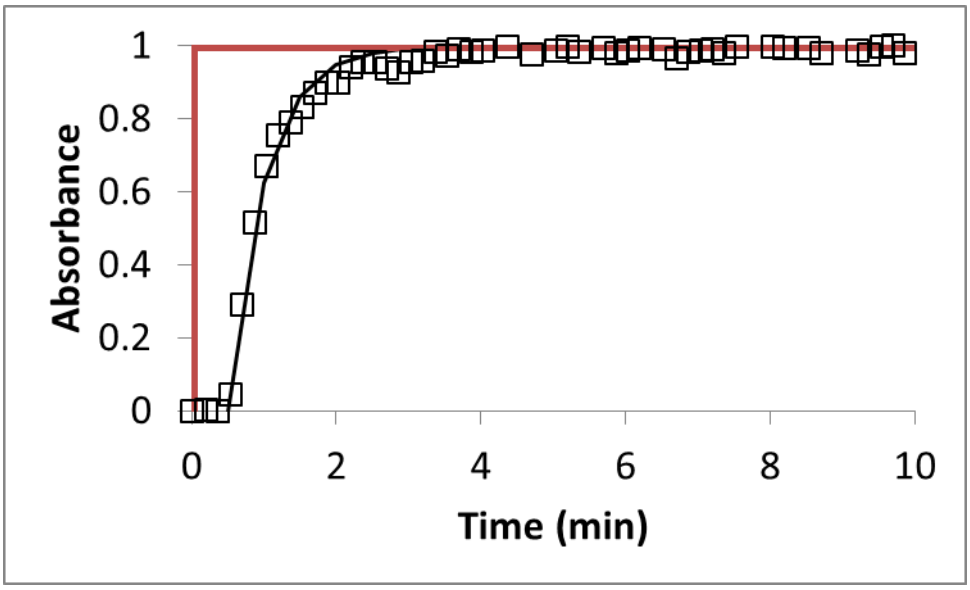


Figure 40. Black curve is the from the concentration model as well and squares are the experimental data. The red line represents the influent concentration at what would have been the column-end of the sample tube. (1/16th inch tube in Figure 33 in the main text). Both the lag time and the mixing observed in the experimental data were incorporated into the model

10.4.4.5. Ancillary Column Data

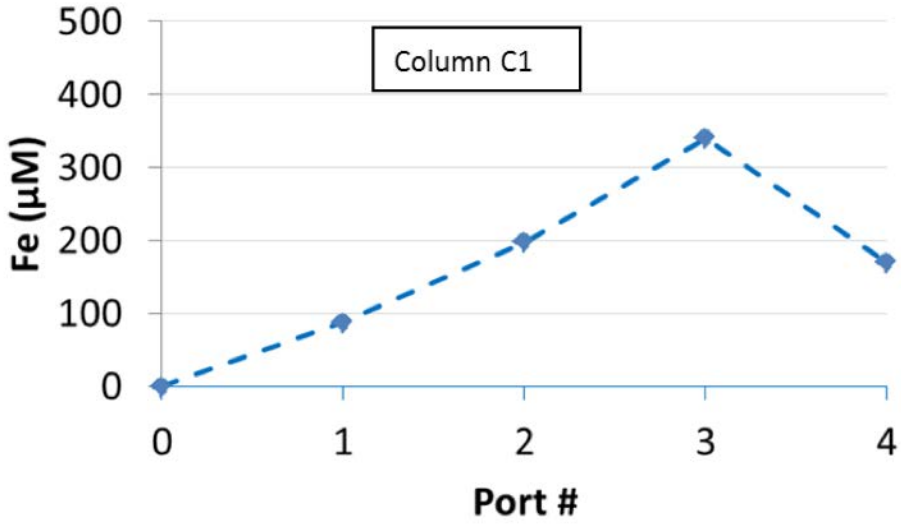


Figure 41. Dissolved iron at sample ports along the control column.

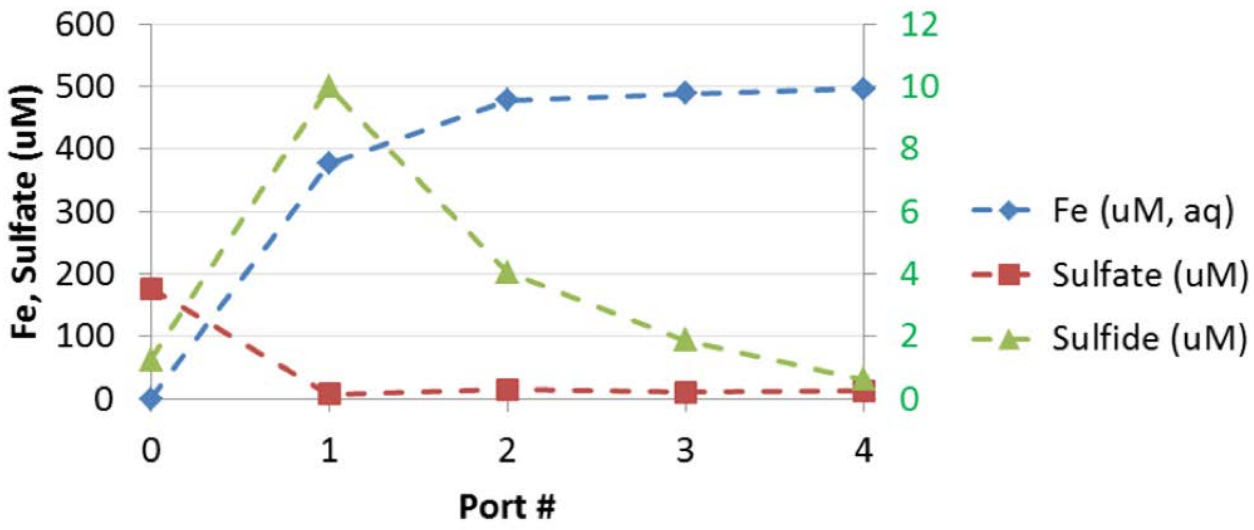


Figure 42. Dissolved iron and sulfate at sample ports along the sulfate column.

10.4.4.6. UV-vis and modeling data for all columns and ports

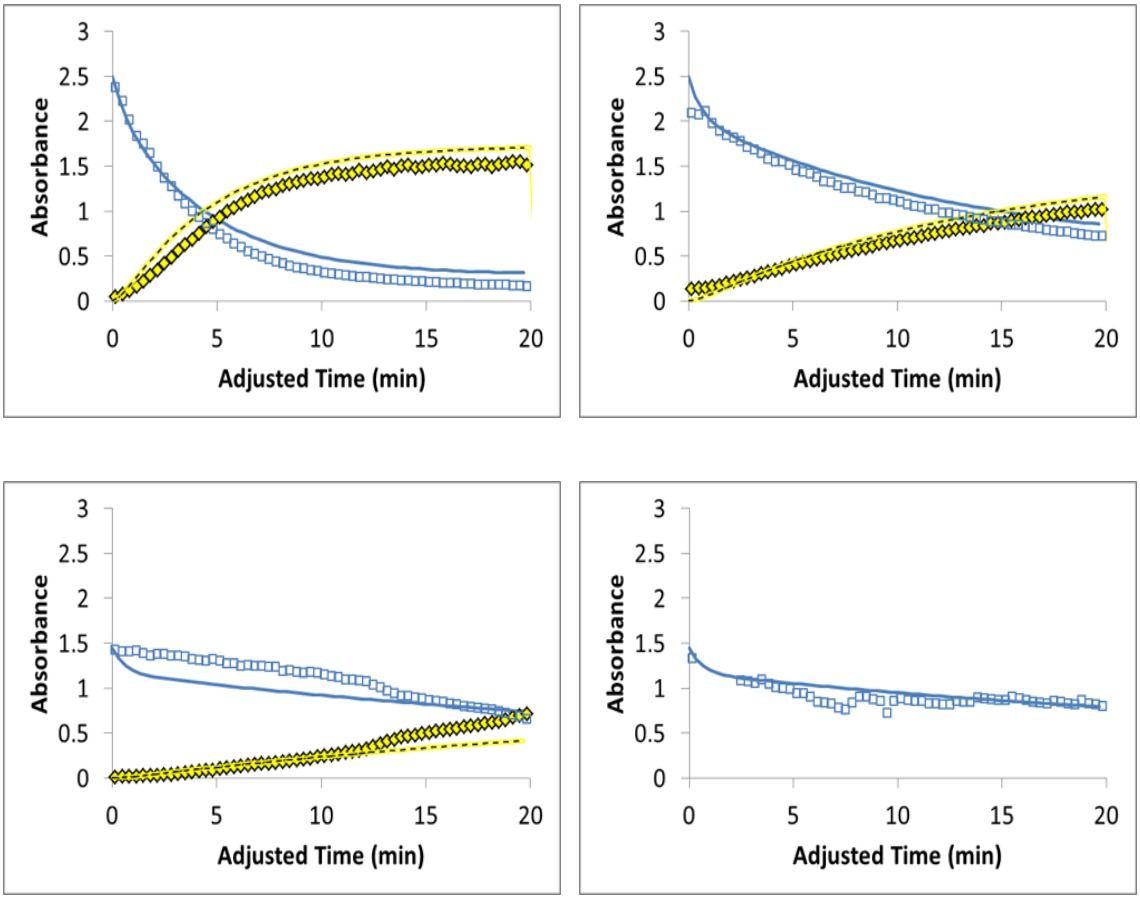


Figure 43. Control column, Ports 1-4. The upper portion of each column (Port 4) was difficult to test because of gas accumulation at the top of the column. For the control column, the quality of the 350 nm data for Port 4 was compromised by dramatically changing baseline, so it was not included in this analysis.

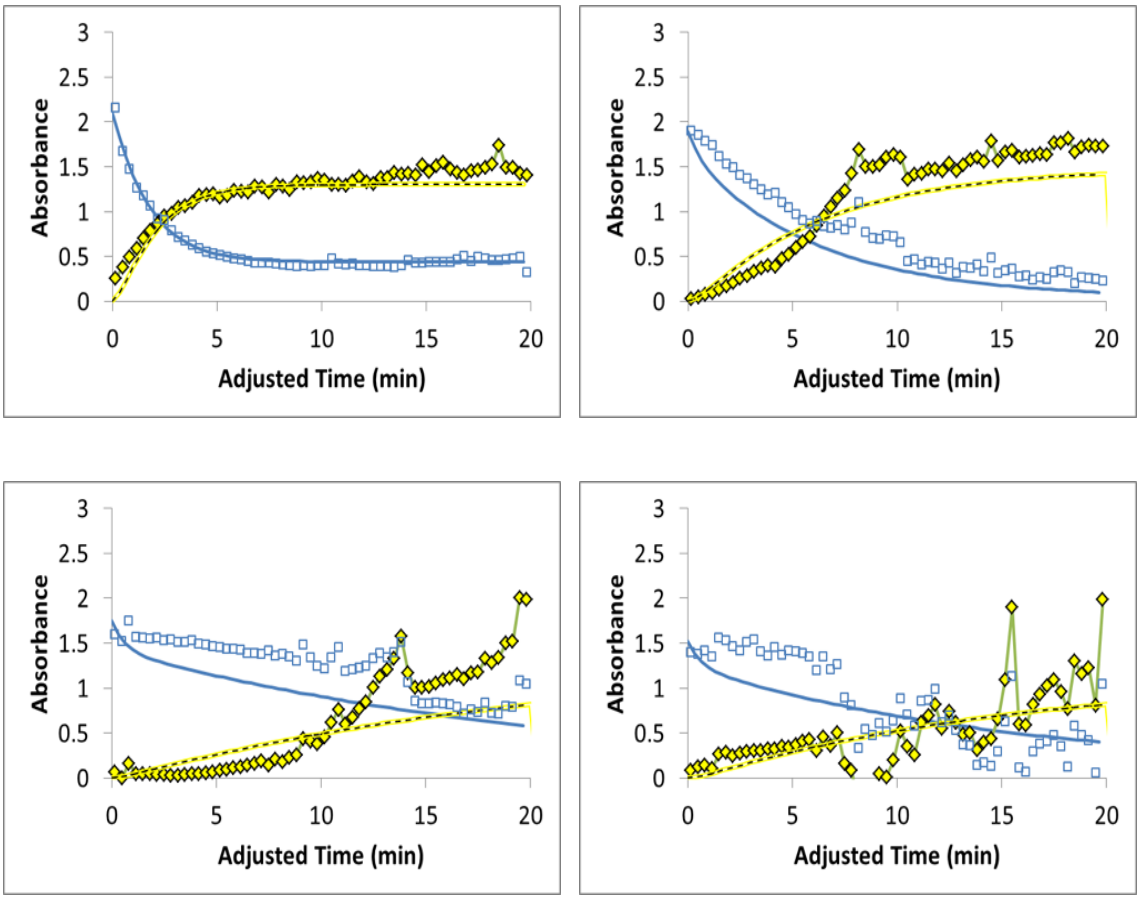


Figure 44. Sulfate column, Ports 1-4.

## 10.5. Objective 4—Outreach and Technology Transfer

### 10.5.1. Collaborations to deploy CRPs for Field Site Characterization

As an early demonstration of the applicability of CRPs for field characterization, we collaborated with the University of Western Ontario (Dr. Denis O'Carroll) to make reduction potential measurements during injection of a sulfidated carboxymethylcellulose nZVI. During this demonstration, the nZVI, which had been sulfidated in the field with dithionite was injected by gravity into a heterogeneous sandy aquifer.

Figure 45. Sample the CMC-nZVI injection test site in Ontario.

Several interesting general observations can be made regarding the injection:

1. In absolute terms the concentration of nZVI measured at the monitoring wells was quite low (generally C/C(0) < 0.02). Conservative tracers also showed significant dilution, indicating that relative transport of the nZVI was relatively good. However, the delivery of nZVI would be insufficient reduction of contaminant mass in a full-scale treatment application.

2. The particles persisted in the mobile aqueous phase for periods of weeks after injection. This is in dramatic contrast to typical nZVI behavior, where aggregation and sticking generally remove particles from the water phase within hours.

The experimental protocol for using CRPs at the site was as follows:

a. One mL of groundwater sample was added to a 10-mL septum vial containing ~140 uM I2S in deoxygenated DI water.

b. The septum vial was then placed in a field spectrophotometer and the absorbance measured as a function of time.

c. In general, the absorbance at 610 nm decrease with time over ~20 minutes and then stabilized.

d. The decrease in 610 nm absorbance could then be related to the amount of nZVI in the sample.

In general terms, the observed concentrations of nZVI in the formation (based on absorbance of the groundwater sample at 800 nm) was quite low, making the tests difficult to perform.

In addition, based on results from the injection solution, the amount of dye reduction occurring was much less than would have been expected based on the amount of iron in the nZVI solution. Based on subsequent work in our lab, we concluded that essentially all of the nZVI had been consumed in the sulfidation process, leaving only FeS, which is much less reactive than nZVI. This result is represented in Figure 46 below. The left figure shows the dye reduction behavior for two samples from the field trial (one from the injection solution and one collected from a groundwater well. In both cases the samples were diluted to a total iron concentration of ~4 mg/L. The data indicate that absorbance at 610 nm reduced from 2.6-2.8 to values of 2.2-2.4. Data with freshly-prepared, but unsulfidated, nZVI in our laboratory is shown in the lower figure. A 4 mg/L concentration of nZVI in that case reduced the sorption from 2.5 to less than 1. These data indicate that there was much less nZVI available in the field injection solution. So, while we were not able to demonstrate the full applicability of the CRP approach at this site, we were able to quickly demonstrate that the nZVI content of the injected solution was much less than was believed to be the case by the UWO field team.

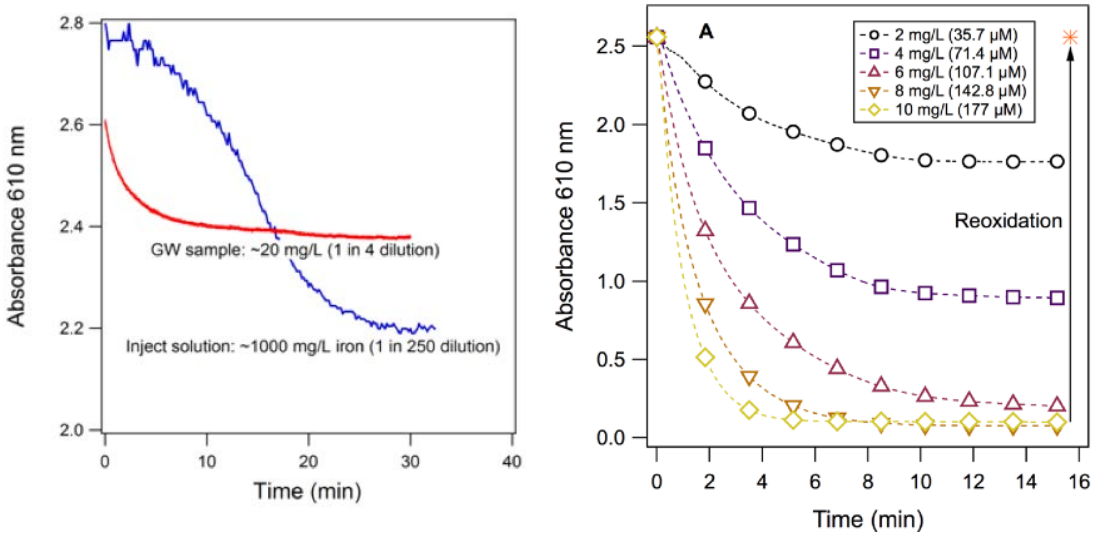


Figure 46. Example data using CRPs to characterization the reduction potential and capacity of CMC-nZVI impacted waters sampled from the Ontario field site.

This result does not mean that reduction of the contaminants would not be successful. Indeed, subsequent data from the site suggests that significant contaminant reduction

occurred. However, it now appears likely that much of this degradation occurred as the result of biological activity, not by iron directly. However, preparation of the report on this test is still in progress at the University of Western Ontario at the time of this report.

### 10.5.2. Other Collaborations on Field Sites

Numerous parties have expressed interesting in testing CRP based methods at their field sites. Most of these were delayed because new laboratory results created an involving understanding of how CRPs might best be applied in the field. The next major steps in this process will be extension of CRPs methods for application to frozen core samples, through ER-2621. Cores samples for this work will be obtained from Indian Head, MD, as part of ESTCP ER-201587 and Parris Island, SC, as part of ESTCP ER-201525.

### 10.5.3. Training via Short Courses and Webinars

#### 10.5.3.1. Short Courses and Webinars

- 2014 Battelle Chlorcon Conference. (~50 attendees) Groundwater Geochemistry and Practical Assessment of Redox-Based Remediation. Instructors: Paul Tratnyek and Richard L. Johnson and Bill Deutsch (Geochemistry Services LLC).
- SERDP/ESTCP Webinar, 8/9/2016 (several hundred attendees). Practical Assessment and Optimization of Redox-Based Groundwater Remediation Technologies
    - https://serdp-estcp.org/Tools-and-Training/Webinar-Series/09-08-2016
    - https://www.youtube.com/watch?v=eB0JVJOQVX0

#### 10.5.3.2. SERDP ESTCP Webinar

- Push-pull with CRP posted on YouTube and SERDP websites. As part of the technology transfer process, we developed a short YouTube video showing the importance of mineral surfaces in controlling the reduction process.
    - https://www.serdp-estcp.org/News-and-Events/Blog/Practical-Assessment-of-Redox-Based-Groundwater-Remediation-Technologies
    - https://www.youtube.com/watch?v=Wr1bSbQz1ck

- The still images below, from that video, show that water extracted from a reactive porous medium (in the case one of our columns) did not reduce a CRP. However, when that CRP was introduced into the medium and then extracted, it was completely reduced (to pink) due to direct contact between the CRP and the mineral surfaces within the column. This early result was translated into quantitative results as part of Objective 3 of this project.

Figure 47. Demonstration of CRP reduction upon contact with aquifer material in a column. Images represent pull, push, and pull, using resazurin at the CRP. Blue to pink indicates reduction.

# 11. OVERALL CONCLUSIONS AND IMPLICATIONS

Chemical redox probes (CRP) for redox characterization:

- There are a wide variety probes are available, some of which are suitable for in situ characterization.
- There are two important advantages of CRPs over conventional electrode measurements. The first is that the CRPs provide direct access to reducing mineral surfaces. The second is that the CRPs have the potential to provide kinetic information as well as thermodynamic measurements.
- An important disadvantage of the approach is that CRPs need to be matched to the conditions in the subsurface, which requires either some a priori information about the redox conditions, or trial and error using difference CRPs.

Detection by Spectrophotometry vs. Potentiometry:

- Spectrophotometry of CRPs is robust in the laboratory, but difficult to do well in the field without taking extraordinary measures.
- Potentiometry is simple, effective, and more familiar to practitioners. However, it should be recognized that the results probably underestimate the actual reduction potential. In addition, they do not provide any information on the kinetics of the reduction process, which may ultimately be key for understanding in situ degradation rates.

# 12. REFERENCES


(1) Stumm, W.; Morgan, J. J. (1985) On the conceptual significance of p*e*. *Am. J. Sci.*, *285*, 856-859.

(2) Hostettler, J. D. (1985) On the importance of distinguishing Eh from p*e*. *Am. J. Sci.*, *285*, 859-863.

(3) Thorstenson, D. C. (1984) The concept of electron activity and its relation to redox potentials in aqueous geochemical systems. *U.S. Geological Survey Open-File Report 84-072*,

(4) Frevert, T. (1979) The pe redox concept in natural sediment-water systems; its role in controlling phosphorus release from lake sediments. *Arch. Hydrobiol., Suppl. 55*, 278-297.

(5) Shi, Z.; Nurmi, J. T.; Tratnyek, P. G. (2011) Effects of nano zero-valent iron (nZVI) on oxidation-reduction potential (ORP). *Environ. Sci. Technol.*, *45*, 1586-1592.

(6) Doyle, R. W. (1968) The origin of the ferrous ion-ferric oxide Nernst potential in environments containing dissolved ferrous iron. *Am. J. Sci.*, *266*, 840-859.

(7) Grundl, T. J.; Macalady, D. L. (1989) Electrode measurement of redox potential in anaerobic ferric/ferrous chloride systems. *J. Contam. Hydrol.*, *5*, 97-117.

(8) Grenthe, I.; Stumm, W.; Laaksuharju, M.; Nilsson, A. C.; Wikberg, P. (1992) Redox potentials and redox reactions in deep groundwater systems. *Chem. Geol.*, *98*, 131-150.

(9) Macalady, D. L.; Langmuir, D.; Grundl, T.; Elzerman, A. (1990) Use of model-generated $Fe^{3+}$ ion activities to compute Eh and ferric oxyhydroxide solubilities in anaerobic systems. In: *Chemical Modeling of Aqueous Systems II*; American Chemical Society: Washington, DC, *Vol. 416*; pp. 350-367.

(10) Breck, W. G. (1972) Redox potentials by equilibration. *J. Mar. Res.*, *30*, 121-139.

(11) Stumm, W. (1966) Redox potential as an environmental parameter; conceptual significance and operational limitations. In: *Advances in Water Pollution Research*; Water Pollution Control Federation: Washington, D.C., *Vol. 1*; pp. 283-308.

(12) Morris, J. C.; Stumm, W. (1967) Redox equilibria and measurements of potentials in the aquatic environment. In: *Equilibrium Concepts in Natural Water Systems*; American Chemical Society: Washington, DC, ACS Symposium Series No. 67; pp. 270-285.

(13) Whitfield, M. (1969) Eh as an operational parameter in estuarine studies. *Limnol. Oceanogr.*, *14*, 547-558.

(14) Spiro, M. (1986) Polyelectrodes: The behaviour and applications of mixed redox systems. *Chem. Soc. Rev.*, *15*, 141-165.

(15) Peiffer, S.; Klemm, O.; Pecher, K.; Hollerung, R. (1992) Redox measurements in aqueous solutions—A theoretical approach to data interpretation based on electrode kinetics. *J. Contam. Hydrol.*, *10*, 1-18.

(16) Chapelle, F. H.; Bradley, P. M.; Lovley, D. R.; Vroblesky, D. A. (1996) Measuring rates of biodegradation in a contaminated aquifer using field and laboratory methods. *Ground Water*, *34*, 691-698.

(17) Lovley, D. R.; Chapelle, F. H. (1995) Deep subsurface microbial processes. *Rev. Geophys.*, *33*, 365-381.

(18) Chapelle, F. H.; Morris, J. T.; McMahon, P. B.; Zelibor, J. L. (1988) Bacterial metabolism and the $^{13}C$ composition of ground water, Floridan aquifer system, South Carolina. *Geology*, *16*, 117-121.

(19) Chapelle, F. H.; McMahon, P. B.; Dubrovsky, N. M.; Fujii, R. F.; Oaksford, E. T.; Vroblesky, D. A. (1995) Deducing the distribution of terminal electron-accepting processes in hydrologically diverse groundwater systems. *Water Resour. Res.*, *31*, 359-371.

(20) Chapelle, F. H.; Haack, S. K.; Adriaens, P.; Henry, M. A.; Bradley, P. M. (1996) Comparison of Eh and $H_2$ measurements for delineating redox processes in a contaminated aquifer. *Environ. Sci. Technol.*, *30*, 3565-3569.

(21) Chapelle, F. H.; Vroblesky, D. A.; Woodward, J. C.; Lovley, D. R. (1997) Practical considerations for measuring hydrogen concentrations in groundwater. *Environ. Sci. Technol.*, *31*, 2873-2877.

(22) Mumford, K. G.; Lamarche, C. S.; Thomson, N. R. (2004) Natural oxidant demand of aquifer materials using the push-pull technique. *J. Environ. Eng.*, *130*, 1139-1146.

(23) Smolen, J. M.; Weber, E. J.; Tratnyek, P. G. (1999) Molecular probe techniques for the identification of reductants in sediments: Evidence for reduction of 2-chloroacetophenone by hydride transfer. *Environ. Sci. Technol.*, *33*, 440-445.

(24) Zhang, H.; Colón, D.; Kenneke, J. F.; Weber, E. J. (2011) The use of chemical probes for the characterization of the predominant abiotic reductants in anaerobic sediments. In: *Aquatic Redox Chemistry*; Tratnyek, P. G.; Grundl, T. J.; Haderlein, S. B., Eds.; American Chemical Society: Washington, DC, ACS Symposium Series, *Vol. 1071*; pp. 539-557.

(25) Field, J. A.; Reed, R. L.; Istok, J. D.; Semprini, L.; Bennett, P.; Buscheck, T. E. (2005) Trichlorofluoroethene: a reactive tracer for evaluating reductive dechlorination in large-diameter permeable columns. *Ground Wat. Monitor. Remed.*, *25*, 68-77.

(26) Parbs, A.; Ebert, M.; Köbert, R.; Plagentz, V.; Schad, H.; Dahmke, A. (2003) Einsatz reaktiver tracer zur bewertung der Langzeitstabilität und Reaktivität von Fe(0)-Reaktionswanden [Application of reactive tracers to evaluate the long-term stability and reactivity of Fe(0)-permeable reactive barriers]. *Grundwasser*, *8*, 146-156.

(27) Tratnyek, P. G. (2010) Chemical reductants for ISCR: The potential for improvement. In: *International Conference on Remediation of Chlorinated and Recalcitrant Compounds, 7th*, Monterey, CA, *Vol.* pp. Paper No. D-054.

(28) Perlinger, J. A.; Buschmann, J.; Angst, W.; Schwarzenbach, R. P. (1998) Iron porphyrin and mercaptojuglone mediated reduction of polyhalogenated methanes and ethanes in homogeneous aqueous solution. *Environ. Sci. Technol.*, *32*, 2431-2437.

(29) Tratnyek, P. G.; Reilkoff, T. E.; Lemon, A. W.; Scherer, M. M.; Balko, B. A.; Feik, L. M.; Henegar, B. D. (2001) Visualizing redox chemistry: Probing environmental oxidation-reduction reactions with indicator dyes. *The Chemical Educator*, *6*, 172-179.

(30) Tratnyek, P. G.; Wolfe, N. L. (1990) Characterization of the reducing properties of anaerobic sediment slurries using redox indicators. *Environ. Toxicol. Chem.*, *9*, 289-295.

(31) Grundl, T. J.; Haderlein, S. P.; Nurmi, J. T.; Tratnyek, P. G. (2011) Introduction to aquatic redox chemistry. In: *Aquatic Redox Chemistry*; Tratnyek, P. G.; Grundl, T. J.; Haderlein, S. B., Eds.; American Chemical Society: Washington, DC, ACS Symposium Series, *Vol. 1071*; pp. 1-14.

(32) Rügge, K.; Hofstetter, T. B.; Haderlein, S. B.; Bjerg, P. L.; Knudsen, S.; Zraunig, C.; Mosbæk, H.; Christensen, T. H. (1998) Characterization of predominant reductants in an anaerobic leachate-contaminated aquifer by nitroaromatic probe compounds. *Environ. Sci. Technol.*, *32*, 23-31.

(33) Totten, L. A.; Jans, U.; Roberts, A. L. (2001) Alkyl bormides as mechanistic probes of reductive dehalogenation: reactions of vicinal dibromide stereoisomers with zerovalent metals. *Environ. Sci. Technol.*, *35*, 2268-2274.

(34) Reilkoff, T. E. (2000) 2-Chloroacetophenone as a Probe Compound for Studying Reduction Reactions in Anaerobic Sediments. M.S. Thesis Thesis, Oregon Graduate Institute.

(35) King, D. W. (2002) A general approach for calculating speciation and poising capacity of redox systems with multiple oxidation states: Application to redox titrations and the generation of pε-pH diagrams. *J. Chem. Educ.*, *79*, 1135.

(36) Naka, D.; Kim, D.; Strathmann, T. J. (2006) Abiotic reduction of nitroaromatic compounds by aqueous iron(ll)-catechol complexes. *Environ. Sci. Technol.*, *40*, 3006-3012.

(37) Kim, D.; Strathmann, T. J. (2007) Role of organically complexed iron(II) species in the reductive transformation of RDX in anoxic environments. *Environ. Sci. Technol.*, *41*, 1257-1264.

(38) Zimmerman, A. P. (1981) Electron intensity, the role of humic acids in extracellular electron transport and chemical determination of pE in natural waters. *Hydrobiologia*, *78*, 259-265.

(39) Trevors, J. T. (1984) Electron transport system activity in soil, sediment, and pure cultures. *Crit. Rev. Microbiol.*, *11*, 83-100.

(40) Merlin, G.; Lissolo, T.; Morel, V.; Rossel, D.; Tarradellas, J. (1995) Precautions for routine use of INT-reductase activity for measuring biological activities in soil and sediments. *Environmental Toxicology and Water Quality*, *10*, 185-192.

(41) Liu, D.; Strachan, W. M. J. (1979) Characterization of microbial activity in sediment by resazurin reduction. *Advances in Limnology*, *12*, 24-31.

(42) Vancheeswaran, S.; Hyman, M. R.; Semprini, L. (1999) Anaerobic Biotransformation of Trichlorofluoroethene in Groundwater Microcosms. *Environ. Sci. Technol.*, *33*, 3284.

(43) Hademan, K. J.; Field, J. A.; Istok, J. D.; Schroth, M. H. (2003) "Forced mass balance" technique for estimating in situ transformation rates of sorbing solutes in groundwater. *Environ. Sci. Technol.*, *37*, 3920-3925.

(44) Glod, G.; Angst, W.; Holliger, C.; Schwarzenbach, R. P. (1997) Corrinoid-mediated reduction of tetrachloroethene, trichloroethene, and trichlorofluoroethene in homogeneous aqueous solution: Reaction kinetics and reaction mechanisms. *Environ. Sci. Technol.*, *31*, 253-260.

(45) Hakala, J. A.; Fimmen, R. L.; Chin, Y. P.; Agrawal, S. G.; Ward, C. P. (2009) Assessment of the geochemical reactivity of Fe-DOM complexes in wetland sediment pore waters using a nitroaromatic probe compound. *Geochim. Cosmochim. Acta*, *73*, 1382-1393.

(46) Miehr, R.; Tratnyek, P. G.; Bandstra, J. Z.; Scherer, M. M.; Alowitz, M. J.; Bylaska, E. J. (2004) The diversity of contaminant reduction reactions by zero-valent iron: Role of the reductate. *Environ. Sci. Technol.*, *38*, 139-147.

(47) Xu, X.; Thomson, N. R. (2008) Estimation of the maximum consumption of permanganate by aquifer solids using a modified chemical oxygen demand test. *J. Environ. Eng.*, *134*, 353-361.

(48) Xu, X.; Thomson, N. R. (2009) A long-term bench-scale investigation of permanganate consumption by aquifer materials. *J. Contam. Hydrol.*, *110*, 73-86.

(49) Urynowicz, M. A.; Balu, B.; Udayasankar, U. (2008) Kinetics of natural oxidant demand by permanganate in aquifer solids. *J. Contam. Hydrol.*, *96*, 187-194.

(50) Costanza, J.; Otaño, G.; Callaghan, J.; Pennell, K. D. (2010) PCE oxidation by sodium persulfate in the presence of solids. *Environ. Sci. Technol.*, *44*, 9445-9450.

(51) Johnson, R. L.; Tratnyek, P. G.; O'Brien Johnson, R. (2008) Persulfate persistence under thermal activation conditions. *Environ. Sci. Technol.*, *42*, 9350–9356.

(52) Haselow, J. S.; Siegrist, R. L.; Crimi, M.; Jarosch, T. (2003) Estimating the total oxidant demand for in situ chemical oxidation design. *Remediation J.*, *13*, 5-16.

(53) Szecsody, J. E.; Fruchter, J. S.; Williams, M. D.; Vermeul, V. R.; Sklarew, D. (2004) In situ chemical reduction of aquifer sediments: Enhancement of reactive iron phases and TCE dechlorination. *Environ. Sci. Technol.*, *38*, 4656-4663.

(54) Ludwig, R. D.; Su, C.; Lee, T. R.; Wilkin, R. T.; Acree, S. D.; Ross, R. R.; Keeley, A. (2007) In situ chemical reduction of Cr(VI) in groundwater using a combination

of ferrous sulfate and sodium dithionite: A field investigation. *Environ. Sci. Technol.*, *41*, 5299-5305.

(55) He, Y.; Su, C.; Wilson, J.; Wilkin, R.; Adair, C.; Lee, T. R.; Bradley, P.; Ferrey, M. (2009) Identification and Characterization Methods for Reactive Minerals Responsible for Natural Attenuation of Chlorinated Organic Compounds in Ground Water, U.S. Environmental Protection Agency, EOA 600/R-09/115.

(56) Liu, D.; Strachan, W. M. J. (1981) A field method for determining the chemical and biological activity of sediments. *Water Res.*, *15*, 353-359.

(57) Brown, R. A.; Wilson, J. T.; Ferrey, M. (2007) Monitored natural attenuation forum: The case for abiotic MNA. *Remediation J.*, *17*, 127-137.

(58) Tratnyek, P. G.; Johnson, R. L.; Lowry Gregory, V.; Brown, R. A. (2014) In situ chemical reduction for source zone remediation. In: *Chlorinated Solvent Source Zone Remediation*; Kueper, B. H.; Stroo, H. F.; Vogel, C. M.; Ward, C. H., Eds.; Springer: New York, SERDP and ESTCP Remediation Technology Monograph Series, *Vol. 7*; pp. 307-351.

(59) He, Y. T.; Wilson, J. T.; Su, C.; Wilkin, R. T. (2015) Review of abiotic degradation of chlorinated solvents by reactive iron minerals in aquifers. *Groundwater Monitoring & Remediation*, *35*, 57-75.

(60) Lee, W.; Batchelor, B. (2002) Abiotic reductive dechlorination of chlorinated ethylenes by iron-bearing soil minerals. 1. pyrite and magnetite. *Environ. Sci. Technol.*, *36*, 5147-5154.

(61) Lee, W.; Batchelor, B. (2002) Abiotic reductive dechlorination of chlorinated ethylenes by iron-bearing soil minerals. 2. green rust. *Environ. Sci. Technol.*, *36*, 5348-5354.

(62) Liang, X.; Paul Philp, R.; Butler, E. C. (2009) Kinetic and isotope analyses of tetrachloroethylene and trichloroethylene degradation by model Fe(II)-bearing minerals. *Chemosphere*, *75*, 63-69.

(63) Butler, E. C.; Dong, Y.; Krumholz, L. R.; Liang, X.; Shao, H.; Tan, Y. (2011) Rate controlling processes in the transformation of tetrachloroethylene and carbon tetrachloride under iron reducing and sulfate reducing conditions. In: *Aquatic Redox Chemistry*; Tratnyek, P. G.; Grundl, T. J.; Haderlein, S. B., Eds.; American Chemical Society: Washington, DC, ACS Symposium Series, *Vol. 1071*; pp. 519-538.

(64) Han, Y.-S.; Hyun, S. P.; Jeong, H. Y.; Hayes, K. F. (2012) Kinetic study of cis-dichloroethylene (cis-DCE) and vinyl chloride (VC) dechlorination using green rusts formed under varying conditions. *Water Res.*, *46*, 6339-6350.

(65) Jeong, H. Y.; Anantharaman, K.; Hyun, S. P.; Son, M.; Hayes, K. F. (2013) pH impact on reductive dechlorination of cis-dichloroethylene by Fe precipitates: An X-ray absorption spectroscopy study. *Water Res.*, *47*, 6639-6649.

(66) Jeong, H. Y.; Anantharaman, K.; Han, Y.-S.; Hayes, K. F. (2011) Abiotic reductive dechlorination of cis-dichloroethylene by Fe species formed during iron- or sulfate-reduction. *Environ. Sci. Technol.*, *45*, 5186-5194.

(67) Ferrey, M. L.; Wilkin, R. T.; Ford, R. G.; Wilson, J. T. (2004) Nonbiological removal of cis-dichloroethylene and 1,1-dichloroethylene in aquifer sediment containing magnetite. *Environ. Sci. Technol.*, *38*, 1746-1752.

(68) Darlington, R.; Lehmicke, L. G.; Andrachek, R. G.; Freedman, D. L. (2013) Anaerobic abiotic transformations of cis-1,2-dichloroethene in fractured sandstone. *Chemosphere*, *90*, 2226-2232.

(69) Schaefer, C. E.; Towne, R. M.; Lippincott, D. R.; Lacombe, P. J.; Bishop, M. E.; Dong, H. (2015) Abiotic dechlorination in rock matrices impacted by long-term exposure to TCE. *Chemosphere*, *119*, 744-749.

(70) Amonette, J. E.; Workman, D. J.; Kennedy, D. W.; Fruchter, J. S.; Gorby, Y. A. (2000) Dechlorination of carbon tetrachloride by Fe(II) associated with goethite. *Environ. Sci. Technol.*, *34*, 4606-4613.

(71) Hofstetter, T. B.; Heijman, C. G.; Haderlein, S. B.; Holliger, C.; Schwarzenbach, R. P. (1999) Complete reduction of TNT and other (poly)nitroaromatic compounds under iron-reducing subsurface conditions. *Environ. Sci. Technol.*, *33*, 1479-1487.

(72) Gorski, C. A.; Scherer, M. M. (2009) Influence of magnetite stoichiometry on $Fe^{II}$ uptake and nitrobenzene reduction. *Environ. Sci. Technol.*, *43*, 3675-3680.

(73) Perlinger, J. A.; Venkatapathy, R.; Harrison, J. F. (2000) Linear free energy relationships for polyhalogenated alkane transformation by electron-transfer mediators in model aqueous systems. *J. Phys. Chem.*, *104*, 2752.

(74) Elsner, M.; Haderlein, S. B.; Kellerhals, T.; Luzi, S.; Zwank, L.; Angst, W.; Schwarzenbach, R. P. (2004) Mechanisms and products of surface-mediated reductive dehalogenation of carbon tetrachloride by Fe(II) on goethite. *Environ. Sci. Technol.*, *38*, 2058-2066.

(75) Elsner, M.; Hofstetter, T. B. (2011) Current perspectives on the mechanisms of chlorohydrocarbon degradation in subsurface environments: Insight from kinetics, product formation, probe molecules and isotope fractionation. In: *Aquatic Redox Chemistry*; Tratnyek, P. G.; Grundl, T. J.; Haderlein, S. B., Eds.; American Chemical Society: Washington, DC, ACS Symposium Series, *Vol. 1071*; pp. 407-439.

(76) Williams, A. G. B.; Scherer, M. M. (2004) Spectroscopic evidence for Fe(II)-Fe(III) electron transfer at the iron oxide-water interface. *Environ. Sci. Technol.*, *38*, 4782-4790.

(77) Gorski, C. A.; Scherer, M. M. (2011) $Fe^{2+}$ Sorption at the Fe oxide-water interface: A revised conceptual framework. In: *Aquatic Redox Chemistry*; Tratnyek, P. G.; Grundl, T. J.; Haderlein, S. B., Eds.; American Chemical Society: Washington, DC, ACS Symposium Series, *Vol. 1071*; pp. 315-343.

(78) Gorski, C. A. (2009) Redox behavior of magnetite in the environment: Moving towards a semiconductor model. Thesis,

(79) Strathmann, T. J.; Stone, A. T. (2002) Reduction of oxamyl and related pesticides by $Fe^{II}$: influence of organic ligands and natural organic matter. *Environ. Sci. Technol.*, *36*, 5172-5183.

(80) Salter-Blanc, A. J.; Bylaska, E. J.; Johnston, H.; Tratnyek , P. G. (2015) Predicting reduction rates of energetic nitroaromatic compounds using calculated one-electron reduction potentials. *Environ. Sci. Technol.*, *49*, 3778–3786.

(81) Shi, Z.; Fan, D.; Johnson, R. L.; Tratnyek , P. G.; Nurmi , J. T.; Wu, Y.; Williams, K. H. (2015) Methods for characterizing the fate and effects of nano zerovalent iron during groundwater remediation. *J. Contam. Hydrol.*, *181*, 17-35.

(82) Silvester, E.; Charlet, L.; Tournassat, C.; Géhin, A.; Grenèche, J.-M.; Liger, E. (2005) Redox potential measurements and Mössbauer spectrometry of $Fe^{II}$ adsorbed onto $Fe^{III}$ (oxyhydr)oxides. *Geochim. Cosmochim. Acta*, *69*, 4801-4815.

(83) Amonette, J. E. (2002) Iron redox chemistry of clays and oxides: Environmental applications. In: *Electrochemistry of Clays*; Fitch, A., Ed.; Clay Minerals Society: Aurora, CO, *Vol. 10*; pp. 89-147.

(84) Strathmann, T. J.; Stone, A. T. (2003) Mineral surface catalysis of reactions between FeII and oxime carbamate pesticides. *Geochim. Cosmochim. Acta*, *67*, 2775-2791.

(85) Sander, M.; Hofstetter, T. B.; Gorski, C. A. (2015) Electrochemical analyses of redox-active iron minerals: A review of nonmediated and mediated approaches. *Environ. Sci. Technol.*,

(86) Orsetti, S.; Laskov, C.; Haderlein, S. B. (2013) Electron transfer between iron minerals and quinones: Estimating the reduction potential of the Fe(II)-goethite surface from AQDS speciation. *Environ. Sci. Technol.*, *47*, 14161-14168.

(87) O'Loughlin, E. J. (2008) Effects of electron transfer mediators on the bioreduction of lepidocrocite (γ-FeOOH) by *Shewanella putrefaciens* CN32. *Environ. Sci. Technol.*, *42*, 6876-6882.

(88) Shi, Z.; Zachara, J. M.; Shi, L.; Wang, Z.; Moore, D. A.; Kennedy, D. W.; Fredrickson, J. K. (2012) Redox reactions of reduced flavin mononucleotide (FMN), riboflavin (RBF), and anthraquinone-2,6-disulfonate (AQDS) with ferrihydrite and lepidocrocite. *Environ. Sci. Technol.*, *46*, 11644-11652.

(89) Liu, C.; Zachara, J. M.; Foster, N. S.; Strickland, J. (2007) Kinetics of reductive dissolution of hematite by bioreduced anthraquinone-2,6-disulfonate. *Environ. Sci. Technol.*, *41*, 7730-7735.

(90) McBride, M. B. (1994) *Environmental Chemistry of Soils*; Oxford Univ. Press.

(91) Elsner, M.; Chartrand, M.; Vanstone, N.; Couloume, G. L.; Lollar, B. S. (2008) Identifying abiotic chlorinated ethene degradation: Characteristic isotope patterns in reaction products with nanoscale zero-valent iron. *Environ. Sci. Technol.*, *42*, 5963-5970.

(92) Zwank, L.; Elsner, M.; Aeberhard, A.; Schwarzenbach, R. P.; Haderlein, S. B. (2005) Carbon isotope fractionation in the reductive dehalogenation of carbon tetrachloride at iron (hydr)oxide and iron sulfide minerals. *Environ. Sci. Technol.*, *39*, 5634-5641.

(93) Chen, S.; Fan, D.; Tratnyek, P. G. (2014) Novel contaminant transformation pathways by abiotic reductants. *Environ. Sci. Technol. Lett.*, *1*, 432-436.

(94) Refait, P.; Charton, A.; Genin, J. M. R. (1998) Identification, composition, thermodynamic and structural properties of a pyroaurite-like iron(II)-iron(III) hydroxy- oxalate Green Rust. *Eur. J. Solid State Inorg. Chem.*, *35*, 655-666.

(95) Scherer, M. M.; Balko, B. A.; Tratnyek, P. G. (1998) The role of oxides in reduction reactions at the metal-water interface. In: *Mineral-Water Interfacial Reactions: Kinetics and Mechanisms*; Sparks, D. L.; Grundl, T. J., Eds.; American Chemical Society: Washington, DC, ACS Symposium Series, *Vol. 715*; pp. 301-322.

(96) Luan, F.; Gorski, C. A.; Burgos, W. D. (2015) Linear free energy relationships for the biotic and abiotic reduction of nitroaromatic compounds. *Environ. Sci. Technol.*, *49*, 3557-3565.

(97) Chun, C. L.; Penn, R. L.; Arnold, W. A. (2005) Kinetic and microscopic studies of reductive transformations of organic contaminants on goethite. *Preprints of Extended Abstracts presented at the ACS National Meeting, American Chemical Society, Division of Environmental Chemistry*, *45*, 622-625.

(98) Colón, D.; Weber, E. J.; Anderson, J. L. (2006) QSAR study of the reduction of nitroaromatics by Fe(II) species. *Environ. Sci. Technol.*, *40*, 4976-4982.

(99) Bishop, E. (1972) *Indicators*; Pergamon: Oxford.

(100) Yanina, S. V.; Rosso, K. M. (2008) Linked reactivity at mineral-water interfaces through bulk crystal conduction. *Science*, *320*, 218-222.

(101) Colón, D.; Weber, E. J.; Anderson, J. L. (2008) Effect of natural organic matter on the reduction of nitroaromatics by Fe(II) species. *Environ. Sci. Technol.*, *42*, 6538-6543.

(102) Stumm, W. (1992) *Chemistry of the Solid-Water Interface: Processes at the Mineral-Water and Particle-Water Interface of Natural Systems*; Wiley: New York.

(103) Gorski, C. A.; Scherer, M. M. (2009) New conceptual model for interpreting the redox behavior of magnetite in anoxic environments. In: American Chemical Society, *Vol.* pp. ENVR-064.

(104) Strathmann, T. J.; Stone, A. T. (2002) Reduction of the pesticides oxamyl and methomyl by $Fe^{II}$: effect of pH and inorganic ligands. *Environ. Sci. Technol.*, *36*, 653-661.

(105) Johnson, T. L.; Scherer, M. M.; Tratnyek, P. G. (1996) Kinetics of halogenated organic compound degradation by iron metal. *Environ. Sci. Technol.*, *30*, 2634-2640.

(106) Rosso, K. M.; Yanina, S. V.; Gorski, C. A.; Larese-Casanova, P.; Scherer, M. M. (2010) Connecting observations of hematite ($\alpha$-$Fe_2O_3$) growth catalyzed by Fe(II). *Environ. Sci. Technol.*, *44*, 61-67.

(107) Katz, J. E.; Zhang, X.; Attenkofer, K.; Chapman, K. W.; Frandsen, C.; Zarzycki, P.; Rosso, K. M.; Falcone, R. W.; Waychunas, G. A.; Gilbert, B. (2012) Electron small polarons and their mobility in iron (oxyhydr)oxide nanoparticles. *Science*, *337*, 1200.

(108) Fan, D.; Bradley, M.; Hinkle, A. W.; Johnson, R. L.; Tratnyek, P. G. (2016) Chemical reactivity probes for assessing abiotic natural attenuation by reducing iron minerals. *Environ. Sci. Technol.*, *50*, 1868-1876.

(109) Klausen, J.; Troeber, S. P.; Haderlein, S. B.; Schwarzenbach, R. P. (1995) Reduction of substituted nitrobenzenes by Fe(II) in aqueous mineral suspensions. *Environ. Sci. Technol.*, *29*, 2396-2404.

(110) Vikesland, P. J.; Heathcock, A. M.; Rebodos, R. L.; Makus, K. E. (2007) Particle size and aggregation effects on magnetite reactivity toward carbon tetrachloride. *Environ. Sci. Technol.*, *41*, 5277-5283.

(111) Danielsen, K. M.; Hayes, K. F. (2004) pH dependence of carbon tetrachloride reductive dechlorination by magnetite. *Environ. Sci. Technol.*, *38*, 4745 -4752.

(112) McCormick, M. L.; Adriaens, P. (2004) Carbon tetrachloride transformation on the surface of nanoscale biogenic magnetite particles. *Environ. Sci. Technol.*, *38*, 1045-1053.

(113) Elsner, M.; Schwarzenbach, R. P.; Haderlein, S. B. (2004) Reactivity of Fe(II)-bearing minerals toward reductive transformation of organic contaminants. *Environ. Sci. Technol.*, *38*, 799-807.

(114) Schwertmann, U.; Cornell, R. M. (1991) *Iron Oxides in the Laboratory*; VCH: Weinheim.

(115) Taylor, R. M.; Maher, B. A.; Self, P. G. (1987) Magnetite in soils: I. The synthesis of single-domain and superparamagnetic magnetite. *Clay Miner.*, *22*, 411-422.

(116) Pecher, K.; Haderlein, S. B.; Schwarzenbach, R. P. (2002) Reduction of polyhalogenated methanes by surface-bound Fe(II) in aqueous suspensions of iron oxides. *Environ. Sci. Technol.*, *36*, 1734-1741.

(117) Kenneke, J. F.; Weber, E. J. (2003) Reductive dehalogenation of halomethanes in iron- and sulfate-reducing sediments. 1. Reactivity pattern analysis. *Environ. Sci. Technol.*, *37*, 713-720.

(118) Maithreepala, R. A.; Doong, R.-A. (2004) Reductive dechlorination of carbon tetrachloride in aqueous solutions containing ferrous and copper ions. *Environ. Sci. Technol.*, *38*, 6676-6684.

(119) Shao, H.; Butler, E. C. (2007) The influence of iron and sulfur mineral fractions on carbon tetrachloride transformation in model anaerobic soils and sediments. *Chemosphere*, *68*, 1807-1813.

(120) Maithreepala, R. A.; Doong, R.-A. (2005) Enhanced dechlorination of chlorinated methanes and ethenes by chloride green rust in the presence of copper(II). *Environ. Sci. Technol.*, *39*, 4082-4090.

(121) O'Loughlin, E. J.; Kemner, K. M.; Burris, D. R. (2003) Effects of AgI, AuIII, CuII on the reductive dechlorination of carbon tetrachloride by green rust. *Environ. Sci. Technol.*, *37*, 2905-2912.

(122) Liang, X.; Butler, E. C. (2010) Effects of natural organic matter model compounds on the transformation of carbon tetrachloride by chloride green rust. *Water Res*, *44*, 2125-2132.

(123) O'Loughlin, E. J.; Burris, D. R. (2004) Reduction of halogenated ethanes by green rust. *Environ. Toxicol. Chem.*, *23*, 41-48.

(124) Butler, E. C.; Hayes, K. F. (2000) Kinetics of the transformation of halogenated aliphatic compounds by iron sulfide. *Environ. Sci. Technol.*, *34*, 422-429.

(125) Lipczynska-Kochany, E.; Harms, S.; Milburn, R.; Sprah, G.; Nadarajah, N. (1994) Degradation of carbon tetrachloride in the presence of iron and sulphur containing compounds. *Chemosphere*, *29*, 1477-1489.

(126) Assaf-Anid, N.; Lin, K.-Y. (2002) Carbon tetrachloride reduction by $Fe^{2+}$, $S^{2-}$, and FeS with vitamin B12 as organic amendment. *J. Environ. Eng.*, *128*, 94-99.

(127) Choi, J.; Choi, K.; Lee, W. (2009) Effects of transition metal and sulfide on the reductive dechlorination of carbon tetrachloride and 1,1,1-trichloroethane by FeS. *J. Hazard. Mater.*, *162*, 1151-1158.

(128) Devlin, J. F.; Muller, D. (1999) Field and laboratory studies of carbon tetrachloride transformation in a sandy aquifer under sulfate reducing conditions. *Environ. Sci. Technol.*, *33*, 1021-1027.

(129) Amir, A.; Lee, W. (2012) Enhanced reductive dechlorination of tetrachloroethene during reduction of cobalamin (III) by nano-mackinawite. *J. Hazard. Mater.*, *235-236*, 359-366.

(130) Butler, E. C.; Hayes, K. F. (1999) Kinetics of the transformation of trichloroethylene and tetrachloroethylene by iron sulfide. *Environ. Sci. Technol.*, *33*, 2021-2027.

(131) Jeong, H. Y.; Hayes, K. F. (2007) Reductive dechlorination of tetrachloroethylene and trichloroethylene by mackinawite (FeS) in the presence of metals: Reaction rates. *Environ. Sci. Technol.*, *41*, 6390-6396.

(132) Liang, X.; Dong, Y.; Kuder, T.; Krumholz, L. R.; Philp, R. P.; Butler, E. C. (2007) Distinguishing abiotic and biotic transformation of tetrachloroethylene and trichloroethylene by stable carbon isotope fractionation. *Environ. Sci. Technol.*, *41*, 7094-7100.

(133) Butler, E. C.; Hayes, K. F. (2001) Factors influencing rates and products in the transformation of trichloroethylene by iron sulfide and iron metal. *Environ. Sci. Technol.*, *35*, 3884-3891.

(134) He, Y. T.; Wilson, J. T.; Wilkin, R. T. (2010) Impact of iron sulfide transformation on trichloroethylene degradation. *Geochim. Cosmochim. Acta*, *74*, 2025-2039.

(135) Nowack, B.; Ranville, J. F.; Diamond, S.; Gallego-Urrea, J. A.; Metcalfe, C.; Rose, J.; Horne, N.; Koelmans, A. A.; Klaine, S. J. (2012) Potential scenarios for nanomaterial release and subsequent alteration in the environment. *Environ. Toxicol. Chem.*, *31*, 50-59.

(136) Lowry, G. V.; Gregory, K. B.; Apte, S. C.; Lead, J. R. (2012) Transformations of nanomaterials in the environment. *Environ. Sci. Technol.*, *46*, 6893-6899.

(137) Maynard, A. D.; Aitken, R. J.; Butz, T.; Colvin, V.; Donaldson, K.; Oberdorster, G.; Philbert, M. A.; Ryan, J.; Seaton, A.; Stone, V.; Tinkle, S. S.; Tran, L.; Walker, N. J.; Warheit, D. B. (2006) Safe handling of nanotechnology. *Nature*, *444*, 267-269.

(138) Wagner, S.; Gondikas, A.; Neubauer, E.; Hofmann, T.; von der Kammer, F. (2014) Spot the difference: Engineered and natural nanoparticles in the environment - Release, behavior, and fate. *Angew. Chem., Int. Ed.*, *53*, 12398-12419.

(139) Tosco, T.; Petrangeli Papini, M.; Cruz Viggi, C.; Sethi, R. (2014) Nanoscale zerovalent iron particles for groundwater remediation: A review. *J. Cleaner Prod.*, *77*, 10-21.

(140) Crane, R. A.; Scott, T. B. (2012) Nanoscale zero-valent iron: Future prospects for an emerging water treatment technology. *J. Hazard. Mater.*, *211-212*, 112-125.

(141) Yan, W.; Lien, H.-L.; Koel, B. E.; Zhang, W.-X. (2013) Iron nanoparticles for environmental clean-up: Recent developments and future outlook. *Environ. Sci.: Processes Impacts*, *15*, 63-77.

(142) O'Carroll, D.; Sleep, B.; Krol, M.; Boparai, H.; Kocur, C. (2013) Nanoscale zero valent iron and bimetallic particles for contaminated site remediation. *Adv. Water Resour.*, *51*, 104-122.

(143) Johnson, R. L.; Nurmi, J. T.; O'Brien Johnson, G.; Fan, D.; O'Brien Johnson, R.; Shi, Z.; Salter-Blanc Alexandra, J.; Tratnyek, P. G.; Lowry, G. V. (2013) Field-scale transport and transformation of carboxymethylcellulose-stabilized nano zero-valent iron. *Environ. Sci. Technol.*, *47*, 1573-1580.

(144) Sarathy, V.; Tratnyek, P. G.; Nurmi, J. T.; Baer, D. R.; Amonette, J. E.; Chun, C.; Penn, R. L.; Reardon, E. J. (2008) Aging of iron nanoparticles in aqueous solution: effects on structure and reactivity. *J. Phys. Chem. C*, *112*, 2286-2293.

(145) Phenrat, T.; Long, T. C.; Lowry, G. V.; Veronesi, B. (2009) Partial oxidation ("aging") and surface modification decrease the toxicity of nanosized zerovalent iron. *Environ. Sci. Technol.*, *43*, 195-200.

(146) Reinsch, B. C.; Forsberg, B.; Penn, R. L.; Kim, C. S.; Lowry, G. V. (2010) Chemical transformations during aging of zerovalent iron nanoparticles in the presence of common groundwater dissolved constituents. *Environ. Sci. Technol.*, *44*, 3455-3461.

(147) Kumar, N.; Omoregie, E. O.; Rose, J.; Masion, A.; Lloyd, J. R.; Diels, L.; Bastiaens, L. (2014) Inhibition of sulfate reducing bacteria in aquifer sediment by iron nanoparticles. *Water Res.*, *51*, 64-72.

(148) Bruton, T. A.; Pycke, B. F. G.; Halden, R. U. (2015) Effect of nanoscale zero-valent iron treatment on biological reductive dechlorination: A review of current understanding and research needs. *Crit. Rev. Environ. Sci. Technol.*, *45*, 1148-1175.

(149) Fajardo, C.; Ortíz, L. T.; Rodríguez-Membibre, M. L.; Nande, M.; Lobo, M. C.; Martin, M. (2012) Assessing the impact of zero-valent iron (ZVI) nanotechnology on soil microbial structure and functionality: A molecular approach. *Chemosphere*, *86*, 802-808.

(150) Němeček, J.; Lhotský, O.; Cajthaml, T. (2014) Nanoscale zero-valent iron application for in situ reduction of hexavalent chromium and its effects on indigenous microorganism populations. *Sci. Total Environ.*, *485-486*, 739-747.

(151) Liu, Y.; Lowry, G. V. (2006) Effect of particle age ($Fe^0$ content) and solution pH on nZVI reactivity: $H_2$ evolution and TCE dechlorination. *Environ. Sci. Technol.*, *40*, 6085-6090.

(152) Tratnyek, P. G.; Salter-Blanc, A. J.; Nurmi, J. T.; Amonette, J. E.; Liu, J.; Wang, C.; Dohnalkova, A.; Baer, D. R. (2011) Reactivity of zerovalent metals in aquatic media: Effects of organic surface coatings. In: *Aquatic Redox Chemistry*; Tratnyek, P. G.; Grundl, T. J.; Haderlein, S. B., Eds.; American Chemical Society: Washington, DC, ACS Symposium Series, *Vol. 1071*; pp. 381-406.

(153) Liu, A.; Liu, J.; Zhang, W.-X. (2015) Transformation and composition evolution of nanoscale zero valent iron (nZVI) synthesized by borohydride reduction in static water. *Chemosphere*, *119*, 1068-1074.

(154) Woo, H.; Park, J.; Lee, S.; Lee, S. (2014) Effects of washing solution and drying condition on reactivity of nano-scale zero valent irons (nZVIs) synthesized by borohydride reduction. *Chemosphere*, *97*, 146-152.

(155) Sun, Q.; Feitz, A. J.; Guan, J.; Waite, T. D. (2008) Comparison of the reactivity of nanosized zero-valent iron (nZVI) particles produced by borohydride and dithionite reduction of iron salts. *Nano*, *3*, 341-349.

(156) Fan, D.; Anitori, R. P.; Tebo, B. M.; Tratnyek, P. G.; Lezama Pacheco, J. S.; Kukkadapu, R. K.; Engelhard, M. H.; Bowden, M. E.; Kovarik, L.; Arey, B. W. (2013) Reductive sequestration of pertechnetate ($^{99}TcO_4^-$) by nano zero-valent iron (nZVI) transformed by abiotic sulfide. *Environ. Sci. Technol.*, *47*, 5302-5310.

(157) Fan, D.; Anitori, R. P.; Tebo, B. M.; Tratnyek, P. G.; Lezama Pacheco, J. S.; Kukkadapu, R. K.; Kovarik, L.; Engelhard, M. H.; Bowden, M. E. (2014) Oxidative remobilization of technetium sequestered by sulfide-transformed nano zerovalent iron. *Environ. Sci. Technol.*, *48*, 7409–7417.

(158) Johnson, R. L.; O'Brien Johnson, R.; Nurmi, J. T.; Tratnyek, P. G. (2009) Natural organic matter enhanced mobility of nano zero-valent iron. *Environ. Sci. Technol.*, *43*, 5455–5460.

(159) He, F.; Zhao, D. (2007) Manipulating the size and dispersibility of zerovalent iron nanoparticles by use of carboxymethyl cellulose stabilizers. *Environ. Sci. Technol.*, *41*, 6216-6221.

(160) Busch, J.; Meißner, T.; Potthoff, A.; Bleyl, S.; Georgi, A.; Mackenzie, K.; Trabitzsch, R.; Werban, U.; Oswald, S. E. (2015) A field investigation on transport of carbon-supported nanoscale zero-valent iron (nZVI) in groundwater. *J. Contam. Hydrol.*, Published Online.

(161) Saleh, N.; Sirk, K.; Liu, Y.; Phenrat, T.; Dufour, B.; Matyjaszewski, K.; Tilton, R. D.; Lowry, G. V. (2007) Surface modifications enhance nanoiron transport and NAPL targeting in saturated porous media. *Environ. Eng. Sci.*, *24*, 45-57.

(162) He, F.; Zhang, M.; Qian, T.; Zhao, D. (2009) Transport of carboxymethyl cellulose stabilized iron nanoparticles in porous media: Column experiments and modeling. *J. Colloid Interface Sci.*, *334*, 96-102.

(163) He, F.; Zhao, D.; Paul, C. (2010) Field assessment of carboxymethyl cellulose stabilized iron nanoparticles for in situ destruction of chlorinated solvents in source zones. *Water Res.*, *44*, 2360-2370.

(164) Kocur, C. M.; O'Carroll, D. M.; Sleep, B. E. (2013) Impact of nZVI stability on mobility in porous media. *J. Contam. Hydrol.*, *145*, 17-25.

(165) Krol, M. M.; Oleniuk, A. J.; Kocur, C. M.; Sleep, B. E.; Bennett, P.; Xiong, Z.; O'Carroll, D. M. (2013) A field-validated model for in situ transport of polymer-stabilized nZVI and implications for subsurface injection. *Environ. Sci. Technol.*, *47*, 7332-7340.

(166) Nurmi, J. T.; Sarathy, V.; Tratnyek , P. G.; Baer, D. R.; Amonette, J. E.; Linehan, J. C.; Karkamkar, A. (2011) Recovery of iron/iron oxide nanoparticles from aqueous media: A comparison of methods and their effects. *J. Nanoparticle Res.*, *13*, 1937-1952.

(167) Baer, D. R.; Tratnyek, P. G.; Qiang, Y.; Amonette, J. E.; Linehan, J.; Sarathy, V.; Nurmi, J. T.; Wang, C.; Antony, J. (2012) Synthesis, characterization, and properties of zero-valent iron nanoparticles. In: *Environmental Applications of Nanomaterials (2nd Edition)*; Imperial College Press; pp. 49-86.

(168) Jones, B. D.; Ingle Jr, J. D. (2001) Evaluation of immobilized redox indicators as reversible, in situ redox sensors for determining Fe(III)-reducing conditions in environmental samples. *Talanta*, *55*, 699-714.

(169) Jones, B. D.; Ingle Jr, J. D. (2005) Evaluation of redox indicators for determining sulfate-reducing and dechlorinating conditions. *Water Res.*, *39*, 4343-4354.

(170) Royer, R. A.; Burgos, W. D.; Fisher, A. S.; Unz, R. F.; Dempsey, B. A. (2002) Enhancement of biological reduction of hematite by electron shuttling and Fe(II) complexation. *Environ. Sci. Technol.*, *36*, 1939-1946.

(171) Clark, W. M. (1960) *Oxidation-Reduction Potentials of Organic Systems*; Williams & Wilkins: Baltimore.

(172) Glavee, G. N.; Klabunde, K. J.; Sorensen, C. M.; Hadjipanayis, G. C. (1995) Chemistry of borohydride reduction of iron(II) and iron(III) ions in aqueous and nonaqueous media. Formation of nanoscale Fe, FeB, and Fe2B powders. *Inorg. Chem.*, *34*, 28-35.

(173) Baer, D. R.; Grosz, A. E.; Ilton, E. S.; Krupka, K. M.; Liu, J.; Penn, R. L.; Pepin, A. (2010) Separation, characterization and initial reaction studies of magnetite particles from Hanford sediments. *Physics and Chemistry of the Earth*, *35*, 233-241.

(174) Mahmoodlu, M. G.; Hassanizadeh, S. M.; Hartog, N. (2014) Evaluation of the kinetic oxidation of aqueous volatile organic compounds by permanganate. *Sci. Total Environ.*, *485–486*, 755-763.

(175) Tratnyek, P. G. (2015) Comment on "Evaluation of the kinetic oxidation of aqueous volatile organic compounds by permanganate" by M. G. Mahmoodlu, S. M. Hassanizadeh, and N. Hartog, in Science of the Total Environment (2014) 485–486: 755–763. *Sci. Total Environ.*, *502*, 722-723.

(176) Liu, T.; Li, X.; Waite, T. D. (2013) Depassivation of aged $Fe^0$ by ferrous ions: Implications to contaminant degradation. *Environ. Sci. Technol.*, *47*, 13712-13720.

(177) Huang, Y. H.; Zhang, T. C. (2005) Effects of dissolved oxygen on formation of corrosion products and concomitant oxygen and nitrate reduction in zero-valent iron systems with or without aqueous $Fe^{2+}$. *Water Res.*, *39*, 1751-1760.

(178) Reardon, E. J. (2005) Zerovalent irons: Styles of corrosion and inorganic control on hydrogen pressure buildup. *Environ. Sci. Technol.*, *39*, 7311-7317.

(179) Velimirovic, M.; Carniato, L.; Simons, Q.; Schoups, G.; Seuntjens, P.; Bastiaens, L. (2014) Corrosion rate estimations of microscale zerovalent iron particles via direct hydrogen production measurements. *J. Hazard. Mater.*, *270*, 18-26.

(180) Paar, H.; Ruhl, A. S.; Jekel, M. (2015) Influences of nanoscale zero valent iron loadings and bicarbonate and calcium concentrations on hydrogen evolution in anaerobic column experiments. *Water Res.*, *68*, 731-739.

(181) Filip, J.; Karlický, F.; Marušák, Z.; Lazar, P.; Černík, M.; Otyepka, M.; Zbořil, R. (2014) Anaerobic reaction of nanoscale zerovalent iron with water: Mechanism and kinetics. *J. Phys. Chem. C*, *118*, 13817-13825.

(182) Kocur, C. M.; Chowdhury, A. I.; Sakulchaicharoen, N.; Boparai, H. K.; Weber, K. P.; Sharma, P.; Krol, M. M.; Austrins, L.; Peace, C.; Sleep, B. E.; O'Carroll, D. M. (2014) Characterization of nZVI mobility in a field scale test. *Environ. Sci. Technol.*, *48*, 2862-2869.

(183) Schöftner, P.; Waldner, G.; Lottermoser, W.; Stöger-Pollach, M.; Freitag, P.; Reichenauer, T. G. Electron efficiency of nZVI does not change with variation of environmental parameters. *Sci. Total Environ.*,

(184) Fan, D.; Chen, S.; Johnson, R. L.; Tratnyek, P. G. (2015) Field deployable chemical redox probe for quantitative characterization of carboxymethylcellulose modified nano zerovalent iron. *Environ. Sci. Technol.*, *49*, 10589-10597.

(185) Saleh, N.; Phenrat, T.; Sirk, K.; Dufour, B.; Ok, J.; Sarbu, T.; Matyjaszewski, K.; Tilton, R. D.; Lowry, G. V. (2005) Adsorbed triblock copolymers deliver reactive iron nanoparticles to the oil/water interface. *Nano Lett.*, *5*, 2489-2494.

(186) Yu, Y. S.; Bailey, G. W. (1996) Redox characterization of the surfaces of seven iron-bearing minerals: Use of molecular probes and uv-visible spectroscopy. *Clays Clay Mineral.*, *44*, 573-586.

(187) ZoBell, C. l. E. (1946) Studies on redox potential of marine sediments. *Bull. Am. Assoc. Petrol. Geol.*, *30*, 477-509.

(188) Istok, J. D. (2013) *Push-Pull Tests for Site Characterization*; Springer-Verlag, Berlin Heidelberg.

(189) Johnson, R. L.; Kocur, C. M.; O'Brien Johnson, G.; Tratnyek, P. G. (2017) In situ thermodynamic and kinetic redox measurements using single-well: "Pull-push-pull" tests and chemical reactivity probes. *Environ. Sci. Technol.*, in prep.

# 13. APPENDICES

## 13.1. Supporting Data

Supporting information are included at the end of each Objective section.

## 13.2. List of Scientific/Technical Publications

Fan, D. (2015) Reactivity of Reducing Iron Minerals in the Subsurface: Implications for Contaminant Remediation. Part I: Remediation of Technetium by Sulfidated Nano Zerovalent Iron. Ph.D. Thesis, Oregon Health & Science University.

Fan, D.; Bradley, M.; Hinkle, A. W.; Johnson, R. L.; Tratnyek, P. G. Chemical reactivity probes for assessing abiotic natural attenuation by reducing iron minerals. (2016) *Environ. Sci. Technol.*, *50*, 1868-1876. [DOI: 10.1021/acs.est.5b05800]

Fan, D.; Chen, S.; Johnson, R. L.; Tratnyek, P. G. Field deployable chemical redox probe for quantitative characterization of carboxymethylcellulose modified nano zerovalent iron. (2015) *Environ. Sci. Technol.*, *49*, 10589-10597. [DOI: 10.1021/acs.est.5b02804]

Fan, D.; O'Carroll, D. M.; Elliott, D. W.; Xiong, Z.; Tratnyek, P. G.; Johnson, R. L.; Garcia, A. N. Selectivity of nano zerovalent iron in in situ chemical reduction: Challenges and improvements. (2016) *Remediation J.*, *26*, 27-40. [DOI: 10.1002/rem.21481]

Fan, D.; O'Brien Johnson, G. S.; Tratnyek, P. G.; Johnson, R. L. Sulfidation of nano zerovalent iron (nZVI) for improved selectivity during in-situ chemical reduction (ISCR). (2016) *Environ. Sci. Technol.*, *50*, 9558–9565. [DOI: 10.1021/acs.est.6b02170]

Johnson, R. L.; Kocur, C. M.; O'Brien Johnson, G.; Tratnyek, P. G. (2017) In situ thermodynamic and kinetic redox measurements using single-well: "Pull-push-pull" tests and chemical reactivity probes. *Environ. Sci. Technol.*, in prep.

Shi, Z.; Fan, D.; Johnson, R. L.; Tratnyek , P. G.; Nurmi , J. T.; Wu, Y.; Williams, K. H. Methods for characterizing the fate and effects of nano zerovalent iron during groundwater remediation. (2015) *J. Contam. Hydrol.*, *181*, 17-35. [DOI: 10.1016/j.jconhyd.2015.03.004]

Xu, C.; Zhang, B.; Wang, Y.; Shao, Q.; Zhou, W.; Fan, D.; Bandstra Joel, Z.; Shi, Z.; Tratnyek , P. G. Effects of sulfidation, magnetization, and oxygenation on azo dye reduction by zerovalent iron. (2016) *Environ. Sci. Technol.*, *50*, 11879-11887. [DOI: 10.1021/acs.est.6b03184]

## 13.3. Other Supporting Materials

No other supporting materials provided.